ÇUKUROVA UNIVERSITY
INSTITUTE OF NATURAL AND APPLIED SCIENCES

Ph.D. THESIS

Tahir DURHASAN

FLOW CONTROL IN THE NEAR WAKE OF A CIRCULAR CYLINDER BY SPLITTER PLATE AND PERFORATED CYLINDER COMBINATION

DEPARTMENT OF MECHANICAL ENGINEERING

ADANA-2017

ÇUKUROVA UNIVERSITY
INSTITUTE OF NATURAL AND APPLIED SCIENCES

FLOW CONTROL IN THE NEAR WAKE OF A CIRCULAR CYLINDER BY SPLITTER PLATE AND PERFORATED CYLINDER COMBINATION

Tahir DURHASAN

PhD. THESIS

DEPARTMENT OF MECHANICAL ENGINEERING

We certify that the thesis titled above was reviewed and approved for the award of degree of the Philosophy of Doctorate by the board of jury on 28/11/2017.

…………………………	…………………….	……………………….
Prof. Dr. Hüseyin AKILLI SUPERVISOR	Prof. Dr. Beşir ŞAHİN MEMBER	Prof. Dr. M. Sami AKÖZ MEMBER
……………………….	………………………………..	
Prof. Dr. Bayram ŞAHİN MEMBER	Asst. Prof. Dr. Cuma KARAKUŞ MEMBER	

This PhD Thesis is written at the Department of Institute of Natural And Applied Sciences of Çukurova University.
Registration Number:

Prof. Dr. Mustafa GÖK
Director
Institute of Natural and Applied Sciences

This thesis was supported by the Scientific and Technological Research Council of Turkey under contract no: 114R0087.

ABSTRACT

PhD THESIS

FLOW CONTROL IN THE NEAR WAKE OF A CIRCULAR CYLINDER BY SPLITTER PLATE AND PERFORATED CYLINDER COMBINATION

Tahir DURHASAN

ÇUKUROVA UNIVERSITY
INSTITUTE OF NATURAL AND APPLIED SCIENCES
DEPARTMENT OF MECHANICAL ENGINEERING

Supervisor : Prof. Dr. Hüseyin AKILLI
Year: 2017, Pages: 115
Jury : Prof. Dr. Hüseyin AKILLI
: Prof. Dr. Beşir ŞAHİN
: Prof. Dr. M.Sami AKÖZ
: Prof. Dr. Bayram ŞAHİN
: Asst. Prof. Dr. Cuma KARAKUŞ

In this study, it is aimed to flow control in the near wake of a circular cylinder by splitter plate and perforated cylinder combination in deep water. The cylinder diameter was kept to constant during the experiments as D=50 mm and corresponding Reynolds number based on the cylinder diameter $Re=5\times10^3$. Experiments were performed in three stages. In the first stage, the effect of perforated cylinder on the flow control was investigated using the PIV measurement technique and also force measurement was performed in the air tunnel in order to calculate the drag and the lift coefficients of the cylinder for β=0.3, 0.4, 0.5, 0.6 and 0.7 at D/D_s=0.4, 0.5 and 0.6. In the second stage, the flow structure in the further downstream of the perforated cylinder was investigated using dye visualization technique. Finally, the effect of the splitter plate and perforated cylinder combination in the near wake was investigated on the flow control with respect to total drag and lift coefficients. The results depicted that the porosity, β and the diameter ratio, D/D_s have substantial effects on the flow control and the drag reduction of the cylinder. The flow control was achieved in the near wake region for β=0.5 and 0.6 at D/D_s=0.4 and 0.5. Also, the drag coefficient of cylinder was reduced by 65% for β=0.5 at D/D_s=0.4. It was observed that using of the splitter plate remarkably affected the flow structure and increased the total lift coefficient.

Key Words: Cylinder, Drag reduction, Flow control, PIV

ÖZ

DOKTORA TEZİ

DAİRESEL SİLİNDİRİN YAKIN ARD İZİNDEKİ AKIŞIN AYIRICI PLAKA VE DELİKLİ SİLİNDİR KOMBİNASYONU İLE KONTROL EDİLMESİ

Tahir DURHASAN

ÇUKUROVA ÜNİVERSİTESİ
FEN BİLİMLERİ ENSTİTÜSÜ
MAKİNE MÜHENDİSLİĞİ ANABİLİM DALI

Danışman : Prof. Dr. Hüseyin AKILLI
Yıl: 2017, Sayfa: 115
Jüri : Prof. Dr. Hüseyin AKILLI
: Prof. Dr. Beşir ŞAHİN
: Prof. Dr. M.Sami AKÖZ
: Prof. Dr. Bayram ŞAHİN
: Yrd. Doç. Dr. Cuma KARAKUŞ

Bu çalışmada derin suda dairesel silindirin ard izindeki akışın ayırıcı plaka ve delikli silindir kombinasyonu ile kontrol edilmesi amaçlanmıştır. Silindir çapı D=50 mm ve bu çapa karşılık gelen Reynolds sayısı $Re=5\times10^3$ deneyler süresince sabit tutulmuştur. Deneyler üç aşamada gerçekleştirilmiştir. Birinci aşamada, geçirgenlik oranı β=0.3, 0.4, 0.5, 0.6 ve 0.7, çap oranı D/D_s =0.4, 0.5 ve 0.6 için delikli silindirin akış kontrolündeki etkisi PIV ölçüm tekniği kullanılarak araştırılmıştır ve ayrıca hava tünelinde silindirin sürükleme ve kaldırma katsayılarını hesaplamak için kuvvet ölçümleri yapılmıştır. İkinci aşamada, delikli silindirin daha uzak ard izindeki akış yapısı boya görselleştirme tekniği kullanılarak araştırılmıştır. Son olarak, ayırıcı plaka ve delikli silindir kombinasyonunun silindirin yakın ard izindeki akış kontrolü üzerine ve sürükleme ve kaldırma katsayısına etkisi incelenmiştir. Sonuçlar geçirgenlik β ve çap oranının, D/D_s girdapları bastırmada ve silindirin sürüklenme katsayısının azaltılmasında önemli bir etkiye sahip olduğunu göstermiştir. Yakın ard izindeki akış kontrolü geçirgenlik oranının β=0.5 ve 0.6, çap oranın D/D_s =0.4 ve 0.5 değerleri için başarılmıştır. Ayrıca, silindirin sürüklenme katsayısı β=0.5 ve D/D_s =0.4 için %65 azaltılmıştır. Ayırıcı plaka kullanımı akış yapısını önemli ölçüde etkilemiş ve toplam kaldırma katsayısının arttığı gözlemlenmiştir.

Anahtar Kelimeler: Silindir, Sürüklemenin azaltılması, Akış kontrolü, PIV

EXPANDED ABSTRACT

The drag reduction and the flow control downstream of the circular cylinder are important research topics in order to reduce or eliminate the adverse effects of vortex induced vibrations (VIV). Flow control techniques can be divided into two categories as an active and passive flow control. The active flow controls need to external energy whereas the passive flow controls. Therefore the passive flow control techniques are more applicable than the active flow control techniques. The illustrative example of the passive flow control techniques can be given such as splitter plate, shroud, control rod, helical strakes. Although the shrouds have been studied in this regard, the controlled wake of shroud has not been fully understood. In this study, it is aimed to investigate the flow structure around the cylinder in the near wake and the effect of perforated cylinder on the drag coefficient of cylinder in deep water. Perforated cylinders were used in this study as shroud. The perforated cylinder, constructed from perforated steel sheet which has 1 mm thickness. The diameter of the cylinder and the free-stream velocity were kept constant as D=50 mm and U_∞=100 mm/s corresponds to a Reynolds number of Re=5×10^3 according to the cylinder diameter, D. The perforated cylinders have five different porosities (β=0.3, 0.4, 0.5, 0.6 and 0.7) and three different diameters (D_s=83.33 mm, 100 mm and 125 mm). Firstly, it was focused on the flow structure in the gap region between the cylinder and the perforated cylinder as well as the near-wake region of the perforated cylinder to investigate the effect of the perforated cylinder on the drag reduction. Secondly, the effect of splitter plate and perforated cylinder combination on the flow control of the circular cylinder was investigated. During the experiments two different plate lengths, L_p which are L_p=3/4 and 1 were used and also the plate was located seven different rotation angles, α which are α=120°, 130°, 140°, 150°, 160°, 170° and 180°. The effect of splitter plate and perforated cylinder combination on the total drag and lift coefficients were also investigated.

It can be concluded in the light of obtained PIV results that the flow structure of the cylinder in the near-wake region are significantly affected by the perforated cylinder for all diameter ratios, D/D_s. The perforated cylinders are dominant on the flow structure for the porosity value of $\beta=0.3$. The negative velocity contours indicate that reverse flow occurs in the near wake region owing to the detainment of the main flow by using perforated cylinder at porosity value of $\beta=0.3$. At the diameter ratio of $D/D_s=0.4$, increasing the number of holes on the perforated cylinder enhances momentum transfer into the gap region between the cylinder and the perforated cylinder and the near-wake region. Thus, the velocity magnitudes of the gap region are higher compared to the porosity value of $\beta=0.3$ and reverse flow is disappeared in the near-wake region for the porosity values of $0.4\leq\beta\leq0.6$. The magnitude of velocity in near-wake region is affected not only by the porosity of perforated cylinder, but also by the diameter ratio of the perforated cylinder. At the diameter ratio of $D/D_s=0.6$, the negative velocity contours for the porosity values of $\beta=0.4$ and 0.5 indicate that narrow gap is inadequate to momentum transfer from inside of perforated cylinder into the near - wake region. Therefore, the reverse flow occurs in the near-wake region as a result of momentum transfer from the shear layers of the perforated cylinder into the near-wake region. On the other hand, the flow control is achieved in the near-wake region for the porosity values of $\beta=0.5$ and 0.6 at the diameter ratios of $D/D_s=0.4$ and 0.5. Also, the drag coefficient of cylinder is reduced by 65% for the porosity value of $\beta=0.5$ at the diameter ratio of $D/D_s=0.4$. However, the vortex formation of the cylinder is still observed in the gap region between the cylinder and the perforated cylinder for all cases.

The results obtained from dye experiments for the further downstream depict that perforated cylinders behave like bare cylinder and dominant on the flow structure for porosity values of $\beta\leq0.4$. The shear layers on the both side of perforated cylinder roll up in to the near wake region and Von Karman Vortex Street emerged from the downstream of cylinder perforated cylinder configuration.

The results obtained for porosity value of β=0.5 indicated that the location of rolling up of shear layers, R_L is shifted to further region of downstream for the diameter ratios $D/D_s \geq 0.5$. However, the results obtained for the porosity value of β=0.5 at the diameter ratio of D/D_s=0.4 is slightly different compared with the case of diameter ratios $D/D_s \geq 0.5$. The wake region exhibits 'S' shaped unsteady oscillating flow behavior similar to Von Karman vortex street. On the other hand, the width of wake regions, W_w are decreased up to porosity values of β<0.6 and they are approximately same at porosity value of $\beta \geq 0.6$ for all dimeter ratios, D/D_s. In addition, the formation of Von Karman vortex street is suppressed in the further downstream at the diameter ratios of D/D_s=0.4 and 0.5.

The use of splitter plate and perforated cylinder combination remarkably affects the flow structure in the near-wake. For the plate angles of $120^o \leq \alpha \leq 140^o$, the incoming flow through the perforated cylinder is blocked by the splitter plate. Therefore, the reverse flow occurs in the near-wake region and re-enters into the gap region between the cylinder and the perforated cylinder. A lower magnitude vorticity in the lower side of the cylinder elongates in the downstream direction and the magnitude of the vorticity dramatically increases in the leading edge of the splitter plate due to the fact that the momentum transfer into the near-wake region increases at this point. On the other hand, the reverse flow disappear in the near-wake region for the porosity values of β=0.5 and 0.6 at the plate angles of $\alpha=170^o$ and 180^o. The plate angle of $\alpha=180^o$ presents the well-known splitter plate method with in the literature and might be the best way of preventing the interaction of vortices formed by the cylinder in the near-wake region. Total drag coefficient which is calculated based on the frontal area of cylinder slightly reduces with the increasing plate angle, α. It is noted that the plate angle has a significant effect on the total lift coefficient. The maximum total lift coefficient is evaluated at the plate angle $\alpha=120^o$ for the porosity of β=0.7 since increasing porosity, β enhances momentum transfer into the gap region between the cylinder and the perforated cylinder and decreasing plate angle, α causes asymmetric flow in the gap region between the cylinder and the perforated cylinder. The total lift coefficient decreases gradually with the increasing plate angle, α. The total lift coefficient values are approximately zero for all porosity at the plate angle of $\alpha=180^o$ due to symmetric flow structure around the cylinder.

ACKNOWLEDGEMENTS

First of all, I am especially indebted to my supervisor, Prof. Dr. Hüseyin AKILLI who have been supportive my career goals and who worked actively to provide me those goals.

I sincerely thank Prof. Dr. Beşir ŞAHİN for his continuous and effective advices to improve myself.

My heartfelt thanks go to Asst. Prof. Dr. Engin PINAR, Asst. Prof. Dr. Göktürk Memduh ÖZKAN, Muhammed M. AKSOY and Hürrem AKBIYIK who always have been with me throughout this study. Without their moral and support it might be so difficult to finish this investigation.

I also thank all members of Mechanical Engineering stuff for their grateful helps throughout my experiments.

Most importantly, I wish to thank my loving and supportive wife, Zeynep, and my wonderful son, Zahit Alp, who provide unending inspiration.

CONTENTS **PAGE**

LIST OF TABLES **PAGE**

LIST OF FIGURES **PAGE**

LIST OF ABBREVIATONS

D	: Cylinder diameter
D_s	: Perforated cylinder diameter
β	: Porosity
L_p	: Splitter plate length
α	: Splitter plate angle
h_W	: Water height
<U>	: Time averaged streamwise velocity
<V>	: Time averaged velocity vectors
<y >	: Time averaged streamline
<ω>	: Time averaged vorticity
U_∞	: Free stream velocity
C_D	: Drag coefficient
C_L	: Lift coefficient

XXI

1. INTRODUCTION

Flow over a bluff body has great research interest since it is a common encountered phenomenon such as marina engineering, platform pillars, pipelines and high-rise buildings. Bluff body flow is characterized by a large region of separated flow where it is named as wake and includes various forms of flow instability. The well-known flow instability is that leading to the regular formation and shedding of spanwise vortices, which are often referred to as Karman vortices (Bearman 1997). These vortices are responsible for generation of unsteady forces effective on the body which are causing structural vibration, acoustic noise and increases in the mean drag and lift fluctuation. These unsteady forces are unacceptable to certain engineering structures. Due to this reason, vortex shedding control has constituted the basis of many numerical and experimental studies.

1.1. Flow around a Circular Cylinder

The circular cylinder is commonly used as a bluff body in the studies due to it has simple geometry and wide range of usage area in the engineering applications. Besides, flow around the circular cylinder involves important flow characteristics depends only on the Reynolds number ($Re=U_\infty D/\nu$ where U_∞ is the free stream velocity far from the cylinder, D is the diameter of the cylinder and ν is the kinematic viscosity) such as the wake, the separated shear layer, the vortex shedding patterns. As a results of a fluid flows around the cylinder, a force occurs that tends to drag the cylinder in the direction of flow. The drag force consists of skin friction and pressure. From creeping flows ($Re \ll 1$) to fully turbulent flows ($Re \gg 10^7$) there are different flow regimes which can be classified as follows (Figure1.1);

i. When Reynolds number is less than 1 so-called creeping flow, the flow behaves like a potential flow. There is no separation and the drag is all due to skin friction in this flow regime.

ii. While the Reynolds number increases, the drag decreases as shown Figure 1.2. At the Reynolds number in the range of 5 to 15, flow separation occurs, a pair fixed of “Foppl” vortices (eddies) first appears in the wake of cylinder and ambient pressure exists at the rear of the cylinder. Drag consists of skin friction and difference of pressure at the front and the rear of the cylinder. The wake is a limited length.

iii. At the Reynolds number ***Re*** = 40, the eddies elongated, become unstable and first periodic driving force begin. While periodicity is governed in low Re range by the wake instability, periodicity is governed in high Re range by the vortex shedding. Vortex shedding regime is laminar.

iv. The Reynolds number in the range of 150 to 300, transition occurs and laminar vortex shedding becomes turbulent vortex shedding. Boundary layer is laminar but vortex street is fully turbulent in the range of $300 < Re < 3x10^5$. This flow regime is often called the subcritical flow regime. The drag is entirely due to pressure and the drag coefficient is constant with a value of approximately 1 and at the range of $10^3 < Re < 10^5$.

v. The Reynolds number in the range of $3x10^5 < Re < 3x10^6$, laminar boundary layer becomes turbulent and the separation point moves further on the rear of the body due to this reason a sudden drop occurs in the drag coefficient. The wake is narrower and vortex street is disappear. After this sudden reduction, an increase in drag coefficient exists at higher Reynolds numbers as seen by Figure 1.2. This can be explained by the increase in frictional drag, i.e. the fluid contacts with larger surface area when the separation angle gets larger values such as 140^o.

vi. Vortex street is re-establishment, the boundary layer is fully turbulent and wake is thinner at the Reynolds number $Re > 3x10^6$.

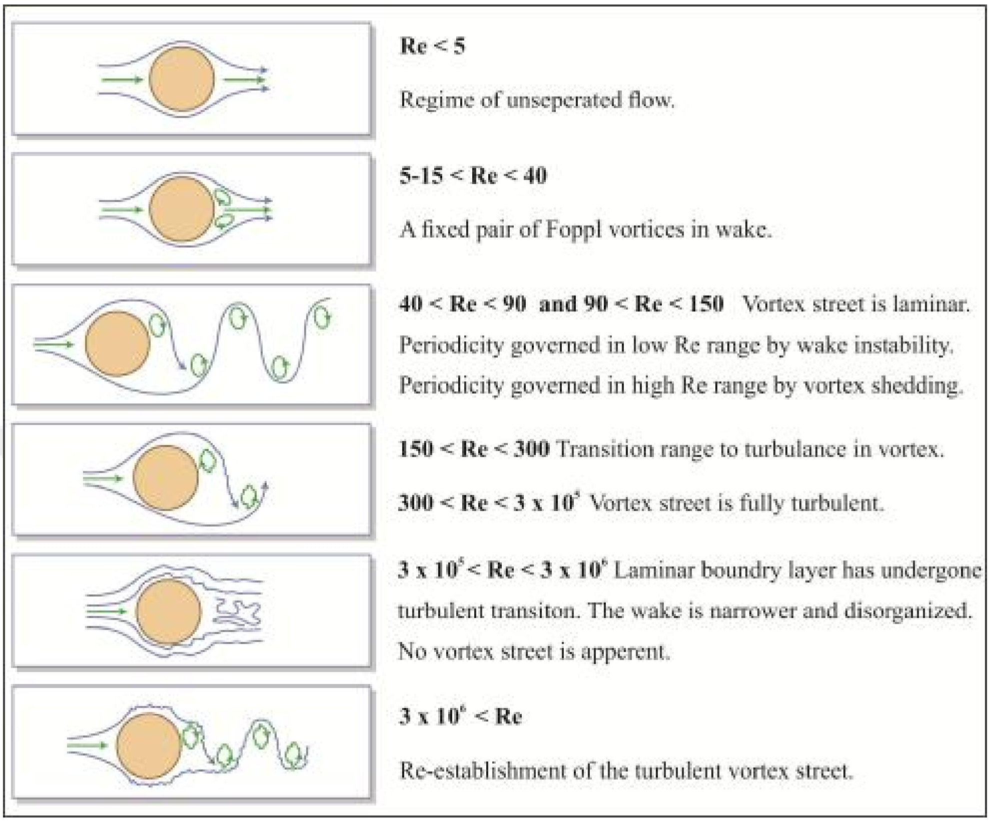

Figure 1.1. Flow regimes of circular cylinder depending on the Reynolds number (Lienhard, 1966 and Figure by MIT OCW.).

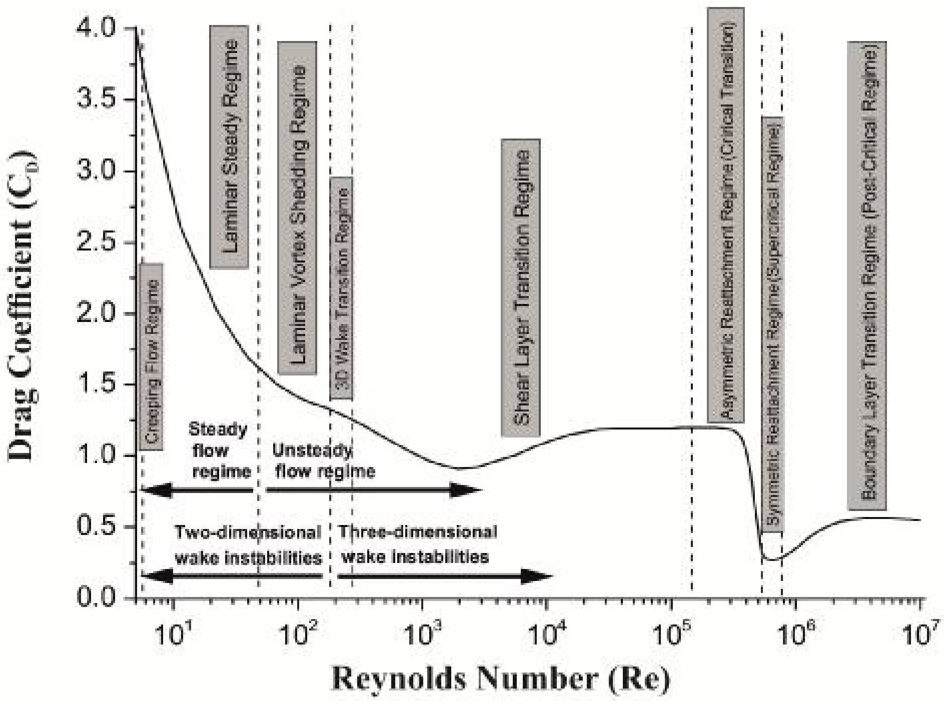

Figure 1.2. Variation of drag coefficient, C_D, with respect to Reynolds number, Re and possible demarcations of flow patterns (Firat, 2015).

1.1.1. Vortex Induced Vibration

Vortex shedding is an unsteady flow that takes place at moderate high Reynolds number. In this flow, the vortices occur at behind of the cylinder and detach periodically either side of the cylinder. The frequency of vortex shedding is related to the non-dimensional Strouhal number. The definition of Strouhal number can be given as $St = f\, D / U_\infty$ (f is the frequency of vortex shedding, D is the diameter of cylinder and U_∞ is the free stream velocity). The Strouhal number has nearly constant at a value of 0.2 for the subcritical flow regime as shown Figure 1.3.

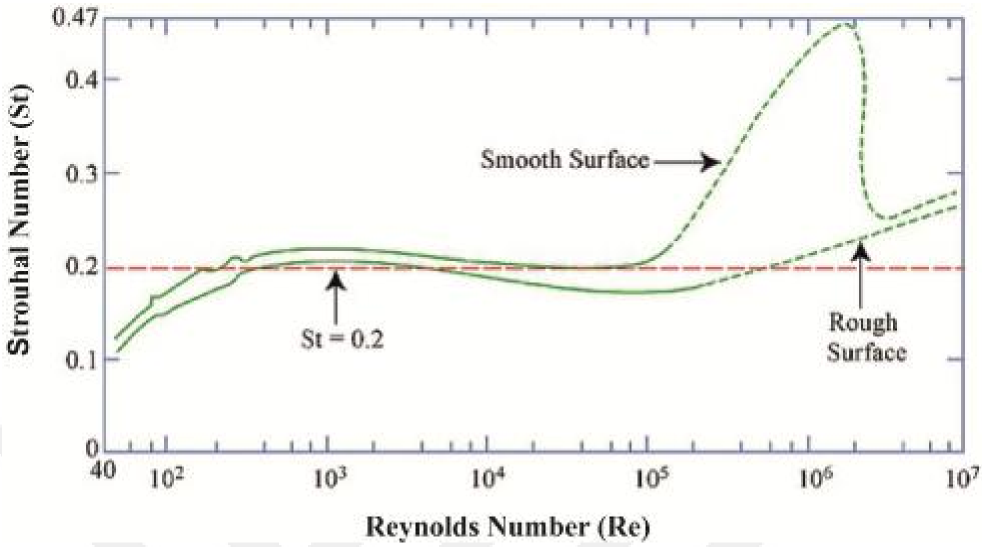

Figure 1.3. Relationship between Strouhal number, St, and Reynolds number, Re for circular cylinders (http://kopootus.jimdo.com/2012/06/27/strouhal-number-vs-reynolds-number-graph).

The vortices exert a fluctuating reaction forces on the cylinder both in direction perpendicular to flow and in the direction of flow, thus vibration occurs on the cylinder. The frequency of vortex shedding is the same as vibrating frequency of the cylinder induced by the flow and this vibration causes acoustic noise. The component of this force, perpendicular to flow direction (the lift direction) has a frequency equal to the vortex shedding frequency, while that in the direction of flow (the drag direction) has a frequency equal to two times of the vortex shedding frequency. When the vortex shedding frequency is close or equal to natural frequency of vibrating of the cylinder, the phenomenon of lock-in occurs which can also be defined as the local synchronization between the vortex shedding frequency and vibrating frequency of the cylinder. Lock-in can occur in either the lift or the drag direction and both have been observed in the nature and many engineering systems such as bridges, stacks, chimneys, transmission lines, aircraft control surfaces, offshore structures, heat exchangers, marine cables, drilling and production risers in petroleum production, tethered structures, buoyancy and spar hulls, pipelines, cable-laying. As a result of phenomenon of lock-in, structure can be destroyed and financial loses can happen. The collapse of Tacoma Narrows Bridge is a well-known example for lock-in phenomenon.

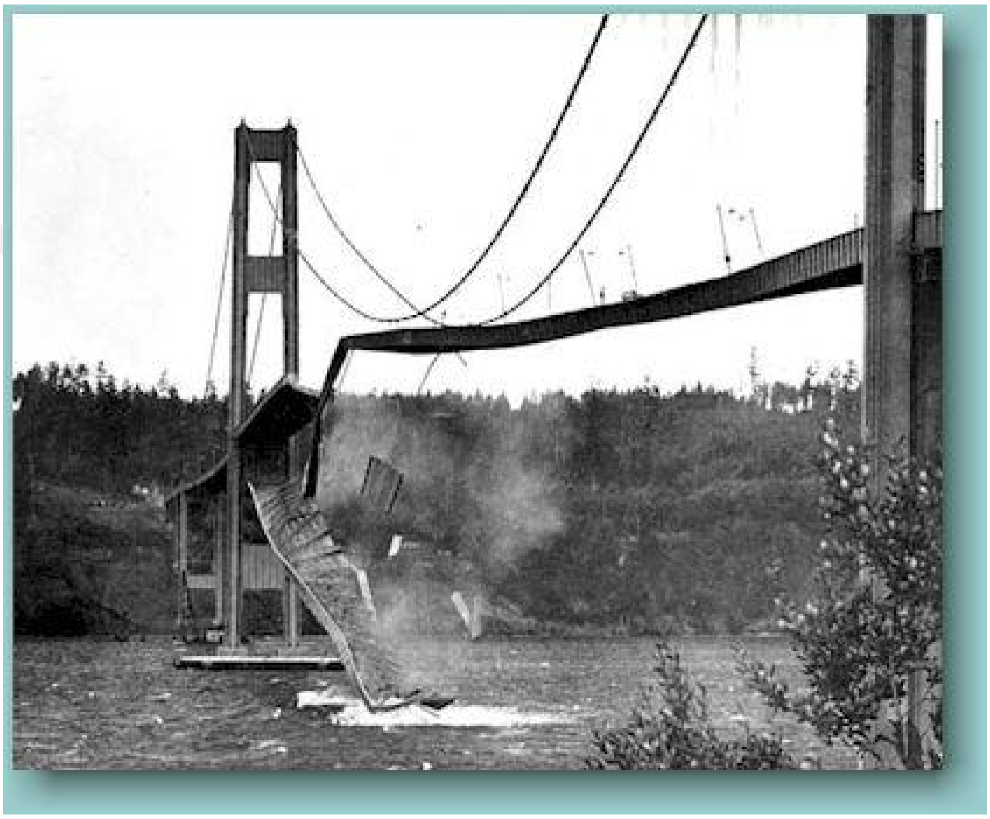

Figure 1.4. The collapse of Tacoma Narrows Bridge because of vortex lock-in (http://www.lib.washington.edu/specialcollections/collections/exhibits/tnb)

1.2. Flow Control around a Cylinder

The aim of flow control is to obtain some desired objectives such as drag or lift reduction, mixing augmentation, heat transfer enhancement, suppression of vortex induced vibration and flow-induced noise suppression etc. Therefore, the flow control may be applied to delay/advance transition, to suppress/enhance turbulence, or to prevent/promote separation depends on desired objectives. The resulting of flow over a cylinder may be the vortex induced vibration, the acoustic noise, the lock-in phenomenon and increasing lift and drag fluctuations, due to aforementioned reasons in the previous section. In order to avoid or minimize this results, the flow control techniques have been studied since discovery of the boundary layer by Prandtl (1945). The flow control techniques bases on the principle of modification of the geometry or the wake flow in order to change the behaviors of the boundary layer or free-shear layers. The flow control techniques can be divided into two categories name as active and passive flow control. The active flow controls need to external energy whereas the passive flow controls. Therefore the passive flow control techniques are more applicable than the active flow control techniques. A comprehensive study on the classification of the flow control techniques was performed by Gad-el-Hak (2000).

1.2.1. Passive Flow Control

The passive flow control techniques are widely applied since they have same advantages of being easier to implement, less expensive in cost and more stable. Zdravkovich (1981) classified the passive flow control techniques in to three categories in accordance with phenomenological mechanism of the vortex shedding as surface protrusions, shrouds and near-wake stabilizers. He also was performed another classification in accordance with direction of flow as omnidirectional and unidirectional. The omnidirectional mean is effective irrespective of the direction of flow, while the unidirectional mean is effective only direction of flow.

1.2.1.1 Surface Protrusion

The surface protrusions affect separation lines and/or separated shear layers. The helical protrusions have been broadly used in the application of offshore engineering and industrial chimneys as shown figure 1.5. The helical protrusions are omnidirectional. Although the helical protrusions are considerably effective on the suppression of the vortex induced vibration, they cause increasing of the mean drag. The helical protrusions are named as cross-section of protrusion. While helical protrusions with rectangular cross section are name as helical strakes, helical protrusions with cylindrical cross section (wire) are named as helical wires. In addition, the surface protrusions have been applied for the flow control such as fin wire, studs and bump. An illustrative sketches are presented in figure 1.6

Figure 1.5. A spar with helical strakes (http://www3.imperial.ac.uk /vortexflows/research/ fluidstruct/vivofrigidstructures).

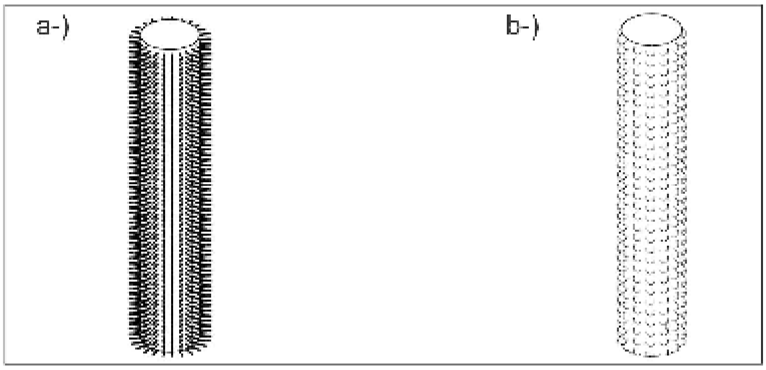

Figure 1.6. Schematic representation of surface protrusions; a) fin, b) bump

1.2.1.2 Shrouds

The shrouds affect the entrainment layers and thus help minimize the vortex shedding forces. The fairings have been used commonly as shroud in offshore, vessel and underwater retrofit operations. The fairings provide unrivaled protection against the vortex induced vibration and also they significantly reduce the mean drag. The fairings can be omnidirectional or unidirectional depending on design. An example of fairing application is presented in Figure 1.7. Introducing a perforated shroud or axial sluts are another way to attenuate the vortex shedding. The perforated shrouds have been applied with circular or rectangular holes. Typically, Figure 1.8 shows the perforated cylinder and the axial slut mounted on a cylindrical body. It consists of a relatively thin metal cylinder that is held off the main cylinder by struts. The main advantage of the perforated shroud (with the circular holes) is that it contributes reducing the drag.

Figure 1.7. An application of faring on the pipeline (http://i.imgur.com/AcKilqY.jpg).

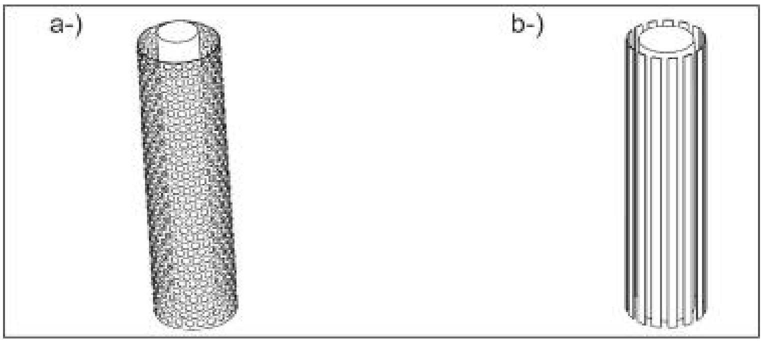

Figure 1.8. Schematic representation of shrouds; a) perforated cylinder, b) axial sluts

1.2.1.3 Near-wake Stabilizers

Near-wake stabilizers prevent the entrainment layers and thus reduce the interaction of two opposite shear layers. A well-known wake stabilizer is splitter plate. The splitter plate provides an important change in the flow structure downstream of the cylinder. The vortex shedding downstream of a circular cylinder completely disappears and the mean drag is significantly reduced. Additionally, elucidator examples can be given for near-wake stabilizers such as guiding vanes, small control rod, base bleed, slits cut across the cylinder etc. Schematic representation of near-wake stabilizers to the circular cylinder are shown in figure 1.9.

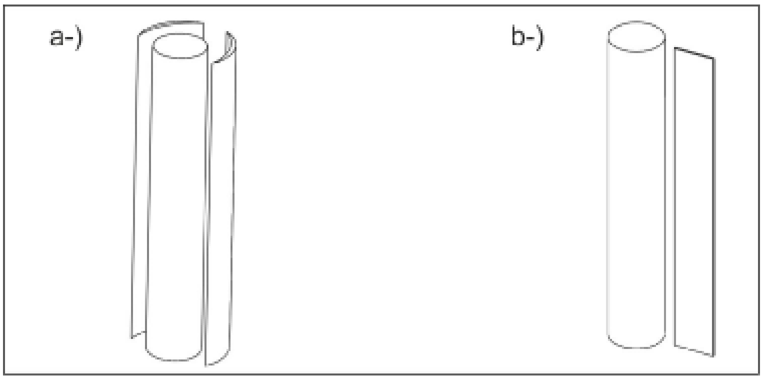

Figure 1.9. Schematic representation of near-wake stabilizers; a) guiding plates, b) splitter plate

1.2.2. Active Flow Control

Active flow control techniques, applying some sorts of energy into the flow, have been developed in order to obtain a beneficial changes on the flow field. The main advantage of the active flow controls can be applied or not depending on the changes flow condition. The active control techniques can be categorized into groups as predetermined or interactive methods. The principle of predetermined method bases on the applying steady or unsteady energy without consideration for the state of the flow field. On the other hand, the principle of interactive methods base on the continuously adjusting of the power input to the actuator depending some form of measurement element. For the interactive control, the control loop can be either a feedforward or feedback loop. The sensor is located upstream of the actuator in the feedforward control loop. For this reason, the parameters of measured flow field and the controlled flow field will change as the flow structures come over stationary sensors and actuators. Some illustrative examples can be given for the active control techniques such as feedback control, electro-magnetic control, rotating cylinder, wake heating, suction and blowing. The active flow controls lie outside the scope of this study and more details on the active flow controls can be got studies of Gad-el Hak (2000). Schematic representation of some active flow controls to the circular cylinder are shown in figure 1.10.

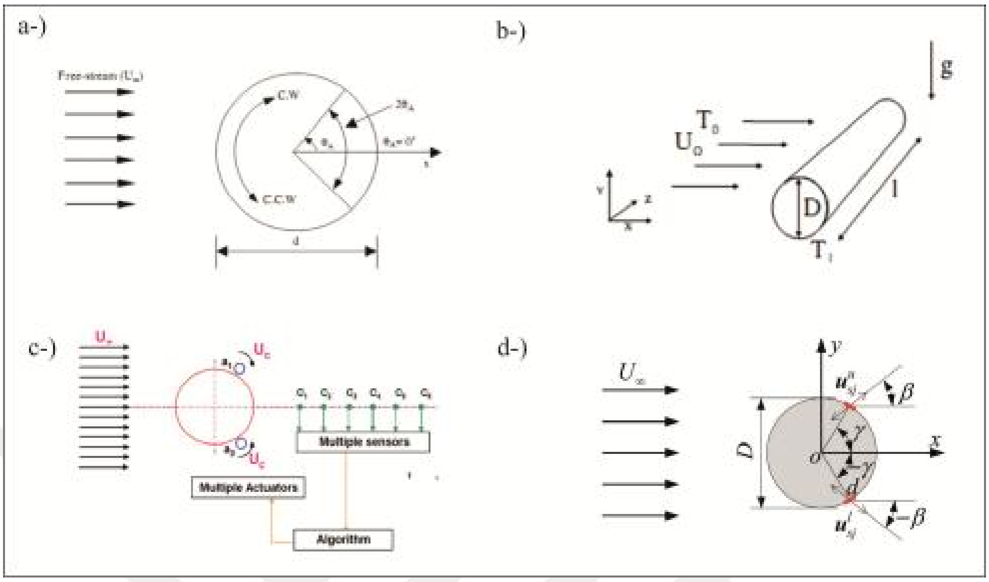

Figure 1.10. Schematic representation of some active flow controls to the circular cylinder; a) rotary oscillations of cylinder (Lee et al., 2006), b) wake heating (Kieft et al., 2007), c) the close-loop feedback control (Muddada and Patnaik (2009), d) synthetic jet (Wang et al.,2015)

1.3. Present Study

The shrouds have been used in order to suppress the vortex shedding downstream of the cylinder such as permeable cylinder (Ozkan et. al 2012, Gozmen et. al. 2014), drop-shaped mesh (Oruc 2012, Oruc et. al. 2016), perforated semi-circular fairing (Durhasan et. al. 2016). Although aforementioned studies have been carried out, the flow structure in the gap between the cylinder and the perforated cylinder has not been extensively studied so far. In this study, it is aimed to investigate the effect of the splitter plate and the perforated cylinder combination on the flow control and the drag coefficient of cylinder in deep water. The perforated cylinder, constructed from perforated steel sheet which has 1 mm thickness. The PIV measurement technique was conducted to obtain velocity vector field and force measurement was performed in the air tunnel in order to calculate the drag and the lift coefficient.

2. PRELIMINARY WORK

2.1. Flow around a Cylinder

Roshko (1954) defined flow regimes predicated on measurement of velocity fluctuation, spectra and frequency for different Reynolds numbers. Gerrard (1966) introduced the formation region of the vortices as seen Figure 2.1. He discussed the physical basis for two simultaneous characteristic lengths of the shedding process.

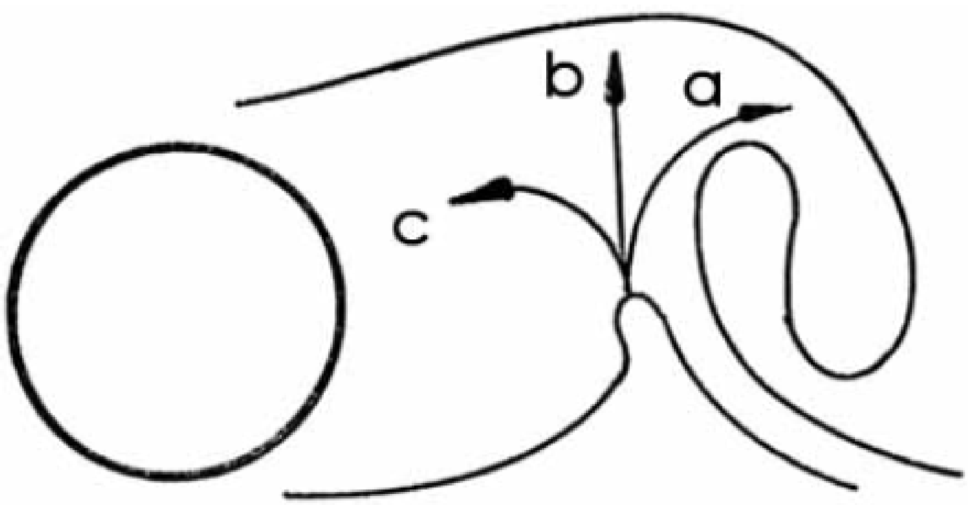

Figure 2.1. Mechanism of vortex formation by Gerrard (1966). a, b – fluid entrainment c – reverse flow

Son and Hanratty (1969) conducted to experimental study in order to measurement velocity gradients at the surface of the cylinder for Re=5x10^3 to 10^5. They noted that flow separation angle of the cylinder increases with the increasing Reynolds number.

Lin and Rockwell (1995) investigated flow structures around cylinder quantitatively using the film based particle image velocimetry technique at three values of Re = 10^3, 5×10^3 and 10^4. They found that representations of velocity, vorticity and streamlines indicated a decrease in the vortex formation length with increasing Reynolds number.

A review on the wake formation mechanics of the cylinder and the associated hydrodynamic forces for wide range Reynolds number was presented by Marris (1964). Similar study on the flow regimes and vortex frequency of cylinder was performed by Linhard (1966). Another comprehensive review was performed by Bearman (2011) on the circular cylinder wakes and vortex-induced vibrations.

Other reviews including vortex shedding and induced vibrations are reported by Parkinson (1974), Sarpkaya (1979), Bearman (1984), Sarpkaya (2004), Gabbai and Benaroya (2005).

2.2. Flow Control Techniques

Flow control researches have been performed since Prandtl (1904) discovered the boundary layer. Pioneering work was performed by Schubauer and Skramstad (1947). They used steady-state tools and mechanisms for flow control. Some of important scientists such as Bearman (1984, 2011), Sarpkaya (2004) and Williamson and Govardhan (2004) overemphasized importance of vortex shedding suppression downstream of a 2-D bluff body such as circular cylinder. A detailed review and analysis were performed by Lachman (1961) and Gad-el Hak (2000). More recently, similar reviews were performed by Choi et al. (2008), Kumar et al. (2008) and Rashidi et. al. (2016). Choi et al. (2008) summarized both active and passive control techniques in his review. He, also, discussed the effect of Reynolds-number, the lowest possible drag by control, and control efficiency. A similar study was carried out by Oruc (2017) on the passive and active flow control strategies for bluff body.

2.2.1. Passive flow control

A comprehensive review on the passive flow control was presented by Zdravkovich (1981). He classified the passive flow control techniques in to three categories according to phenomenological mechanism of vortex shedding as surface protrusions, shrouds and near-wake stabilizers. A review of drag reduction technique and surface modification methods were performed by Bandyopadhyay (1986). Moreover, many studies have been performed about the effects of surface modifications on turbulent boundary layers. Another familiar review by Kumar et al. (2008) mentioned only passive control methods. The review indicates that patented passive control techniques are used for practical applications such as marine deep water environments.

2.2.1.1. Surface Protrusion

Ahmed and Bays-Muchmore (1992) experimentally investigated flow around the wavy cylinder. They pointed out that despite of symmetrical geometry, asymmetrical flow structure is occurred. Their results also showed that the sectional drag coefficients at the geometric nodes are greater than at the geometric saddle.

Nebres and Batill (1993) was conducted experimental study in wind tunnel in order to investigate the effect of the single perturbation on the flow characteristics of circular cylinder. They found that Strouhal number is affected significantly by perturbation angular position, perturbation size and Reynolds number.

Lee and Kim (1997) conducted to experimental study in order to reveal the f1ow characteristics of the downstream of a circular cylinder with helically wrapped three small wires with various pitches. They indicated that the surface protrusions remarkably affected the wake formation of the cylinder. The vortex formation region elongated and the vortex shedding frequency and wake width elongated compared to the bare cylinder.

Owen et al. (2001) experimentally investigated that the effect of simple geometry modification of a circular cylinder on the drag and vortex-induced vibration reduction. They achieved vortex shedding suppression and drag reductions up to 47% for the body with a sinuous axis. They also noted that the cylinder with bumps decreased drag and vortex shedding suppression up to 25% compared to the circular cylinder case.

Bearman and Brankovic (2004) investigated the vortex-induced vibration of a circular cylinder and using surface protrusion devices: strakes and bumps at the Reynolds number within the range of 10^3 to 10^4. They observed that the regular vortex shedding in the wakes of fixed cylinders with strakes or bumps appears little or no evidence. Although the amplitudes of vibration were found, they are less than plain cylinder.

Lim and Lee (2004) show that using of O-rings reduce drag force acting on the cylinder. They were carried out experiments for various combinations of pitch interval at Reynolds numbers in the range $\boldsymbol{Re} = 78\times10^2 - 120\times10^3$. It is observed that the maximum drag reduction of about 9% compared with the smooth cylinder was obtained at $Re = 12\times10^4$, the cylinder fitted with O-rings of $\boldsymbol{d} = 0.0167\boldsymbol{D}$ in a pitch interval of $0.165D$. Although the vortex shedding frequencies of the O-ring cylinders are close to that of the smooth cylinder up to a Reynolds number of 32×10^3, the shedding frequency increases and evidence of vortex shedding almost disappears at high Reynolds numbers.

Lam et al. (2004) carried out and experimental investigation to measure the velocity profiles of the wake downstream of a sinusoidal cylinder in the range of $Re=3\times10^3–9\times10^3$ using a Laser Doppler Velocimetry (LDV) system. They concluded that the long vortex formation length of wavy cylinder should causes the drag reduction and suppression of vortex induced vibration.

Nakamura and Igarashi (2008) studied reduction of the drag and fluctuating forces of the cylinder with attaching cylindrical rings along the span of a cylinder at an interval of several diameters at Reynolds numbers in the range of $Re = 3\times10^3$ and 38×10^3. They reported that the drag force of the cylinder with attaching cylindrical ring was lower than for the 2D cylinder, even though the projected area of the cylinder with attaching cylindrical ring was higher than the 2D cylinder.

They showed that maximum reduction of drag force was obtained by 15% for D/d = 1.3, W/d = 1.0, and P/d = 6 at Re=30×10^3, where D is the ring diameter, W is the spanwise width of the ring, and P is the spanwise pitch of the ring.

Zou and Lin (2009) carried out numerical investigation of cross-flow around a sinusoidal wavy cylinder at Re = 3×10^3 by introducing the load cell measurement for the validation test. In the study, they introduced the load cell measurement for the validation test and they compared the mean flow field and the near wake flow structures of the sinusoidal wavy cylinder with the circular cylinder at the same Reynolds number. They found that the mean drag coefficient for the wavy cylinder is reduced due to the formation of a longer wake vortex generated by the wavy cylinder. The fluctuating lift coefficient of the wavy cylinder is also greatly reduced. From that study, they also showed that such free shear layers only roll up into mature vortices at further downstream position and significantly modify the near wake structures and the pressure distributions around the wavy cylinder.

Kiu et al. (2011) conducted the experimental investigation in order to reveal the effects of uniform surface roughness on vortex-induced vibration of cylinders representative of offshore spar platforms at subcritical Reynolds numbers. They indicated that the roughness of cylinder is increased the Strouhal number, although drag coefficient reduced when compare with the smooth cylinder.

Gao et al. (2015) examined the effects of surface roughness on the vortex induced vibration (VIV) response of a flexible cylinder. Their results indicated that the surface roughness remarkably effects on the VIV response and displacement response decreases and the vortex-shedding frequency increases with the increasing surface roughness. It was also found that lock-in region of rough cylinder is narrower than a smooth cylinder.

Recently, flow around the smooth, grooved and dimpled cylinders were studied by Zhou et al. (2015) in order to compare flow structure of those cylinders.

Their results indicate that the strength of vertex shedding of the grooved and the dimpled cylinders become weaker and also drag of those cylinders is lower than the smooth cylinder.

Wang et al. (2015) employed a water drop-shaped fairing for controlling the wake and suppressing Karman vortex street formation downstream of a circular cylinder using CFD technique. The fairing elements evidently lowered the drag and lift forces as well as influenced the frequency of vortex shedding compared to the bare cylinder.

Ozkan et al. (2017) researched the effect of attached permeable plates on the suppression of the vortex shedding from a circular cylinder. They indicated that using of a permeable plate remarkably suppressed the vortex shedding downstream of the circular cylinder for the porosity value of β=0.4 and 0.5 with the plate angle in the range of $35^o \leq \theta \leq 90^o$.

2.2.1.2. Shrouds

First experimental study on the using of shroud cylinder as passive flow control devices was performed by Price (1956). He examined various porous shrouds in order to investigate their effects on suppression of the vortex- excited vibrations. He showed that the vortex-excited vibrations is suppressed by shrouded cylinders due to the delay in forming the normal Karman Street.

Zdravkovic and Soutworth (1973) investigated that the effect of shroud eccentricity on suppression of flow induced vibrations. Their results revealed that an eccentricity in any direction and of any magnitude always reduced the amplitude of vibration subcritical flow region in comparison with that of a concentrically shrouded cylinder.

Every et al. (1982) reviewed the practical aspects of vortex excited structural vibrations in a marine environment with particular emphasis on methods of their suppression. In a part of their study, they focused on the effect of shrouds on the flow control, reported a comprehensive literature and stated that shrouds with the optimum dimension gave a 50% reduction in oscillations of a plain study on suppressing flow induced vibrations (Every and King, 1979).

Molin (1993) showed computational outcomes of how vortex induced vibrations being alleviated by using shroud through various range of cylinder and shroud couples.

Boorsma et al. (2010) illustrated that perforated fairings could reduce noise of landing gears depends on the location of perforation and the porosity of fairing.

Zhao and Cheng (2010) performed a numerical research in order to investigate the effect of porous media on the reduction of lift coefficient of circular cylinder. They observed that the amount of reduction widely depends on the Reynolds number, the permeability.

Ozkan et al. (2012) have brought out permeable cylinders with different porosities to control the flow structure of wake region of various circular cylinders owing to different diameter ratios. It was stated that shear layers on each side of the blunt body being lengthened through streamwise direction as a proof of attenuation of organized vortex street in their experiments.

Ruck et al. (2012) investigated the effect of porous coating on the drag resistance of cylinder. They observed that the coating only on leeward side can reduce the drag forces. This can be conceived as a combination of a smooth surface on the windward (lowest friction) and permeable wall layer on the leeward side.

Gozmen et al. (2014) performed experimental study to flow control downstream of a circular cylinder using permeable cylinder in deep water. Their PIV results show that the permeable cylinder remarkably suppresses the vortex shedding downstream the cylinder with increasing porosity.

Flow past a semi-circular cylinder was investigated numerically by Mimeau et al. (2014). They indicated that introducing porous layers only at the top and bottom of the solid body permits to better manipulate the vortex shedding and to achieve relevant control performances.

Oruc et al. (2016) investigated the effect of a drop shaped mesh on the suppress Karman vortex street formation in the near wake of the cylinder. It was observed that large scale vortical flow structure was not developed and the peak values of both turbulent kinetic energy and Reynolds shear stress distributions were strongly attenuated.

Durhasan et al. (2016) experimentally investigated the effect of the perforated semi-circular fairing on the vortex street suppression by employing PIV technique in the shallow water. They observed that the suppression of vortex street in the downstream is achieved for porosity of β= 0.6 and arc angle α=180^{o}.

2.2.1.3. Near-wake Stabilizers

Roshko (1954) was notably one of the first to report periodic vortex formation suppression using a circular cylinder connected with a splitter plate for a Reynolds number of 1.45×10^{4}. He also showed that, by positioning this splitter plate at different fixed distances in the fully developed cylinder-wake, the Strouhal number St diminishes as the distance between the cylinder and the plate increases up to a limit position (G »2.7D). He also observed that a splitter plate of chord 5D, attached to the cylinder, results in suppression of shedding. A plate of chord 1D does not inhibit formation of vortices but changes the shedding frequency slightly.

Roshko (1955) observed flow changes at Re=1.45×10^{4} when splitter plates were inserted behind a cylinder. When the plate was attached on the cylinder base and the length of the splitter plate, l was larger than 5D, the vortex shedding disappeared, and thus drag was significantly reduced. On the other hand, he also observed flow changes as the plate of l=d moved downstream. When the splitter plate was located downstream less than 4d, the Strouhal number, St decreased and the base pressure increased as the splitter plate moved downstream. However, when the splitter plate was located farther downstream, the flow field did not show much difference from the natural vortex shedding.

Using of base bleed substantially affected the formation process of vortices from a streamlined body with a blunt trailing edge was demonstrated by Wood (1964, 1967) and Bearman (1967).

Bearman (1965) investigated the flow downstream of a two-dimensional model with a blunt trailing edge and fitted with splitter plates at Reynolds numbers between 14×10^3 and 256×10^3. He measured the base pressure and shedding frequency and showed that the existence of a splitter plate increases the base pressure significantly (thereby reducing the pressure drag), even for very short plate length. These studies suggest that the effect of the splitter plate and base bleed is to delay the upper and lower separated shear layers interacting with each other and hence they increase the formation length (position at which the vortices are fully formed or, in a time-average sense, the length of the mean recirculation region). As a result, vortex shedding disappears for a connected splitter plate length L_{sp} equal to 2D.

Another approach, which is equivalent to the aforementioned concept of base bleed, is self-bleed through a slit cut along the entire span of the cylinder, as described by Igarashi (1978), who demonstrated that the region of vortex formation was displaced significantly downstream, relative to the case of a plain cylinder.

Wong (1985) pursued a more advanced approach involving self-injection at two locations near the base of the cylinder, whereby the injection flow was through an annulus opened at the forward stagnation point. This technique was applied to an elastically mounted cylinder, and it was demonstrated that vibrations could be suppressed completely when the effective injection rate was very small. In all of these investigations involving base bleed, with some exceptions, relatively little information is available on the quantitative flow structure associated with the concept of base bleed.

Unal and Rockwell (1987) divided the wake region into two separate regions: the pre-vortex formation region and the post-vortex formation region. They found that the pressure on the splitter plate was suddenly changed when the plate moved from the pre-vortex formation regime to the post-vortex formation regime.

Unal and Rockwell (1988) performed a similar study with a plate that is detached from the cylinder. They found that by placing the plate appropriately, compared to a cylinder with no control, it is possible to obtain more than double the vortex formation length. For low the Re the vortex shedding is completely eliminated while for the higher Re the large scale shedding is suppressed but the shear layer instability remains.

An experimental investigation was carried out by Mansingh and Oosthuizen, (1990) to study the effect of a splitter plate on the two-dimensional wake of a bluff body with fixed separation points. This experimental study has shown that the characteristics of the wake downstream of a bluff body with fixed separation points can be considerably altered by placing a splitter plate on the wake centerline downstream of the bluff body. The effect of splitter plates on the wake flow characteristics of a rectangular cylinder with a splitter plate shows a relatively small change in the Reynolds number.

Cimbala and Garg (1991) investigated the effect of the attached splitter plate on the flow characteristics downstream of a fixed cylinder and a freely rotating cylinder, respectively. For the case of a freely rotating cylinder, the flow field with the plate of $L>2D$ was similar to that of the fixed cylinder with an attached plate. However, when $L<2D$, the flow field was similar to that without the splitter plate. They also showed for the case of a fixed cylinder that the Strouhal number, St increased for $D<L<2D$ and it decreased as the length of the plate further increased.

Miau et al. (1993) carried out measurements of instantaneous pressure fluctuations on a trapezoidal cross-sectional cylinder. Their results indicate that the low frequency variations embedded in the vortex-shedding process can be successfully suppressed by insertion of a splitter plate whose length is twice the maximum width of the trapezoidal cylinder.

The angular motion of a freely rotatable cylinder with splitter plate has been studied numerically by Xu et al. (1993). It is found that, for subcritical the Reynolds numbers, the splitter plate aligns itself in the flow direction. With the increasing Reynolds number, a symmetry breaking bifurcation appears and the splitter plate migrates to a stable off-axis position.

Roshko (1993) controlled the flow around a circular cylinder by attaching a splitter plate downstream of the cylinder and investigated the suppression of vortex shedding. When the gap between the cylinder and splitter plate was large, the effect of the splitter plate became strong. The parameter that had the greatest effect on the vortex shedding was the gap width rather than the length of splitter plate.

Lin and Wu (1994) conducted a numerical study for the Re_D =100 flow to see the effect of a splitter plate. They found that a splitter plate of length 2D attached to the cylinder is sufficient to completely suppress vortex shedding. It was also found that a splitter plate whose upstream edge is located at more than 2.5D from the cylinder is ineffective of suppressing vortex shedding.

Vortex shedding from bluff bodies with splitter plates was experimentally investigated by Nakamura, 1996. It was shown that vortex shedding from bluff bodies with extended splitter plates is characterized by the impinging shear layer instability, where the Strouhal number, St in terms of splitter plate length increases in stepwise direction with increasing splitter plate length.

Recently, Kwon and Choi (1996) investigated the effect of the splitter plate on the laminar vortex shedding downstream of a circular cylinder at Reynolds numbers of 80-160. They showed that for $Re \geq 120$ the shedding frequency changed similarly as just described, whereas for $Re \leq 100$ the shedding frequency monotonically decreased as the plate length increased. They attributed the increased shedding frequency at $L > D$ in the case of $Re \geq 120$ to a generation of the secondary vortex at the tip of the splitter plate. This secondary vortex near the tip of the splitter plate may also be a strong source of the flow-induced noise.

Ozono (1999) studied the effect of a plate of length 1D kept at various locations, including those away from the wake centerline, downstream of the cylinder for $6.7\times10^3 < Re < 2.5\times10^4$. Beyond a certain critical gap between the plate and the cylinder, for a certain range, the Strouhal number, St exceeds the natural one. This is because of a flow mode in which the shear layer separated from the cylinder is forced to interact with the splitter plate.

A numerical work by Mittal and Raghuvanshi (2001) was performed to study the influence of putting of a control cylinder in the near wake of the main cylinder for flows at low Reynolds numbers in the range of $60 \le Re \le 100$. Results were compared with those from flow past a single cylinder at similar Reynolds numbers. It has been observed that the suitable placement of the control cylinder resulted with a nearly complete suppression of the vortex shedding downstream of the main cylinder.

Akıllı et al. (2005) investigated the effect of splitter plate on the suppression of vortex shedding in shallow water using the Particle Image Velocimetry (PIV) technique. Splitter plates with a length of 50 mm, which is equal to the diameter of the cylinder (D), were used during the experiments. Gap distance between the base of the cylinder and the leading edge of the splitter plate ranged from 0 to 2D. Velocity vector field and corresponding vorticity contours and streamline topology and Reynolds stress concentrations were used to explain the characteristics of the flow. The splitter plates having different thicknesses presented the same influence on the flow characteristics. The splitter plate has a substantial effect on suppression of the vortex shedding for the gap ratio between 0 and 1.75D. For this gap ratios, shear layers extend up to the trailing edge of the splitter plate preventing the entrainment of the free-stream flow into the base region. For G/D=1.75, the normalized Reynolds stress has a peak value of 0.0158 which is approximately 8.5 times smaller than the concentrations occurring for a bare cylinder. After passing the splitter plate, the flow starts to oscillate with smaller frequency compared to the natural frequency of the bare cylinder. When the splitter plate was located at 2D location, no effect of the splitter plate was observed.

Kuo et al. (2007) numerically studied the passive wake control downstream of a circular cylinder in uniform flow for Re ranging from 80 to 300. They used two small control cylinders, with diameter ratio d/D = 1/8, placed at x/D = 0.5 and y/D = ±6 and Reynolds numbers is varied from 80 to 300. Their mechanism, which can significantly reduce the fluctuating lift force F_L and the form drag force F_D on the main cylinder, is explored without completely suppressing the vortex street for Re = 80–300. They reported that, by this control, the vortex street downstream of the main cylinder is still maintained but the fluctuating lift force F_L and the form drag force F_D on the main cylinder decreases monotonously with increasing the Reynolds number.

Passive flow control using two-dimensional hydrofoils to reduce vortex-induced vibrations (VIV) and drag force F_D on a cylinder of circular cross-section was studied by Galvao et al. (2008). They tested the hypothesis that by using foils to bend the streamlines around the cylinder, and hence forcing the flow to approach potential flow-like patterns VIV and drag will be reduced. They showed that properly positioned foils can significantly alter the flow around a circular cylinder to eliminate VIV and reduce drag.

Akıllı et al. (2008) investigated experimentally passive control of vortex shedding downstream of a circular cylinder by splitter plates of various lengths attached on the cylinder base in shallow water flow ($Re=63\times10^2$). At this study, the length of the splitter plate was varied from L/D=0.2 to L/D=2.4 in order to see the effect of the splitter plate length on the flow characteristics. Instantaneous and time-averaged flow data clearly indicated that the length of the splitter plate has a substantial effect on the flow characteristics. They found the flow characteristics in the wake region of the circular cylinder sharply change up to the splitter plate length of L/D=1.0 and above this plate length, small changes occur in the flow characteristics.

Kuo and Chen (2009) revealed the wake flow structures downstream of a circular cylinder manipulated by two small control cylinders and elucidate the primary mechanism that leads to a reduction of the lift and the pressure drag on the main cylinder. They found that the fluctuating lift on the main cylinder shows a 70–80% reduction without completely suppressing the vortex street.

Shukla et al. (2009) studied the problem of a hinged-splitter plate in the wake of a circular cylinder where the splitter plate can rotate about the hinge at the base of the cylinder due to the unsteady fluid forces acting on it, and hence the communication between the two sides of the wake is not totally disrupted as in the rigid splitter plate case. They investigated that this problem in the limit where the stiffness and internal damping associated with the hinge are negligible, and the mass ratio of the splitter plate is small. It is concluded that the splitter plate oscillations increase with Reynolds numbers at low values of Re, and are found to reach a saturation amplitude level at higher Re, such as Re > 40×10^3.

Assi et al. (2009) achieved suppression of cross-flow and in-line VIV of a circular cylinder, with resulting drag coefficients C_d less than that for a fixed plain cylinder using two-dimensional control plates. He demonstrated how vortex-induced vibration can be practically eliminated by using free-to-rotate, two-dimensional control plates and further conclusion is that these devices achieve VIV suppression with drag reduction. He found the largest drag reduction to have a drag coefficient equal to about 60% of that for a plain, fixed cylinder over the Reynolds number range of the experiments, up to 30×10^3.

Baek and Karniakidis (2009) numerically investigated the hydrodynamic effect of a slit in circular cylinders with the goal of finding a geometric modification that minimizes vortex-induced vibrations (VIV) without any energy consumption. A slit parallel to the incoming flow is introduced and found to be very effective in suppressing VIV by either weakening or detuning vortex shedding. Through a series of simulations, they found the optimal size of the slit to suppress VIV at Reynolds number of 500; this size is smaller at a higher Re = 10^3.

They confirmed the effectiveness of the slit in suppressing VIV over a wide range of values of the reduced velocity. They also reported that the jet flow through a slit changes the stability in the wake of cylinder by inducing two small pockets of absolute instability at the back of the cylinder followed by bands of convectively and absolutely unstable regions.

Assi et al. (2010) studied on a pair of circular cylinders to investigate the effectiveness of pivoting parallel plates as wake-induced vibration suppressors. Measurements of amplitude of vibration and average drag are presented for a circular cylinder, free to respond in the cross-flow direction, with mass ratio of 2 and a damping level of 0.7% of critical damping. Reduced velocities were up to nearly 30, with associated Reynolds numbers up to $2.3x10^4$ and the results presented are for a center-to-center separation of cylinders of 4 diameters. They showed how vortex-induced vibration and wake-induced vibration of the downstream cylinder of a tandem pair can be practically eliminated by using free to rotate parallel plates. They also presented the results for a single splitter plate and helical strakes for comparison.

Gozmen et al. (2013) investigated the effects of splitter plates having different heights and lengths located in the downstream of the circular cylinder. The length of the splitter plate (L) was varied within the range of $0.5 \leq L/D \leq 2$ and ratio of plate height (h_p) to water height (h_w) is between 0.25 to 1.0. They obtained that flow structures changed significantly with height and length ratios of splitter plates in shallow water. The wake region downstream of the cylinder was elongated along the streamwise direction with increasing plate length and depth. The case of $h_p/h_w=0.75$ for L/D=2 was the most effective case on the control of vortex shedding. The transverse Reynolds normal stress was more effective on the attenuation of turbulent kinetic energy than the streamwise Reynolds normal stress. The peak value of transverse Reynolds normal stress was reduced to 90% of that of the bare cylinder at most.

Bao and Tao (2013) numerically investigated the wake control of a circular cylinder by dual plates symmetrically attached at the rear surface of the cylinder within the low Re number regime. The two flat plates were placed in parallel form and the angle was varied in the range θ_f=0 – 90^o. The results showed that dual plates increased drag reduction and caused stronger wake suppression at relatively shorter plate lengths. The attachment angle had a crucial effect on the control efficiency. For the range of 40^o≤ θ_f≤50^o, the free shear layers reattached on the outside surface of the control plates. So, this regime between 40^o≤ θ_f≤50^o was the most effective range associated with the maximum drag reduction.

2.2.2. Active Flow Control

Rotating cylinder was investigated numerically for low Reynolds number by Ingham (1983), Badr et al. (1990) and Ingham and Tang (1990). They indicated that the rotation delays and even inhibits the boundary-layer separation, although vortex shedding is not observed downstream of the cylinder.

Yu and Monkewitz (1990) studied the effect of temperature change in controlling the wake region by using heat input on cylinders. Their study gave useful information about the parameter range in which flow oscillations are self-excited. An other active flow control methods are electromagnetic turbulence control (EMTC). Experiments of EMTC performed by Nosenchuck et. al (1995) indicated that using a specific electromagnetic force distribution may reduce viscous drag by as much as 90%..

Hsiao and Shyu (1991) carried out experimental investigated to measure velocity and pressure field of circular cylinder under internal acoustic excitation. Their results depicted that the internal acoustic excitation causes an increase in lift and a dramatic reduction in drag.

The surface pressure distributions around a circular cylinder under internal excitation was investigated using fluidic actuators by Amitay et al. (1997). He showed that drag reduction of the circular cylinder is achievable up to 25% using that method at Re=75500.

Lorentz force was studied as an active control method by Weier et al. (1998) and Kim and Lee (2001). The effect of Lorentz force on the suppression of vortex shedding of circular cylinder and flow separation was demonstrated by Weier et al. (1998) and Kim and Lee (2001).

Delaunay and Kaiktsis (1999) performed numerical study to investigate the effects of base suction and blowing on the weak structure of the circular cylinder at Re<47. They noted that suction remarkably reduced the shedding frequency, although blowing have insignificant effect on the shedding frequency shedding at supercritical Reynolds Numbers.

He et al. (2000) studied active flow control around a circular cylinder using oscillatory rotation, blowing and suction. They applied the computational methods in order to predict optimal control strategies in reducing drag. They noted that the formation of vortex street is completely suppressed and the drag remarkably reduced up to Re=200 by using three blowing-suction slots.

An excellent review on the evolution of a synthetic jet and flow mechanisms of its interaction with a cross flow was presented by Glezer and Amitay (2002).

Li et al. (2003) studied optimal control based on adjoint formulation using suction and blowing method to investigate the effect of this method on the vortex shedding suppression of a cylinder. The results of their study showed that the vortex shedding of the cylinder is completely controlled for Reynolds number up to 110.

Chen and Aubry (2003) was carried out numerical study to develop an efficient active control algorithm for controlling downstream of a circular cylinder. They showed that the location of applying Lorentz force on the cylinder surface significantly affect the wake structure and mean drag of the cylinder.

Fujisawa and Takeda (2003) performed experimental study on flow control and the drag reduction using acoustic excitation. They noted that the wake of the cylinder is elongated to downstream direction and the drag is reduced about 30% depends on control parameter such as the slit angle, the forcing Strouhal number and the excitation amplitude.

Jukes and Choi (2009) experimentally studied to control the flow over a cylinder using pulsed DBD surface plasma. The near wake structure of the cylinder investigated by employing PIV measurement at Re=15000. They observed that the suppression of the vortex shedding can be achieved when the surface plasma localize the near separation point of the cylinder. They also noted that the lift fluctuations and drag are reduced significantly.

Muddada and Patnaik (2010) numerically studied the flow over a circular cylinder with the aid of a control algorithm using multiple-feedback sensors and actuators at the sub-critical Reynolds number. They demonstrated the effect of rotary type actuators on the flow structure downstream of the circular cylinder.

Zhang et al. (2010) performed numerical study to control the flow downstream of a cylinder employing alternative direction implicit algorithm and Fast Fourier Transform. They found that the total drag coefficient is decreased and oscillations of drag and lift are suppressed remarkably.

Feng and Wang (2010) studied on control of a flow around a circular cylinder by blowing and suction. It positioned at the mean rear stagnation point and experiments were performed in a water channel at Re=950. They noted that although the synthetic jet remarkably affect the global flow field, it is still dominated by the large -scale coherent structures.

Son et al. (2011) examined feedback control in order to suppress the vortex shedding of the circular cylinder. They found that applying P, PI and PD controls to cylinder significantly reduced the mean drag and lift fluctuations.

A numerical investigation on the flow control downstream of porous cylinder using exerting an external magnetic field was performed by Bovand et al.

(2015). They observed that the vortex shedding is suppressed significantly by the external magnetic field for small Darcy number.

3. MATERIAL AND METHOD

3.1. Experimental Model

In this study, it was aimed to investigation of flow structure and control of flow in the near wake of cylinder by splitter plate and perforated cylinder combination. A circular cylinder (inner cylinder) which are made of plexi glass material was surrounded by the perforated cylinder which is constructed from perforated steel sheet which has 1 mm thickness and diameter value of hole d=10 mm. In order to prevent the interaction of vortices generated by inner cylinder, splitter plate which has 1 mm thickness is located in the gap between cylinder and perforated cylinder. Schematic representations of experimental model is showed in Figure 3.1.

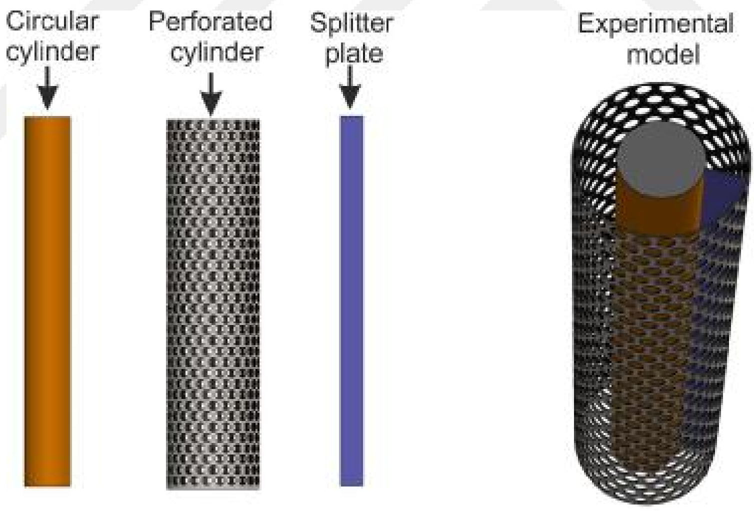

Figure 3.1. Schematic representations of experimental model.

3.1.1. Investigation Parameters

Firstly, in order to constitute reference experiments were performed for bare cylinder (D=50mm). Secondly, the effect of perforated cylinders on the flow control were investigated for three different diameter ratios, D/D_s (D/D_s=0.4, 0.5, 0.6) and five different porosities, β (β=0.3, 0.4, 0.5, 0.6 and 0.7). The porosity, β is defined as the ratio of the open gap area on the body to whole body surface area (Figure 3.2b) Diameter ratio is ratios of the diameter of the inner cylinder, D to the diameter of the perforated cylinder, D_s. Thirdly, it was aimed to control of flow in near wake of cylinder using the splitter plate and perforated cylinder. Dimensionless length of plate, L_p is defined as Lp=[(2L)/(D_s-D)]. During the experiments two different the plate lengths, L_p which are L_p=3/4 and 1 were used and also the plate was located seven different rotation angles, α which are α=120°, 130°, 140°, 150°, 160°, 170° and 180° (figure 3.2a). Moreover, for the length of plate, L_p=3/4, the splitter plate was positioned as in contact with the perforated cylinder and the cylinder (Figure 3.2c and 3.2d).

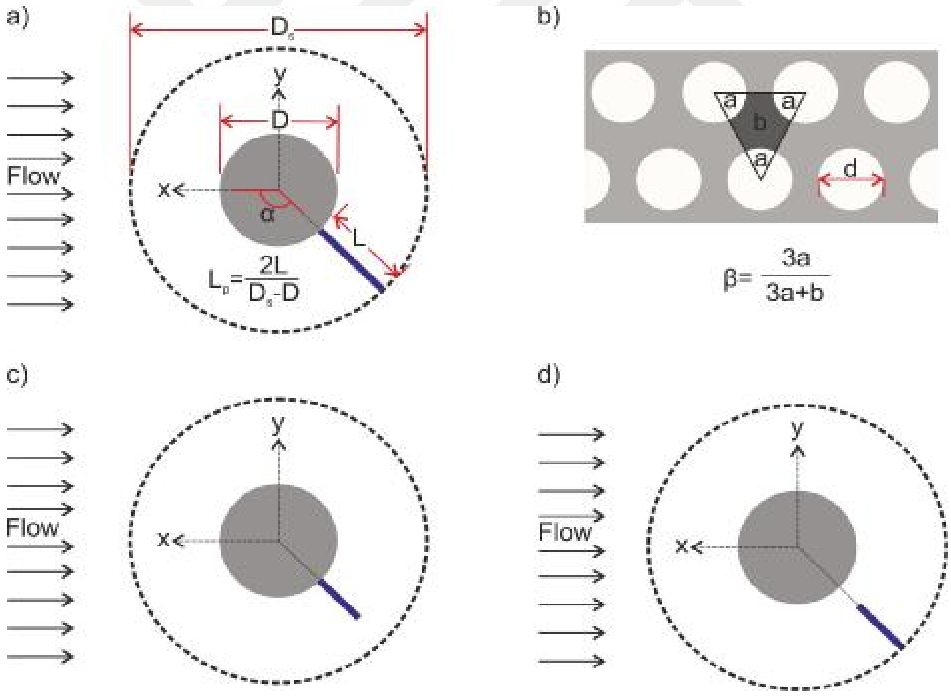

Figure 3.2. Schematic representation of using of splitter plate in annular region of perforated cylinder: a) representation plate angle, α and dimensionless plate length, L_p b) definition of porosity, β, c) the plate in contact with cylinder, d) the plate in contact with perforated cylinder.

3.2. Experimental Setup

Experiments were performed in a large-scale water channel located in the Fluid Mechanical Laboratory of the Department of Mechanical Engineering at Çukurova University. The water channel (see Figure 3.3) test section which has of 8000x1000x750 mm was constructed from a 15 mm thick transparent plexiglass sheet with upstream and downstream fiberglass reservoirs. Water flow speeds were controlled by a 15 kW centrifugal flow pump with a variable speed control unit. A flow straightener system is located at the entrance of the contraction in order to minimize the free-stream turbulence, which is expected to be less than 1%. The temperature of the Fluid Mechanics Laboratory was kept constant of 22° C throughout the experiments.

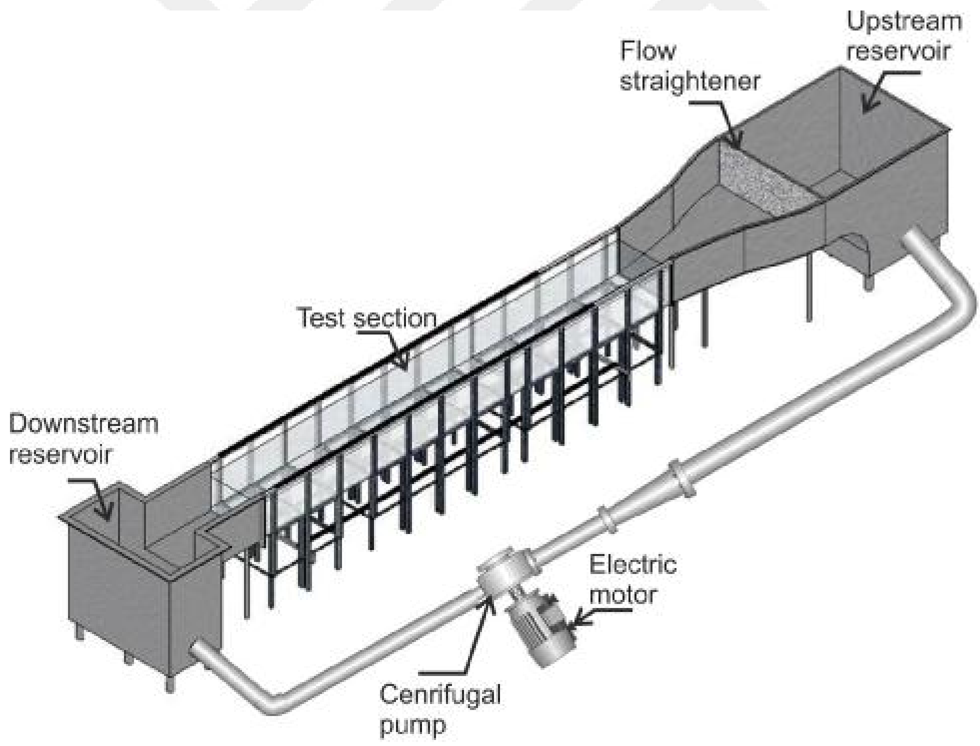

Figure 3.3. The water channel with its arrangements.

The width of the channel is large enough to avoid the effect of the side walls on the observed flow field. All experiments were carried out above a platform, having a length of 2300 mm, width of 980 mm. The height between top surface of the platform and bottom surface of the channel was adjusted 200 mm. The distance from the leading edge of the platform to the cylinder was 1800 mm to obtain fully-developed boundary layer was established during the experiments. The total depth of the water in the channel was adjusted to a 550 mm height from bottom surface of the channel. During all experiment, the water level was (H_w) maintained at the depth of 330 mm and laser sheet was located parallel to the upper surface of platform at the height of H_L=165 mm. A schematic representation of experimental setup is shown in Figure 3.5. Free-surface velocity is U_∞=100 mm/s, which corresponds to the Reynolds number of Re= 5×10^3. $\mathrm{Re} = (U_\infty D)/\nu$, based on the cylinder diameter, D. Here, ν is the kinematics viscosity, and U_∞ is the free-stream velocity.

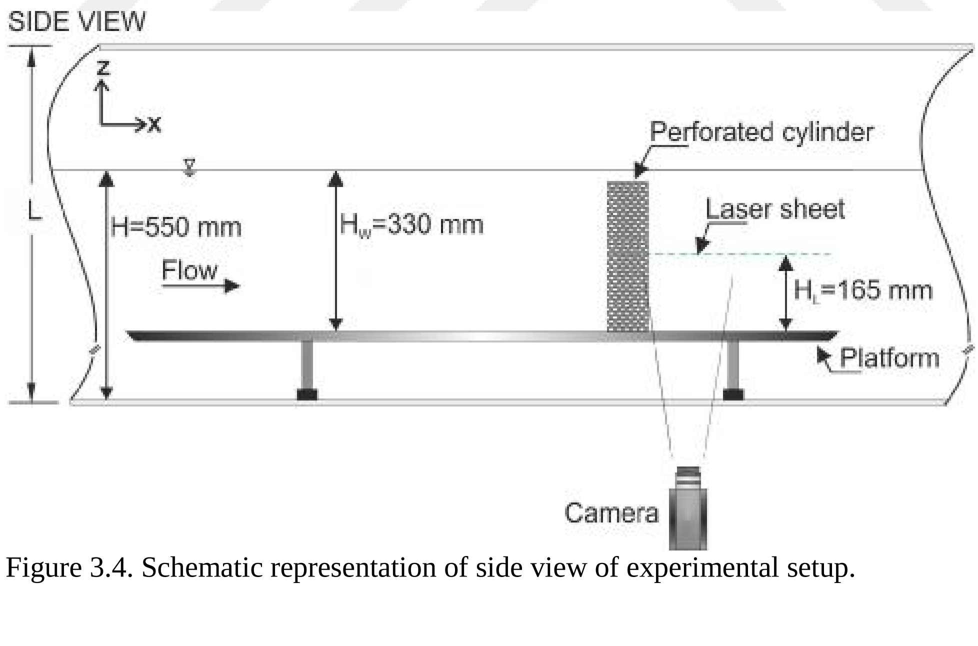

Figure 3.4. Schematic representation of side view of experimental setup.

3.3. Experimental Method

Throughout this study, three experimental systems were used in order to analyze the two dimensional flow structure for a defined flow field. One of the systems used is the flow visualization and the other is the Particle Image Velocimetry (PIV) technique. Dye flow visualization experiments were performed in order to have a direct observation of the flow structure qualitatively in the investigated flow field whereas the PIV experiments was used to measure the velocity vector field which is one of the best non- intrusive techniques within the velocity measurement systems, quantitively. Finally, force measurement was performed in order to investigate effect of the current method on the drag coefficient of cylinder.

3.3.1. Flow Visualization Technique

The Main purpose of flow visualization study was to understand the effect of important parameters which are porosity ratio, diameter ratio on the flow structure of downstream of cylinder with perforated cylinder qualitatively. The dye visualization technique aims to visualize flow by spreading some amount of Rhodamine type dye that shines under the laser light exposure in the desired flow field. The dye visualization technique offers no numerical analysis or data to use, but shows a brief demonstration of the flow that gives an idea about the flow field and the vortices. Dye must inject very small injection tube to avoid the formation of a large wake. Merzkirch (1987) reports that hypodermic needles are suitable for injecting dye into water, because of their very small outer diameters. Dye is well suited to the visualization of low-speed water flows, because it is neutrally buoyant, has good visibility and low diffusivity. Dye came from a container, which were located 75 cm above the free surface of the water channel and went through the plastic tube.

Visualization of the experimental results were recorded with a high speed SONY 80X handy cam type digital video recorder to examine the flow behaviors in detail. The video camera is used to capture the instantaneous video images of the vortex flow structures. Each experiment is recorded approximately three minutes. This duration is increased up to fifteen minutes for some critical situations. Figure 3.5 shows schematic representation of dye experimental setup.

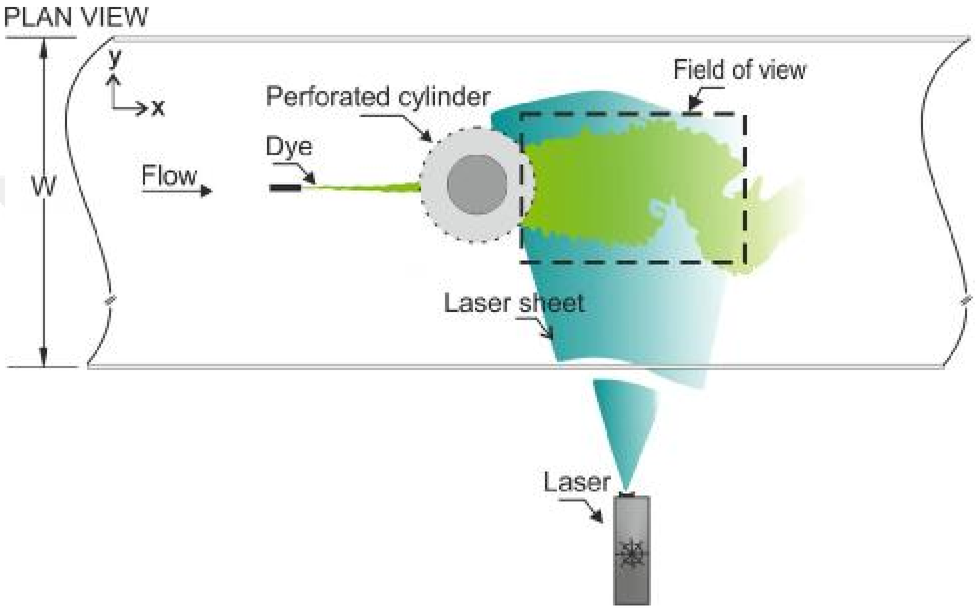

Figure 3.5. Schematic representation of dye experimental setup.

3.3.2. Particle Image Velocimetry (PIV) Technique

The Particle Image Velocimetry (PIV) technique is one of the most reliable method for flow velocity measurement in modern fluid mechanics. Main principle of PIV is based on the definition of speed which is distance over time. In PIV, the flow property actually measured is the distance traveled by particles in the flow field within a known time interval. These particles are added to the flow and known as seeding. Different types of seeding particle are used depending on the nature of the flow for PIV experiments. The type of seeding particle is chosen to follow the flow, and in order to detect their movement, an area of the flow field is illuminated by a light-sheet. The light-sheet, which is generated by a laser and a system of optical components, is not continuous/permanent, but pulsed to produce a stroboscopic effect, freezing the movement of the seeding particles. The time between the light pulses is the denominator. To detect the position of the illuminated seeding particles, a CCD-camera (CCD = Charge Coupled Device) is positioned at right angles to the light-sheet, and particle positions will appear as light specks on a dark background on each camera frame. The pulsing light-sheet and the camera are synchronized so that particle positions at the instant of light pulse number 1 are registered on frame 1 of the camera, and particle positions from pulse number 2 are on frame 2. (Older generations of CCD cameras couldn’t switch frames fast enough, so both the first and the second pulse of the light sheet were recorded on the same camera frame). The camera images are divided into square regions called interrogation areas (Figure 3.6) or interrogation regions, and for each of these interrogation areas the image from the first and the second pulse of the light-sheet are correlated to produce an average particle displacement vector. Doing the same process for all interrogation regions produce a vector map of average particle displacements.

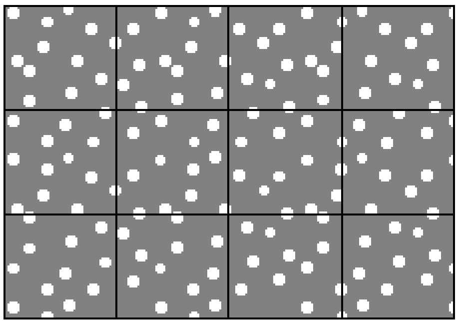

Figure 3.6. Interrogation areas.

Dividing with the known time between the two images captured the displacement vectors are converted into a map of so-called raw velocity vectors. Then validation algorithms can be applied to the raw vector maps, so that outliers, the term for erroneous vectors, can be detected and removed. In the FlowMap PIV system, for reasons of experimental reproducibility, the raw vector map is archived and a new validated vector map is output, and further analysis can produce streamlines, vortices and so on.

From the basic principles the following main topics of PIV emerge:

- Seeding
- Illumination
- Cameras
- Synchronization
- Correlation
- Validation and further analysis

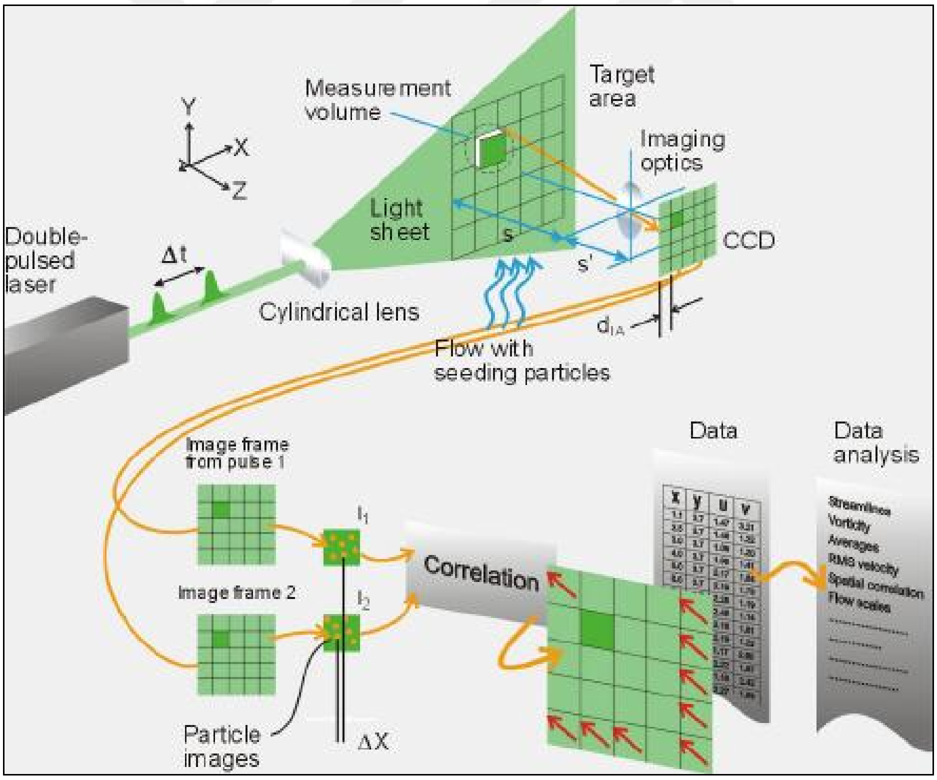

Figure 3.7. Basic PIV analysis process (Schiwietz, Westermann, 2004).

The experiments were performed and the measured data were processed using Dantec Dynamics PIV system and Dynamic Studio 2015a Software installed on a computer. The measurement field was illuminated by a thin and an intense laser light sheet by using a pair of double-pulsed Nd:YAG (yttrium aluminum garnet) laser units each having a maximum energy output of 120 mJ at 532 nm wavelength. The two orientations of the laser system use a combination of spherical and cylindrical lenses. The image capturing was performed by an 8 bit cross-correlation charge-coupled device (CCD) camera having a resolution of 1600 × 1200 pixels (Dantec Dynamics, FlowSense 2M), equipped with a Nikon AF Micro 60 *f* /2.8 *D* lens. In the image processing, 32×32 rectangular interrogation pixels were used and an overlap of 50% was employed. A total of 7326 (99×74) velocity vectors were obtained for an instantaneous velocity field at a rate of 15 frames per second. The plan view of measuring planes covers the downstream of the cylinder with the area of 147 mm x 198 mm for all configurations and the image magnification was 0.0709 mm/pixel. The laser sheet was oriented parallel to the bottom surface of the water channel and the experiments were carried out at the mid-plane of the water height. Figure 3.8 shows schematic representation of plan view setup. The time interval between pulses was 1.75 ms for all experiments and the thickness of the laser sheet illuminating the measurement plane was approximately 2 mm. The time interval and the laser sheet thickness were selected such that the maximum amount of particles in the interrogation window was obtained (With the help of a synchronizer, the time between the images to be taken and the laser pulses is synchronized and the velocity vectors of the flow field were measured by comparing the particle movement between two consecutive images). The number of particles in an interrogation area was in between 20 and 25. The uncertainty in velocity relative to depth averaged velocity is about 2% in the present experiments. The water was seeded with approximately 10 µm diameter aluminum coated sphere particles. The instantaneous images were captured, recorded, and stored in order to obtain averaged-velocity vectors and other statistical properties of the flow field. Spurious velocity vectors (less than 3%) were removed using the local median-filter technique and replaced by using a bilinear least squares fit technique between surrounding vectors. The velocity vector field was also smoothed to avoid dramatic changes in the velocity field using the Gaussian smoothing technique. The vorticity value at each grid point was calculated from the circulation around the eight neighboring points.

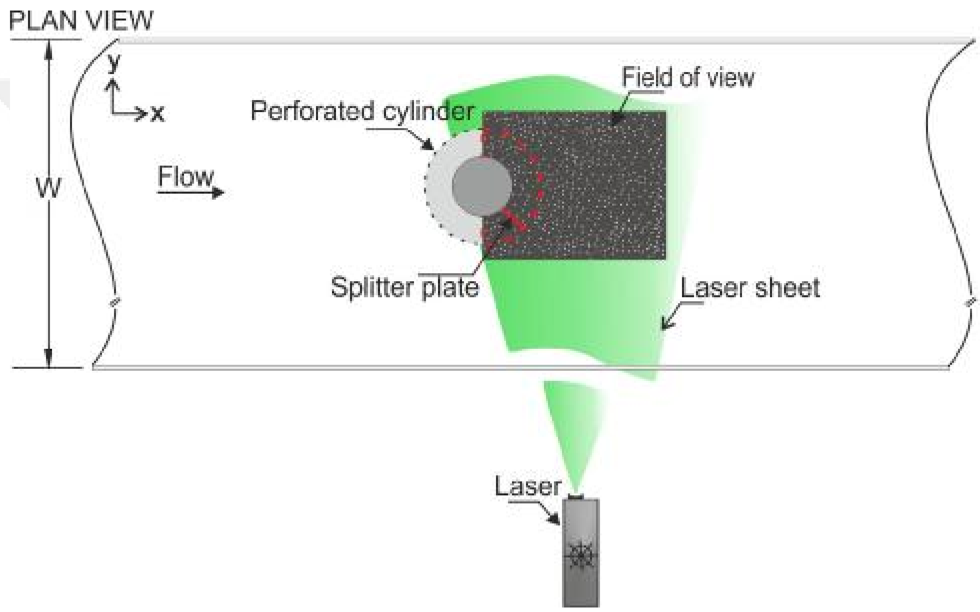

Figure 3.8. Schematic representation of PIV experimental setup.

3.3.3. Force Measurement Technique

The present force measurements were carried out using suction type, open circuit, subsonic wind tunnel with a square test section of 570 mm × 570 mm and a length of 1000 mm in the Fluid Mechanical Laboratory of the Department of Mechanical Engineering at Niğde Ömer Halis Demir University. The wind tunnel consists of contraction (nozzle), test section, diffuser and fan section. Three screens with fine mesh mounted across the entrance to straighten the flow and to reduce the turbulence intensity. The contraction has a ratio of 6.3:1. The walls of test section were expanded with a divergence angle of 0.3˚ from inlet to outlet so as to ensure constant static pressure along the whole test section.

Figure 3.9. Subsonic wind tunnel

The free-stream velocity in the test section can be changed from 3 m/s to 20 m/s by the axial fan that controlled via frequency controller. A Pitot-static tube in connection with an electronic micromanometer (Schiltknecht Messtechnik AG, model MonoAir500) was installed into the test section with test model in order to calibrate the free-stream velocity (Figure 3.10). The calibration was conducted at ambient temperature of T_∞ = 26 ˚C and local atmospheric pressure of P_∞ = 85 kPa and data was depicted below.

Figure 3.10. Pitot-static tube and micromanometer

Force measurements were conducted by using a six axis force/torque (F/T) measurement system (ATI Industrial Automation). The system consists of following components:

- Transducer (converts the obtained force and torque into analog strain gage signals)
- Power supply (supplies power to the transducer and electronics, as well as conditioning the transducer signals to be used with a data acquisition system)
- Data acquisition (DAQ) card (converts the transducer signals from analog voltages into data that computer can use and supplies raw power to the transducer system)
- ATI F/T software with calibration data (converts transducer load information into useable force and torque data)

Resonant frequencies in *x*, *y* and *z* directions of the transducer were more than 32 times higher than that of the vortex shedding frequency of the single circular cylinder at Re = 15×10^3. ATI DAQ F/T software with loaded transducer calibration was used to set the sampling rate (2×10^3 Hz), number of samples (60×10^3), angle of rotation to compensate the forces besides acquiring the F/T data. A rotary unit (isel Germany AG, ZD30) was used to precisely adjust the attack angle of the test model. Dantec Dynamics application software (MiniCTA) and traverse controller unit were used to communicate with the rotary unit. The minimum step (positional accuracy) of the rotary unit is 2.5 arcmin (0.042˚) for half-step operation. In order to avoid the effect of wind tunnel vibration on the force measurements, the load cell was mounted on a rotary unit which was mounted on a one-dimensional (1-D) relatively rigid frame detached from the wind tunnel (Figure 3.11).

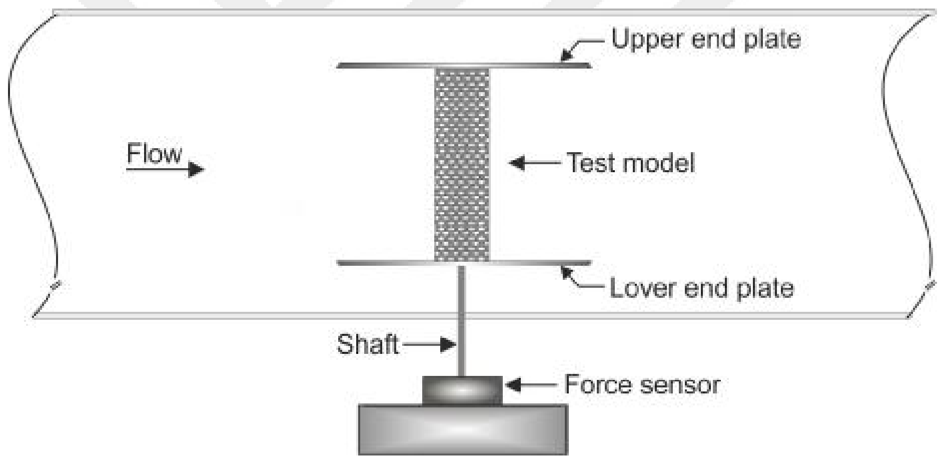

Figure 3.11. Schematic representation of force experimental setup

4. RESULTS AND DISCUSSIONS

4.1. Flow around the Bare Cylinder

First of all, the flow characteristics of bare cylinder in the wake flow region are determined in order to constitute reference and carry out comparison flow characteristics by using perforated cylinder. The first row of Figure 4.1 presents time-averaged vorticity contours, <ω> and time averaged velocity vector map, <V> superposed with dimensionless stream-wise velocity contours, <u>, respectively and second row of Figure 4.1 shows time-averaged streamline topologies, <ψ> and instantaneous dye visualization image, respectively. Here, both the minimum and incremental values were taken as ±1 and 1 for time averaged vorticity contour, <ω> respectively. Negative and positive vorticity contours which have symmetrical structure formed on the upper and lower shear layers of the circular cylinder get closer to each other as an indication of interaction and the consequent shedding of the vortices downstream of the cylinder. The substantial region of reverse flow is evident at the bare cylinder case as a result of the momentum transfer from the free-stream flow into wake flow region. The time-averaged streamline topologies, <ψ> are indicated that the fluid flow gets zero velocity which is called as saddle point designated by S in the Figure. The location of the saddle point, S also defines the vortex formation length, i.e. the vortex formation length is defined as the distance from the base of the cylinder to the saddle points on the centerline (Aydin et al., 2010). The separated and recirculating flow in the near wake region with the help of visualizing tools is clearly seen for the bare cylinder. It is seen from the dye picture that alternating vortex shedding and the well-known Karman Vortex Street occurs downstream of the cylinder. This vortex structure applies unsteady loads on the bluff bodies or any object located downstream of these bluff bodies. These unsteady loads cause fatigue and shorten the life of bluff bodies and objects. In the meantime, these vortices are an environmental issue. They cause erosions and transport sediments and pollutants from the bottom of the rivers and shallow lakes.

Scientists have been studying to control the unsteady vortex structure with different methods throughout past years.

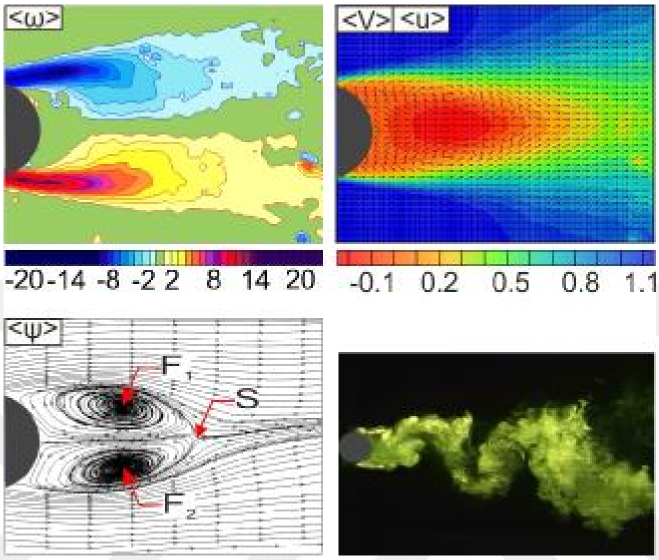

Figure 4.1. The results of bare cylinder: Time averaged vorticity contours, <ω>, time averaged velocity vector map, <V> superposed with stream-wise velocity contours, <u>, time averaged streamline topology, <Ψ> and instantaneous dye visualization picture.

4.2. Flow Structure in the Near Wake of Cylinder Surrounded by Perforated Cylinder

Time averaged velocity vector map, <V> superposed with stream-wise velocity contours, <u> in the near-wake region for various porosity, β at different diameter ratio, D/D_s are presented sequentially in Figures 4.2a and 4.2b. In each figure, first column, second column, and third column present diameter ratio, $D/D_s=0.4$, $D/D_s=0.5$, and $D/D_s=0.6$, respectively, and each rows show porosities of perforated cylinder, which are β=0.3, 0.4, 0.5, 0.6 and 0.7, respectively. For the porosity value of β=0.3, the perforated cylinder has a few holes on the surface, so it reduces momentum transfer into the gap region between the cylinder and the perforated cylinder. Therefore, the magnitude of velocity in the gap region is considerably lower than the porosity value of $\beta \geq 0.4$. The negative velocity contours indicate that reverse flow occurs in the near-wake region owing to the prevention of the main flow by perforated cylinder at porosity value of $\beta=0.3$. At the diameter ratio of $D/D_s=0.4$, increasing the number of holes on the perforated cylinder enhances momentum transfer into the gap region and the near-wake region. Thus, the flow velocity magnitudes through the gap are high compared to the porosity value of $\beta=0.3$ and reverse flow is disappeared in the near-wake region for the porosity value of $0.4 \leq \beta \leq 0.6$. The magnitude of velocity in the near-wake region is affected not only by the porosity of perforated cylinder, but also by the diameter ratio of perforated cylinder. At the diameter ratio of $D/D_s=0.6$, the negative velocity contours for the porosity value of $\beta=0.4$ and 0.5 indicate that narrow gap region is inadequate to transfer the momentum from inside of perforated cylinder into the near-wake region. Therefore, the reverse flow occurs in the near-wake region as a result of momentum transfer from shear layers of the perforated cylinder into the near-wake region. It is clearly seen from Figure 4.3b that the perforated cylinders have insignificant effect on the velocity distribution of the near-wake region for the porosity value of $\beta \geq 0.6$ at the diameter ratio of $D/D_s \geq 0.5$. The reverse flow occurs in the near-wake region due to the prevention of the main flow by the cylinder. Moreover, at the porosity value of $\beta=0.7$, the momentum transfer into the gap region is soared due to increasing number of hole on the perforated cylinder for all diameter ratios, D/D_s. Therefore, the magnitude of flow velocity in the gap region increases compared to the porosity value of $\beta<0.7$.

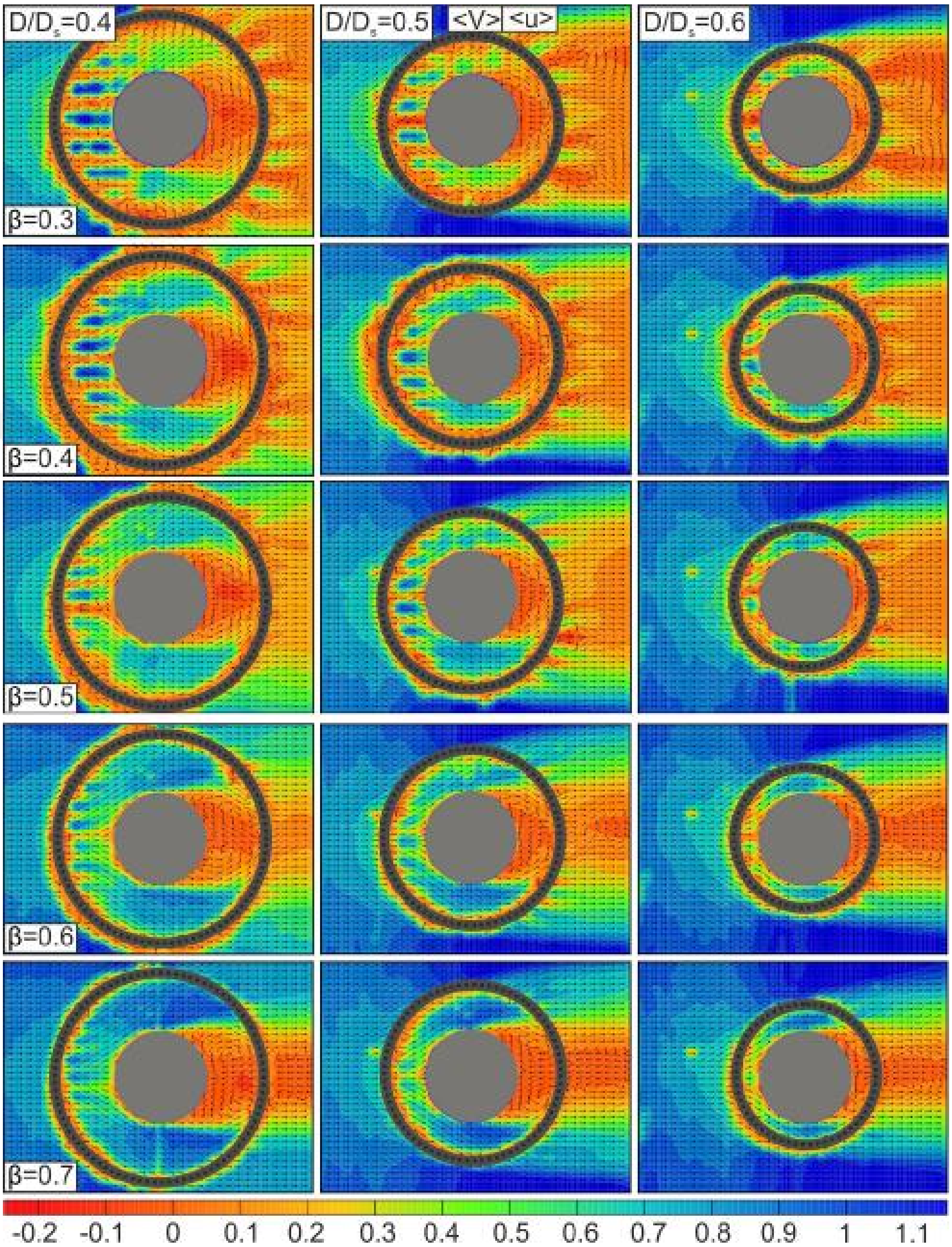

Figure 4.2a. Time averaged velocity vector map, <V>, superpose with velocity contours, <u> for various porosity, β at different diameter ratio, D/D_s.

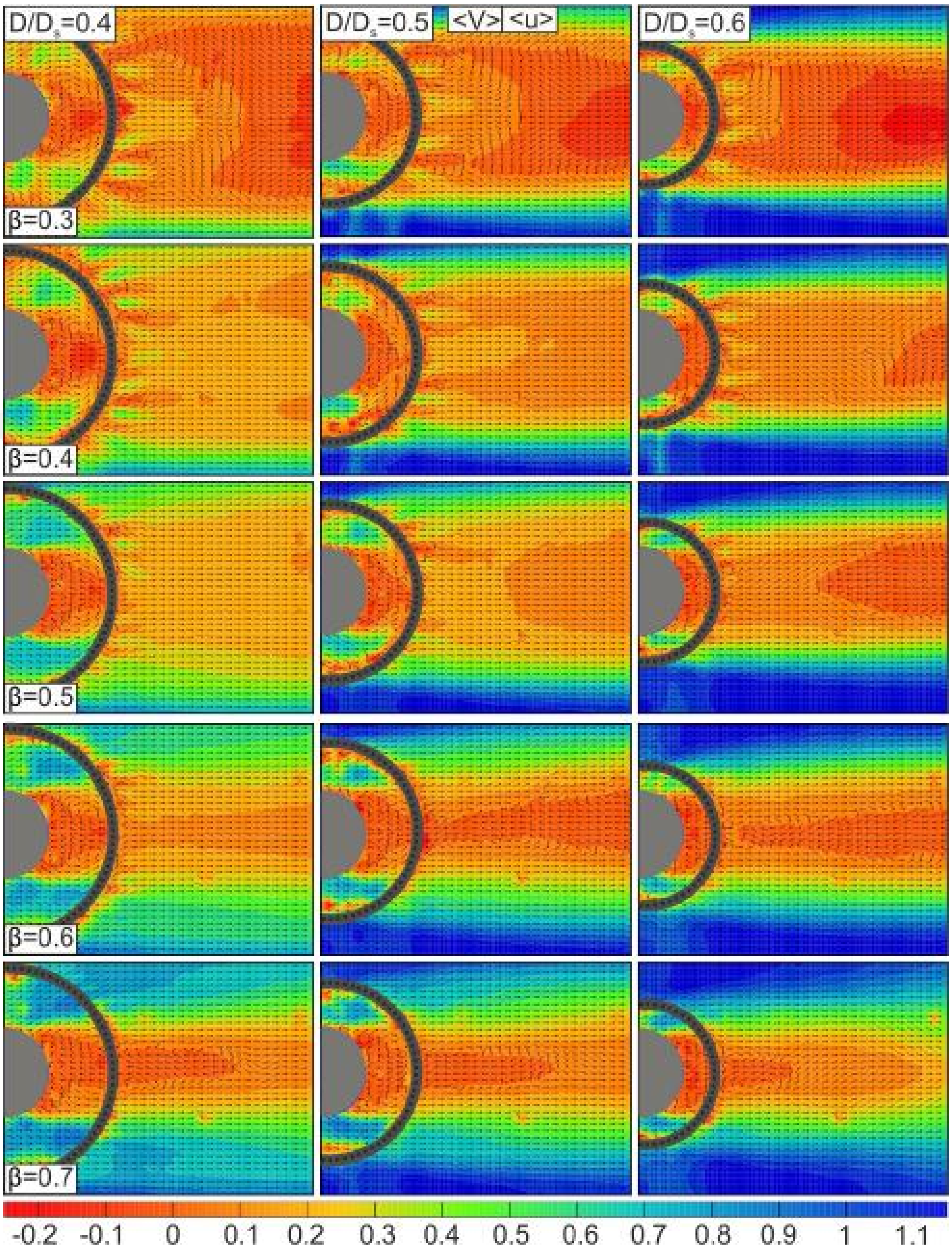

Figure 4.2b. Time averaged velocity vector map, <V>, superpose with velocity contours, <u> in the near-wake region for various porosity, β at different diameter ratio, D/D_s.

Figure 4.3 presents time averaged streamline topology, $<\psi>$ for various porosity, β at different diameter ratio, D/D_s. The recirculation zone of the cylinder and corresponding location of the generated foci and saddle points are significantly affected by perforated cylinders compared to the bare cylinder. For porosity values of $\beta \leq 0.5$, time averaged streamline topologies, $<\psi>$ demonstrate a saddle point, S and two foci, F_1 and F_2 occurring in the gap region between the cylinder and the perforated cylinder at diameter ratio, D/D_s=0.4, 0.5 and 0.6. This situation shows that the recirculation zone of the cylinder is restricted by the perforated cylinder. Moreover, the size of the recirculation zone decreases with the increasing diameter ratio, D/D_s. The results obtained for the porosity value of β=0.3 with the diameter ratio of D/D_s=0.4 reveal that the other two foci which are designated by F_3 and F_4 occur in the gap region between the cylinder and the perforated cylinder. On the other hand, the foci F_3 and F_4 occur in the outside of perforated cylinder for the porosity value of β=0.3 at the diameter ratio of D/D_s=0.6, since occurrence of reverse flow in the near-wake region restricts to momentum transfer from the inside of perforated cylinder into the near-wake region. However, formations of foci F_1 and F_2 are asymmetrical with respect to the centerline of the cylinder and the saddle point, S disappears for the porosity value of β=0.6 at the diameter ratios of D/D_s=0.4 and 0.5. The perforated cylinder begins to lose its effect on the flow structure and the foci F_3 and F_4 occurs as a result of reverse flow in the near-wake region for the porosity values of $\beta \geq 0.6$. Furthermore, for the porosity value of β=0.7 with the diameter ratio of D/D_s=0.6, the occurrence of foci F_1 and F_2 in the near-wake region indicates that the wake flow patterns of this case behaves like a bare cylinder.

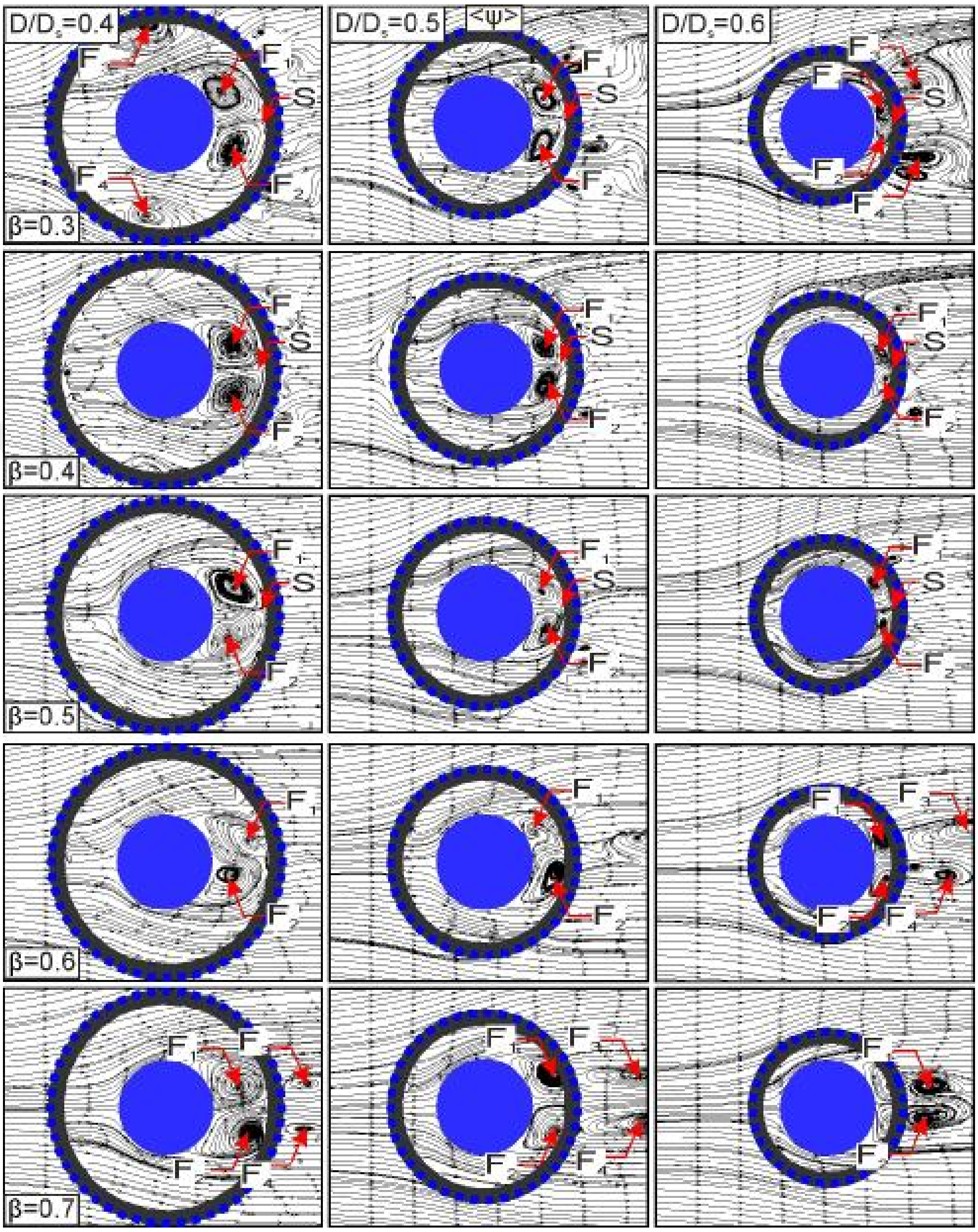

Figure 4.3. Time averaged streamline topology, <ψ>, for various porosity, β at different diameter ratio, D/D_s.

Figures 4.4a and 4.4b present the time averaged vorticity contours, <ω> inside of perforated cylinder and the near-wake region for various porosity, β at different diameter ratios, D/D_s. First of all, Figure 4.4a shows that two distinct vorticity pairs which are designated by A and B, respectively occur in the gap region between the cylinder and the perforated cylinder for all cases. The vorticity pair 'A' stems from the cylinder, while the vorticity pair 'B' develops out of internal surface of perforated cylinder. The vortex formation length of the cylinder 'A' is shorter compared to the bare cylinder case due to the fact that the shear layers on the both side of the cylinder are restricted by internal surface of the perforated cylinder at the porosity value of $\beta \leq 0.5$ for all diameter ratios, D/D_s. Also, the vortex formation length of the cylinder 'A' decreases with the increasing diameter ratio, D/D_s. Furthermore, the magnitude of the vorticity pairs 'A' and 'B' gradually increase with the increasing porosity, β since the perforated cylinder enhances the momentum transfer into the gap region between the cylinder and the perforated cylinder. Figure 4.4b shows that another vorticity pair, which is designated by 'C', occurs in the near-wake region due to external surface of perforated cylinder. The vorticity pair 'C' formed in the near-wake region indicates that the porosity, β and the diameter ratio, D/D_s have a significant effect on the flow structure. Contrary to the magnitude of vorticity pair, 'B', the magnitude of vorticity pair, 'C' decreases with the increasing porosity, β for all diameter ratios, D/D_s. Moreover, for the porosity value of β=0.6 with the diameter ratio of D/D_s=0.4, a distinct difference is determined when compared with the diameter ratios, D/D_s=0.5 and 0.6. At the diameter ratio of D/D_s=0.4, the low magnitude vorticity pair 'A' appears in the near-wake region owing to the fact that the shear layers of the cylinder elongate to the stream-wise direction. However, the vorticity pair 'A' interacts with vorticity pair 'C' in the near-wake region for diameter ratio of $D/D_s \geq 0.5$. At porosity value of β=0.7, it is observed that the elongated vorticity pair 'A' appears in the near-wake region for diameter ratios of D/D_s=0.4 and 0.5. For the porosity value of β=0.7 with the diameter ratio D/D_s=0.6, the combined vorticity pair is obtained in the near-wake region for porosity value of β=0.6.

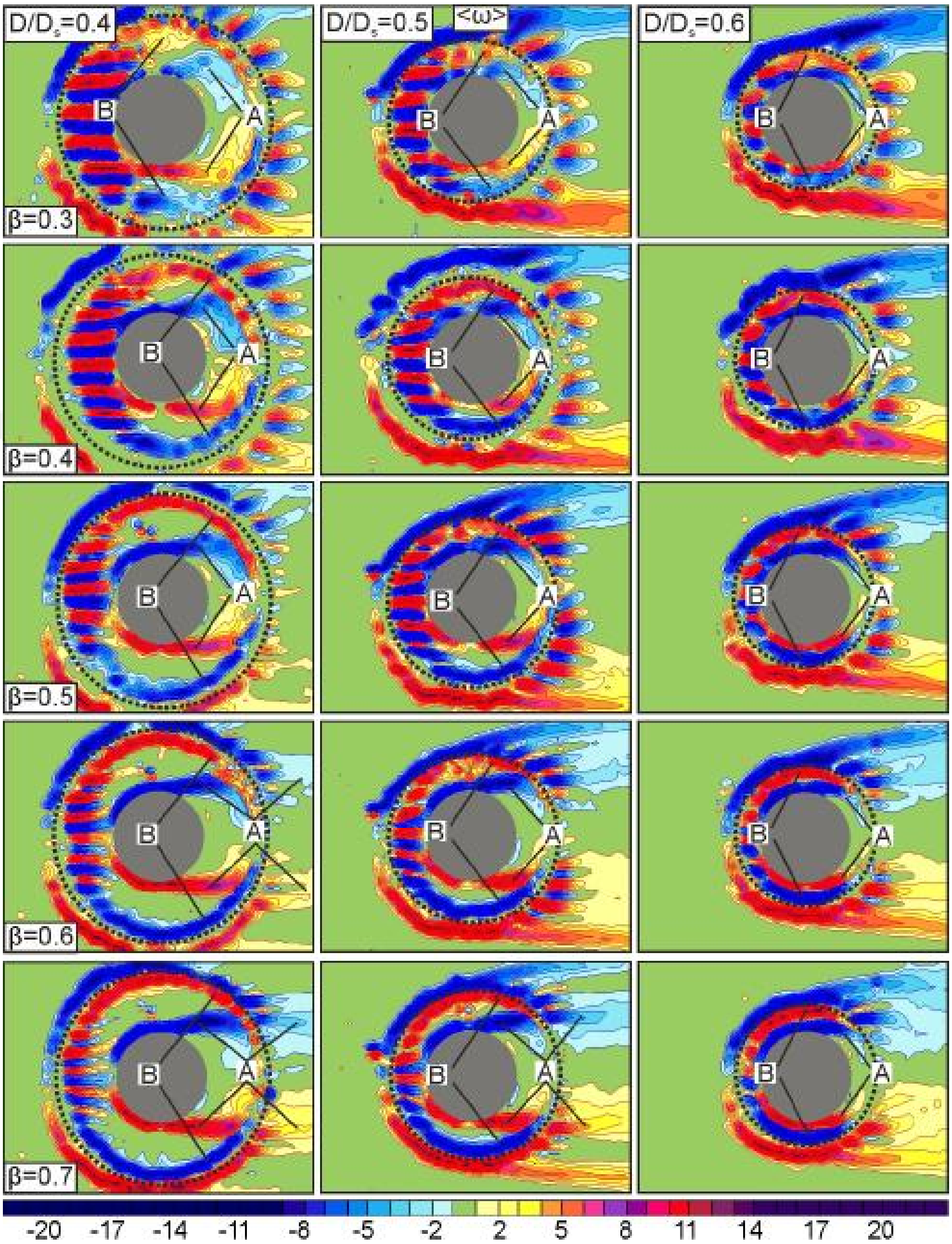

Figure 4.4a. Time averaged vorticity contours, <ω>, for various porosity, β at different diameter ratio, D/D_s.

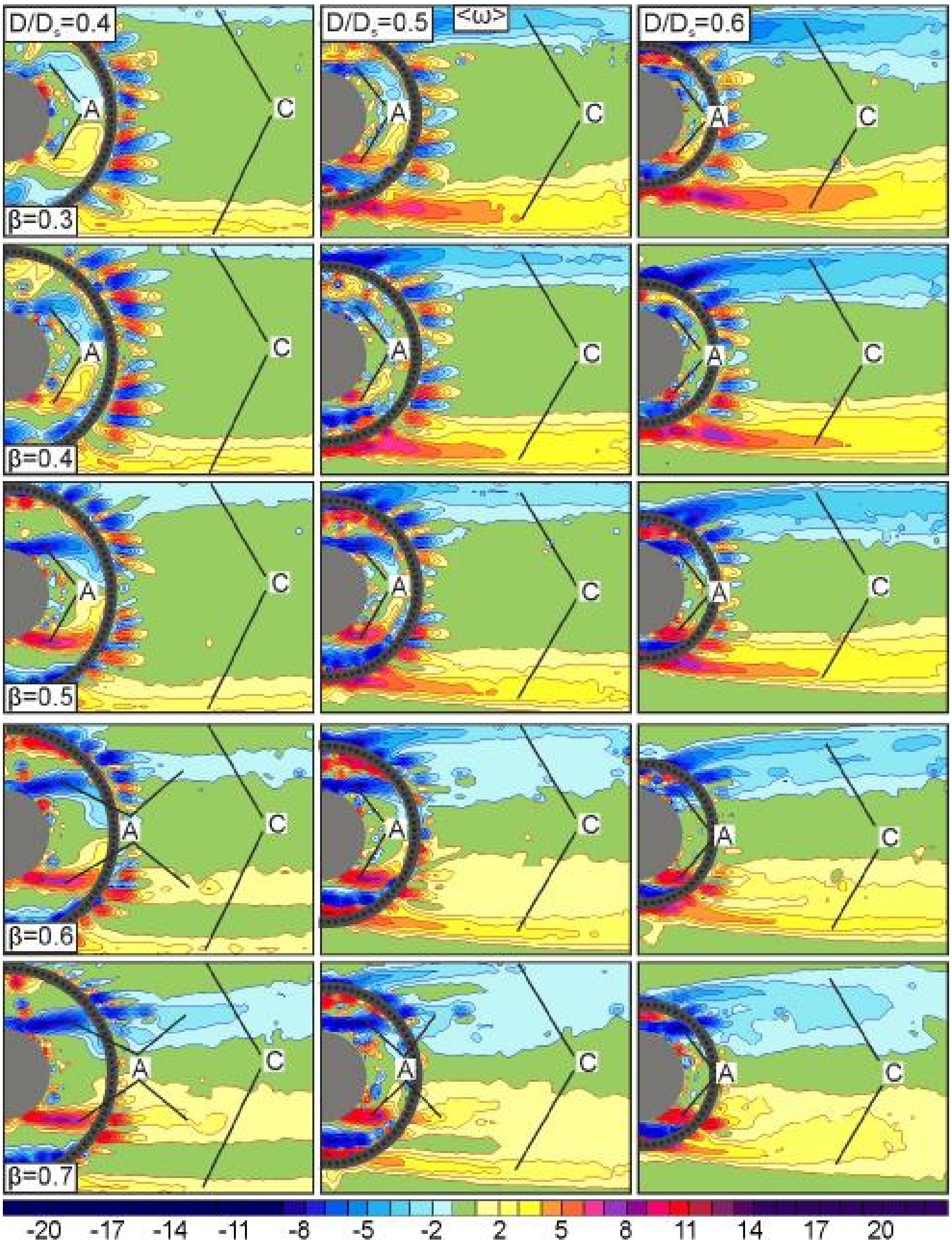

Figure 4.4b. Time averaged vorticity contours, <ω>, in the near-wake region for various porosity, β at different diameter ratio, D/D_s.

In order to perform better analysis in the near-wake region, profiles of mean stream-wise velocity, U/U_∞ measured at locations of x/D=1.2, 2 and 3.2 are presented in Figure 4.5 for various porosities, β and diameter ratios, $D/D_{s.}$ For comparison purposes, the results for the bare cylinder are also included. It is clearly seen that the wake width narrows with both increasing porosity, β and increasing diameter ratio, D/D_s. At the location of x/D=1.2, the negative velocity value occurred in the near-wake region indicates the formation of vortices for the bare cylinder and β=0.7. The influence of perforated cylinder is weakened as the stream-wise distance increases to x/D=2 and the region of negative velocity is also observed for β=0.3 and 0.6 at D/D_s=0.5 and for β=0.3, 0.5 and 0.6 at D/D_s=0.6. The velocity deficit decreases for the bare cylinder and β=0.7 cases. Further downstream at the location of x/D=3.2, the perforated cylinder loses its effect on the control and velocity deficit increases for β=0.3 at all diameter ratio, D/D_s. For the diameter ratio of D/D_s=0.4, the velocity profiles of β=0.5 and 0.6 indicate that the vortices are suppressed in the near-wake region at x/D=1.2, 2 and 3.2.

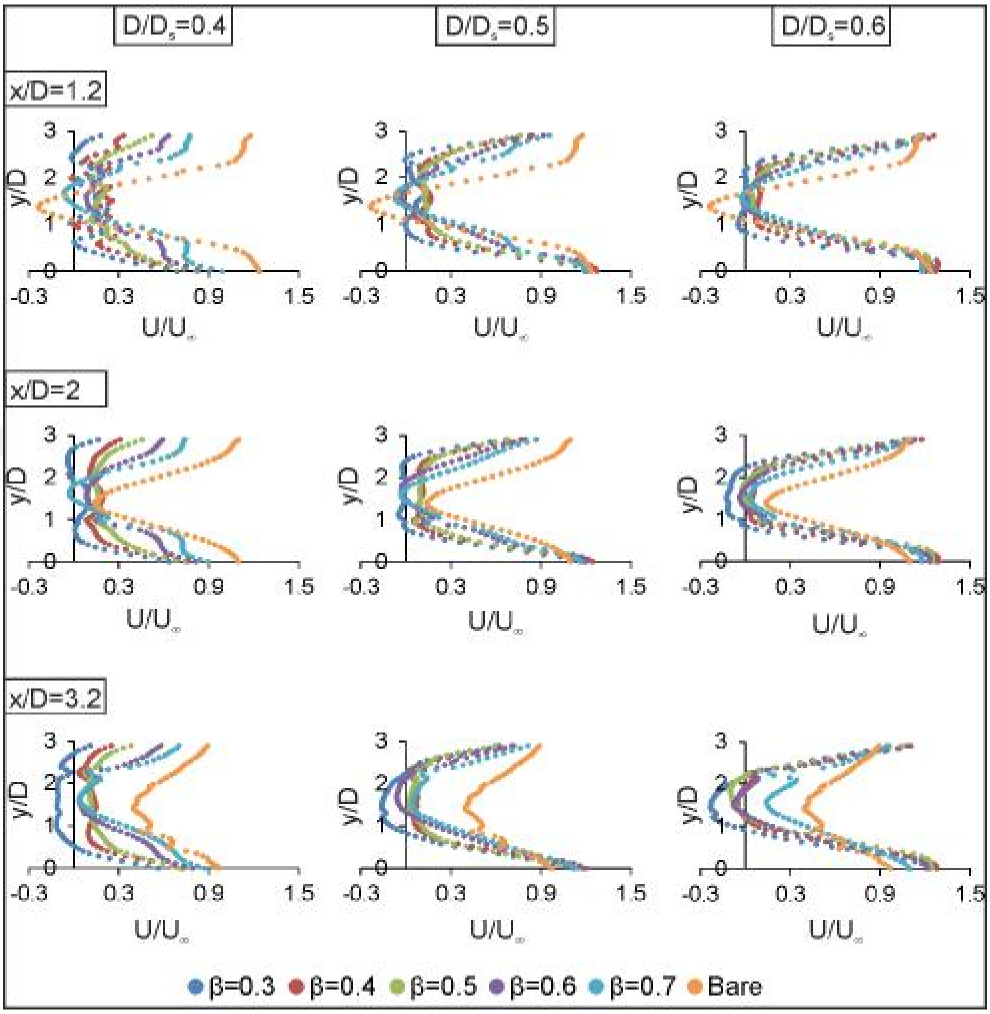

Figure 4.5. Profiles of mean stream-wise velocity for cases of D/D_s=0.4, 0.5 and 0.6 and various porosity, β at x/D=1.2, 2 and 3.2.

Figure 4.6 shows variation of the time averaged drag coefficient of the cylinder, $<C_D>$ with respect to porosity, β for D/D_s=0.4, 0.5 and 0.6 at $Re=5\times10^3$ and 15×10^3. First of all, force measurement is performed for the bare cylinder in order to compare the magnitude of drag coefficient, $<C_D>$ with results of current control method. The time averaged drag coefficient of the bare cylinder is calculated as $<C_D>$ =1.11 and 1.22 for the Reynolds number $Re=5\times10^3$ and

15×10^3, respectively. Using the perforated cylinder remarkably affects the drag coefficient, $<C_D>$ of the cylinder. It is obtained that the variation of the drag coefficient, $<C_D>$ of the cylinder with the porosities of perforated cylinder have similar trend for $Re=5\times10^3$ and 15×10^3. The drag coefficient, $<C_D>$ of the cylinder is reduced by 89% for the porosity value of β=0.3 at the $Re=15\times10^3$. Especially for low porosity value of perforated cylinder, the momentum transfer into the gap region is reduced, so that the drag coefficient, $<C_D>$ of the cylinder is remarkably lower than the bare cylinder. The drag coefficient, $<C_D>$ of the cylinder increases with the increasing the porosities of perforated cylinders due to the increasing momentum transfer into the gap region. Moreover, it should also be pointed out that even for the porosity value of β=0.7, the drag coefficient, $<C_D>$ of the cylinder is obtained with 26% and 30% lower than the bare cylinder case at $Re=5\times10^3$ and 15×10^3, respectively.

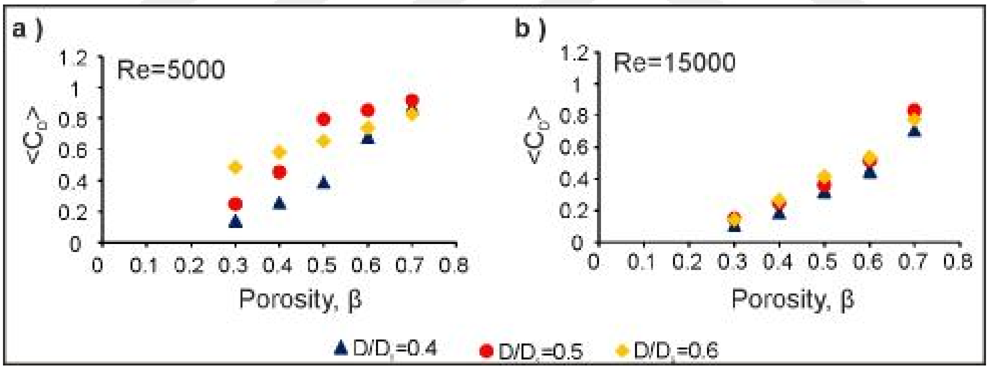

Figure 4.6. Variation of the time averaged drag coefficient of the cylinder, $<C_D>$ with respect to the porosity, β for $D/D_s=0.4$, 0.5 and 0.6 at the $Re=5\times10^3$ and 15×10^3.

The force measurements were also performed for the cylinder along with perforated cylinders, and also the total drag coefficient was separately calculated based on both the frontal area of cylinder and perforated cylinder. Figure 4.7 presents the variation of the total drag coefficient with the porosities of perforated cylinder, β for the diameter ratios of D/D_s=0.4, 0.5 and 0.6 at Re=5×10^3 and 15×10^3. Figures 4.7a and 4.7c indicate that total drag coefficients, $<C_{DC}>$ which are calculated based on the frontal area of cylinder, remarkably increases when compared to the bare cylinder case for Re=5×10^3 and 15×10^3, respectively. It is observed that the total drag coefficient, $<C_{DC}>$ slightly decreases with increasing porosity, β. Diameter ratio, D/D_s affects total drag coefficient, $<C_{DC}>$ remarkably. The minimum total drag coefficient, $<C_{DC}>$ is obtained for the diameter ratio of D/D_s=0.6 owing to decreasing cross sectional area of the perforated cylinder. The variation of the total drag coefficient, $<C_{DS}>$ which is calculated based on the frontal area of perforated cylinder, with the porosity of cylinder, β are shown in Figures 4.7b and 4.7d for Re=$5\times10^3$and 15×10^3, respectively. The total drag coefficient, $<C_{DS}>$ is obtained approximately same for all diameter ratio, D/D_s and the porosity of perforated cylinder, β.

It can be concluded in the light of obtained PIV results that the flow structure of the cylinder in the near-wake region is significantly affected by the presence of perforated cylinder for all diameter ratios, D/D_s. The perforated cylinder is dominant on the flow structure for the porosity value of β=0.3. The diameter ratio of D/D_s=0.6 is insignificant effect on the flow control of the cylinder for all porosities, β. Additionally, the flow control is achieved in the near-wake region for the porosity values of β=0.5 and 0.6 at the diameter ratio of D/D_s=0.4 and 0.5. The drag coefficient, $<C_D>$ of cylinder is also reduced by 65% for the porosity value of β=0.5 at the diameter ratio of D/D_s=0.4. However, the vortex formation of the cylinder is observed in the gap region between the cylinder and the perforated cylinder for all cases.

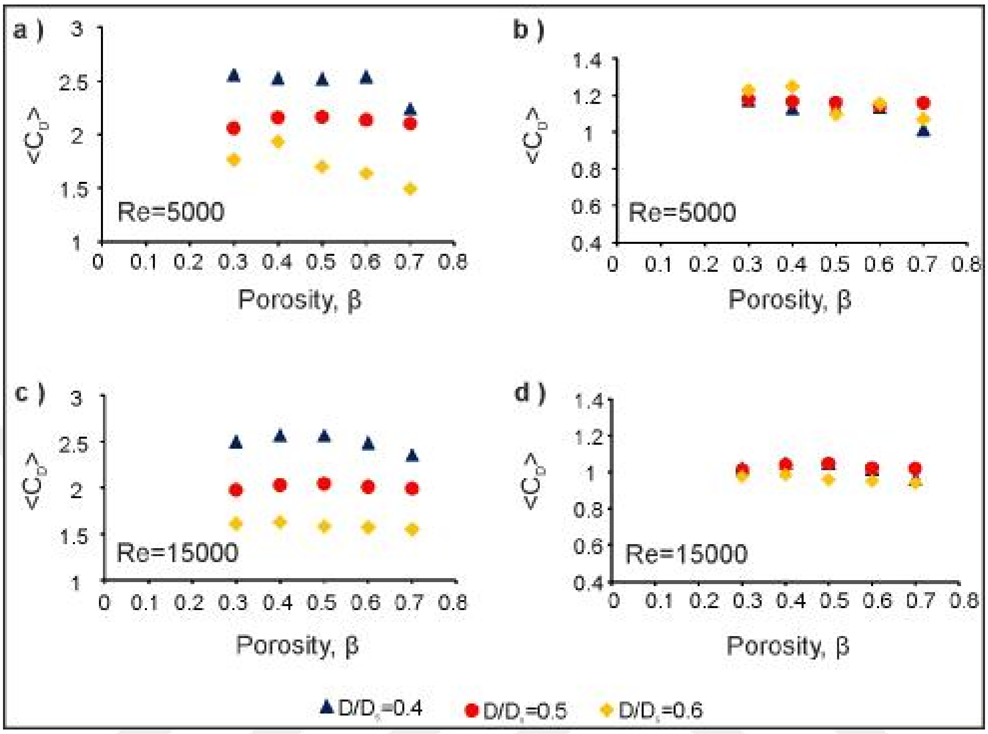

Figure 4.7. Variation of total drag coefficient, $<C_D>$ a) the drag coefficient, $<C_{DC}>$ at the Re=5×10^3, b) the drag coefficient, $<C_{DS}>$ at the Re=5×10^3 c) the drag coefficient, $<C_{DC}>$ at the Re=15×10^3, d) the drag coefficient, $<C_{DS}>$ at the Re=15×10^3.

4.3. Flow Visualization Downstream of Cylinder Surrounded by Perforated Cylinder

The dye experiments were carried out in order to investigate the effect of porosity of perforated cylinder and diameter ratio on the flow characteristics further downstream of the shrouded cylinder. The dye (Rhodamine 6G) was injected from the base of the perforated cylinder in which the flow is not affected by the injection. Typical visualization images of instantaneous flow field downstream of the cylinder with perforated cylinders are shown in Figure 4.8. In this figure each column presents diameter ratios of D/D_s=0.4, 0.5 and 0.6 and each rows show porosities of perforated cylinders such as β=0.3, 0.4, 0.5, 0.6 and 0.7, respectively. It is clearly seen that the width of downstream wake of the cylinder with perforated cylinder, W_w and the location of rolling up of shear layers, R_L on the both side of the solid cylinder and the perforated cylinder configuration are remarkably affected by the porosity of the perforated cylinders and diameter ratios. For the value of $\beta \leq 0.4$, the downstream flow behavior of the perforated cylinders would be similar to the bare cylinder case. The shear layers on the both side of perforated cylinder rolls up in to the near wake region and von Karman vortex street occurs downstream of the cylinder for the perforated cylinder configuration. The width of wake region, W_w decreases and the location of rolling up of shear layers, R_L closes to the perforated cylinder depends on the increasing diameter ratio, D/D_s. The results obtained for the porosity value of β=0.5 indicate that the location of rolling up of shear layers, R_L is shifted to further region of downstream for diameter ratio $D/D_s \geq 0.5$. However, the results obtained for porosity value of β=0.5 at the diameter ratio of D/D_s=0.4 is slightly different compared with the case of diameter ratios $D/D_s \geq 0.5$. The wake region exhibits ‘S’ shaped unsteady oscillating flow behavior similar to the von Karman vortex street. On contrary, the width of wake regions, W_w are decreased up to porosity values of β<0.6 and they are approximately same at porosity value of $\beta \geq 0.6$ for all dimeter ratios, D/D_s. In addition to this result, the formation of von Karman vortex street is suppressed at the diameter ratios of D/D_s=0.4 and 0.5. Moreover, for the diameter ratio of D/D_s=0.6 at the porosity value of β=0.6, a distinct difference is determined that the location of rolling up of shear layers, R_L is close to perforated cylinder by comparing with the porosity value of β=0.5. The results obtained for porosity value of β=0.7 show that the perforated cylinder has insignificant effect on the flow structure for all diameter ratios, D/D_s. The shear layers roll up in-to the near wake region, alternately and von Karman Vortex Street occurs downstream of the cylinder for perforated cylinder configuration.

In conclusion, the flow structure downstream of cylinder is significantly affected by the diameter ratio, D/D_s and the porosity of perforated cylinder, β. The drag results and the PIV measurements are in close agreement with each other in the scope of this investigation. The porosity values of β=0.5 and 0.6 are most effective cases in suppression of the vortex street in the downstream of the cylinder for perforated cylinder configuration for the diameter ratios D/D_s=0.4 and 0.5.

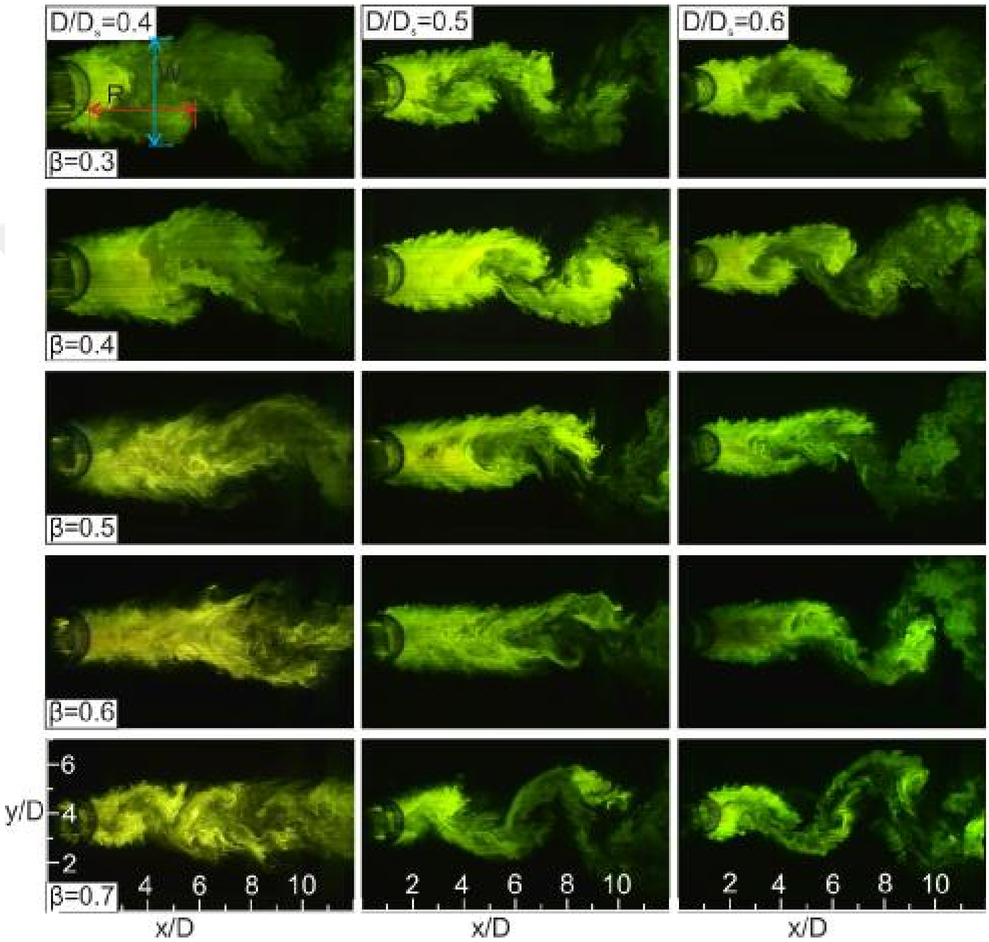

Figure 4.8. Instantaneous dye visualization pictures for various porosity of perforated cylinder, β at different diameter ratios, D/D_s.

4.4. Flow Control in the Near Wake by Splitter Plate and Perforated Cylinder Combination

As mentioned in the previous section, the use of perforated cylinder is significantly effective on the controlling of vortex formation in the near-wake region for several cases. However, the vortex formation is observed in the gap region for the porosity values of $\beta \geq 0.5$ at the diameter ratios of $D/D_s \leq 0.5$. Therefore, it is mainly focused on the control of the vortex formation in the gap region flow between the cylinder and the perforated cylinder by the splitter plate in this section, for the porosity value of $\beta \geq 0.5$ at the diameter ratio of $D/D_s \leq 0.5$. In Figures of 4.9a and 4.9b, each column presents the porosity of perforated cylinders, β=0.5, 0.6 and 0.7 and each row shows the angle of splitter plates, $\alpha = 120^o$, 130^o, 140^o, 150^o, 160^o, 170^o and 180^o, respectively. In order to interpret the differences, the results of the perforated cylinder without any splitter plate (no-plate case) are also presented in the first row of the figures.

Figure 4.9a presents the time averaged velocity vector map, <V> superposed with the stream-wise velocity contours, <u> for the plate length of L_p=1 case for the plate angles of $120^o \leq \alpha \leq 140^o$ at the diameter ratio of $D/D_s = 0.4$. For the plate angles of $120^o \leq \alpha \leq 140^o$, the incoming flow through the perforated cylinder is blocked by the plate. Therefore, the reverse flow occurs in the near-wake region and re-enters into the gap region. The magnitude of reversed flow in the near-wake region increase with the increasing porosity of the perforated cylinder due to increasing momentum transfer into the gap region. Furthermore, the width of the wake region and the size of reversed flow zone gradually decreases with the increasing plate angle compared to the no-plate case. On the other hand, the recirculation zone disappears in the lower side of the cylinder, and the size of recirculation zone increases in the upper side of the cylinder for the plate angle of $\alpha = 120^o$. By increasing plate angle, the recirculation zone can exist in the lower side of the cylinder and the size of recirculation zone decreases in the upper side of the cylinder.

Figure 4.9b provides the time averaged velocity vector map, <V> superposed with the stream-wise velocity contours for the plate angles of $150^o \leq \alpha \leq 180^o$ to understand the effects of larger angles. It is obviously seen that the width of the wake region is same for the plate angles of $150^o \leq \alpha \leq 180^o$. However, the magnitude of velocity in the near-wake region increases and the size of reversed flow zone decreases in comparison with the plate angles of $120^o \leq \alpha \leq 140^o$. For the porosity values of β=0.5 and 0.6, the reverse flow disappears in the near-wake region at the plate angle of $\alpha=170^o$ and 180^o. Especially for the porosity value of β=0.6 at the plate angle of $\alpha=180^o$, the magnitude of the velocity in the gap region between the cylinder and the perforated cylinder, and the near-wake region is increased compared to the no-plate case.

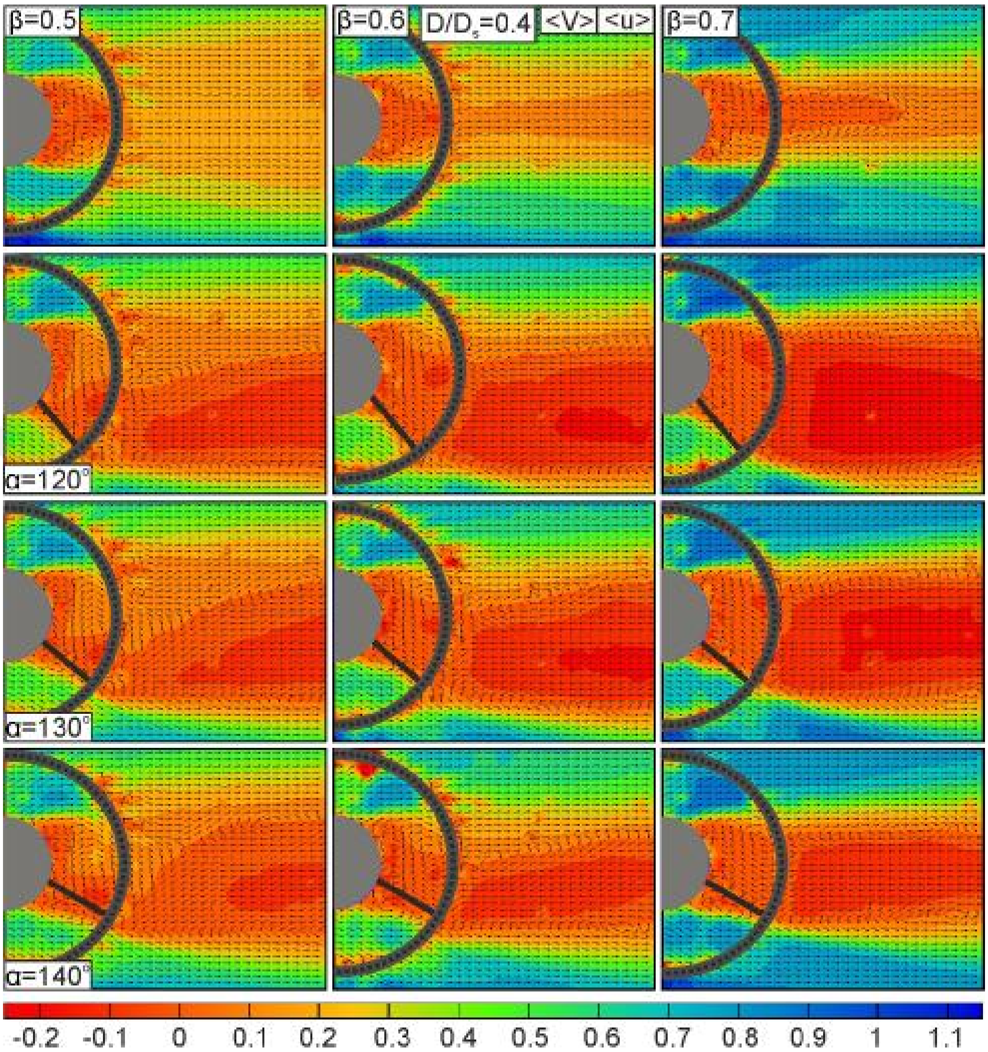

Figure 4.9a. Time averaged velocity vector field, <V> superposed with the stream-wise velocity contours, <u> for $120^o \leq \alpha \leq 140^o$ plate angles for various porosity of the perforated cylinders, β at the diameter ratio of D/D_s=0.4.

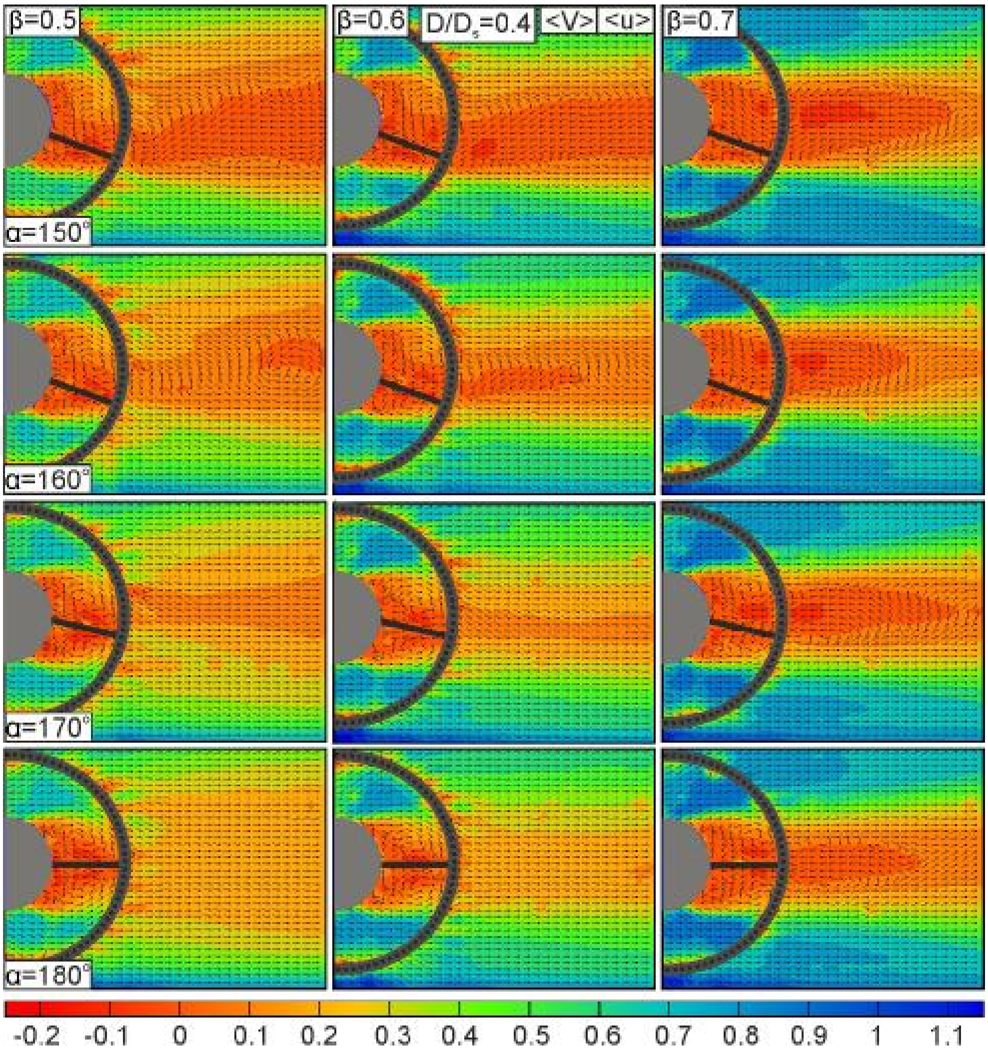

Figure 4.9b. Time averaged velocity vector field, <V> superposed with the stream-wise velocity contours, <u> for $150^o \leq \alpha \leq 180^o$ plate angles for various porosity of the perforated cylinders, β at the diameter ratio of $D/D_s=0.4$.

Figure 4.10a shows the time averaged vorticity contours, $<\omega>$ for the porosity values of the perforated cylinders β=0.5, 0.6 and 0.7 cases for the plate angles of $120^o \leq \alpha \leq 140^o$ at the diameter ratio of D/D_s=0.4. The main mechanism to control the flow is to prevent or attenuate the interaction of shear layers of the cylinder. A lower magnitude of the vorticity, $<\omega>$ in the lower side of the cylinder would elongate in the downstream direction and the magnitude of the vorticity dramatically increases in the leading edge of the plate due to the fact that transfer of the momentum into the near-wake region increases at this specific point. Also, this high magnitude of the vorticity, $<\omega>$ interacts with the vorticity, $<\omega>$ of the perforated cylinder in the lower side, which is designated by 'C' at the no-plate case, in the near-wake region for the plate angle of $\alpha=120^o$. It should be pointed out that for plate angle of $\alpha=130^o$, the magnitude of the vorticity, $<\omega>$ in the leading edge increases in comparison with the plate angle of $\alpha=120^o$, even though the magnitude of the vorticity, $<\omega>$ in the leading edge decreases with the increasing plate angle. It is clearly seen that the interaction of the vorticity in the leading edge with the vorticity, $<\omega>$ in the lower side of the perforated cylinder becomes to decrease for the plate angle of $\alpha=140^o$ at the porosity value of β=0.5. For the porosity values of β=0.6 and 0.7 at the plate angle of $\alpha=140^o$, the vorticity, $<\omega>$ in the leading edge occurs separately in the near-wake region contrary to the plate angle of $\alpha<140^o$.

The larger effective plate angles, α are presented in Figure 4.10b for the plate angles of $150^o \leq \alpha \leq 180^o$ and the diameter ratio of D/D_s=0.4. For the porosity value of β=0.5 at the plate angle of $\alpha=160^o$, it is observed that the vorticity, $<\omega>$ in the leading edge occurs separately in the near-wake region and it has low magnitude compared to the plate angle of $\alpha < 160^o$. For the plate angle of $\alpha >160^o$, similar flow structure with the no-plate case are obtained at all porosity values. The plate angle of $\alpha=180^o$ presents the well-known splitter plate method with in the literature and would be the best way of preventing the interaction of vortices formed by the cylinder in the gap region between the cylinder and the perforated cylinder.

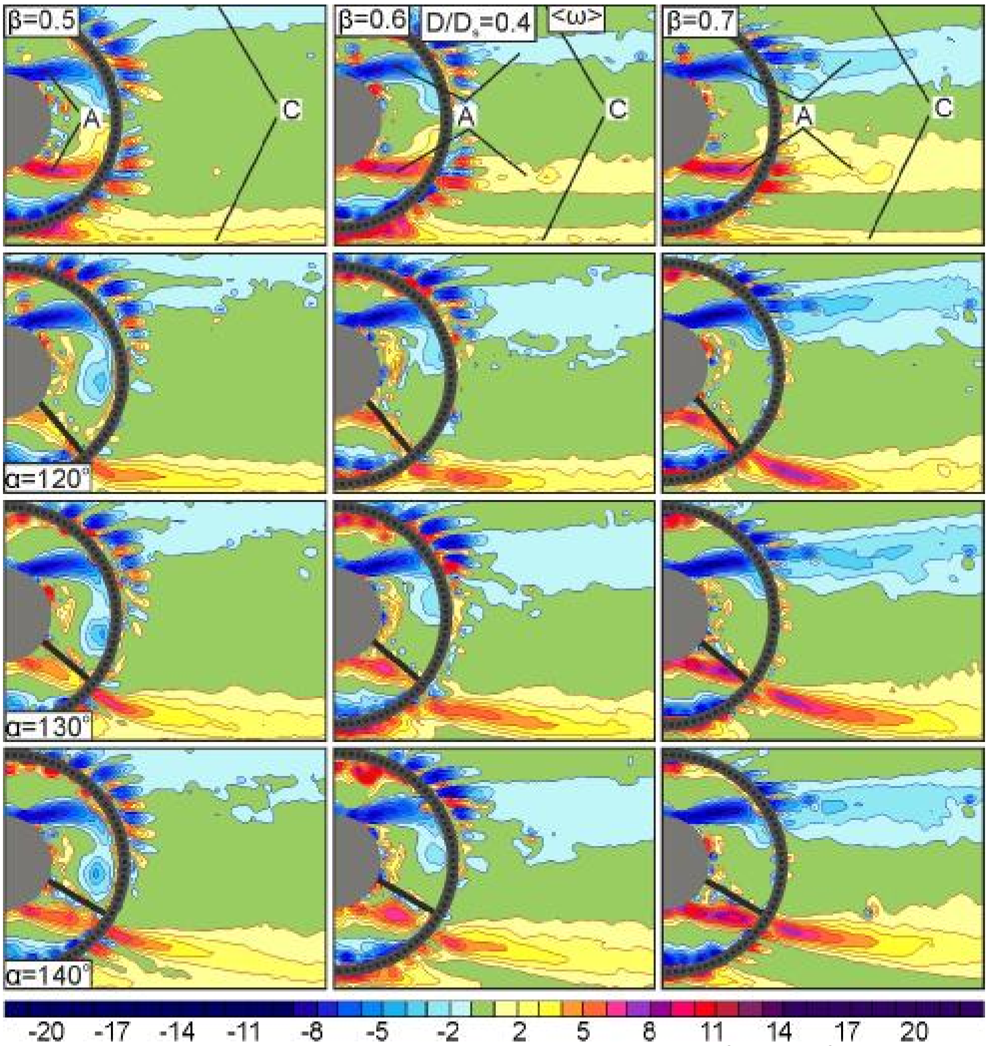

Figure 4.10a. Time averaged vorticity contour, <ω> for $120^o \leq \alpha \leq 140^o$ plate angles for various porosity of the perforated cylinders, β at the diameter ratio of D/D_s=0.4.

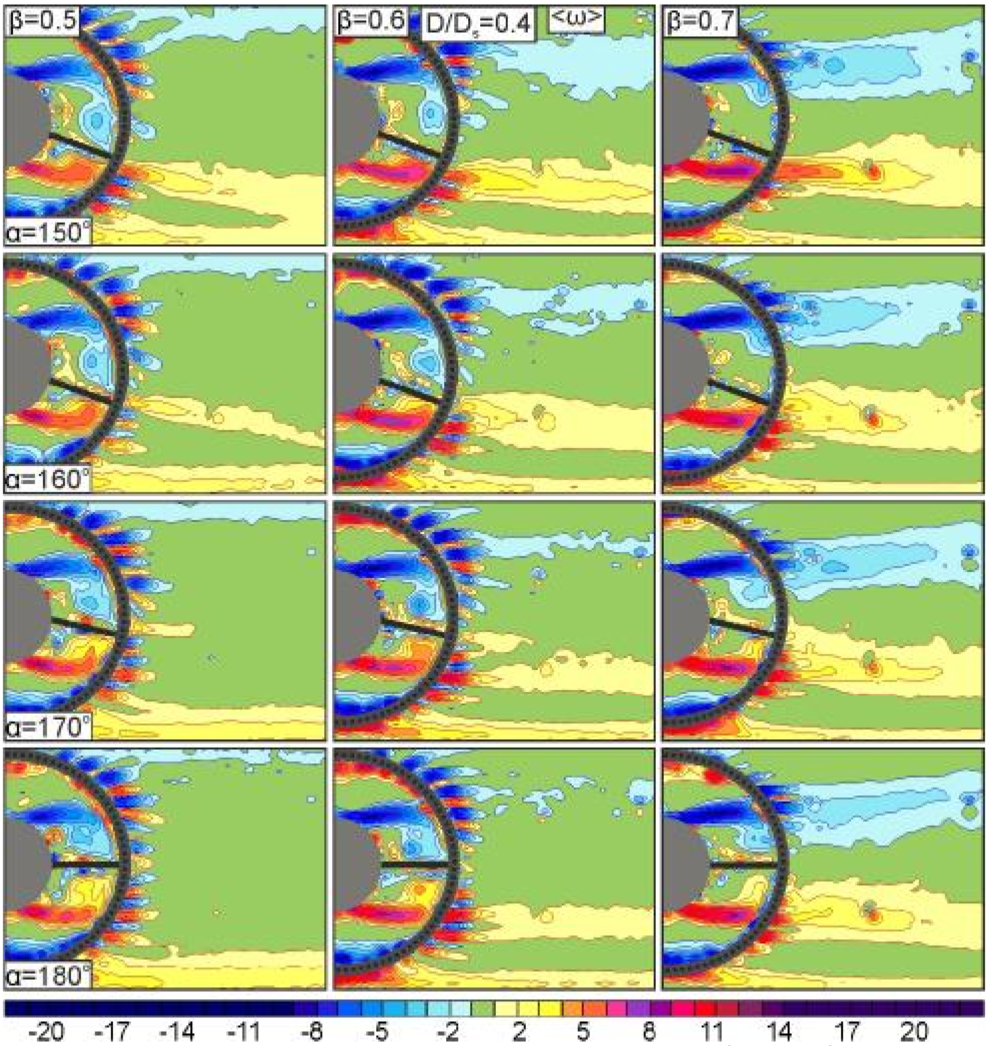

Figure 4.10b. Time averaged vorticity contour, <ω> for $150^o \leq \alpha \leq 180^o$ plate angles for various porosity of the perforated cylinders, β at the diameter ratio of D/D_s=0.4.

Figure 4.11 shows the profiles of mean stream-wise velocity downstream of the cylinder for various splitter plate angles, α and porosity, β at the different locations, x/D. In order to constitute reference and carry out comparison, the results for the bare cylinder and no-plate case are also included. For the plate angle of $\alpha=120^o$ and 140^o, the mean stream-wise velocity has larger deficiency compared with other two plate angle cases at all locations. Moreover, the negative velocity value occurred in the region of y/D grows with the increasing porosity, β for the plate angle of $\alpha=120^o$ and 140^o. This situation indicates that the cases of the plate angle of $\alpha=120^o$ and 140^o cause more momentum transfer from the lower shear layer into the near - wake region. It is interesting to note that the velocity deficit increases at the further downstream locations for the plate angle $\alpha=120^o$ and 140^o. Moreover, it is observed that the velocity profile of $\alpha=180^o$ is nearly similar with the no-plate case for all porosity, β at all locations.

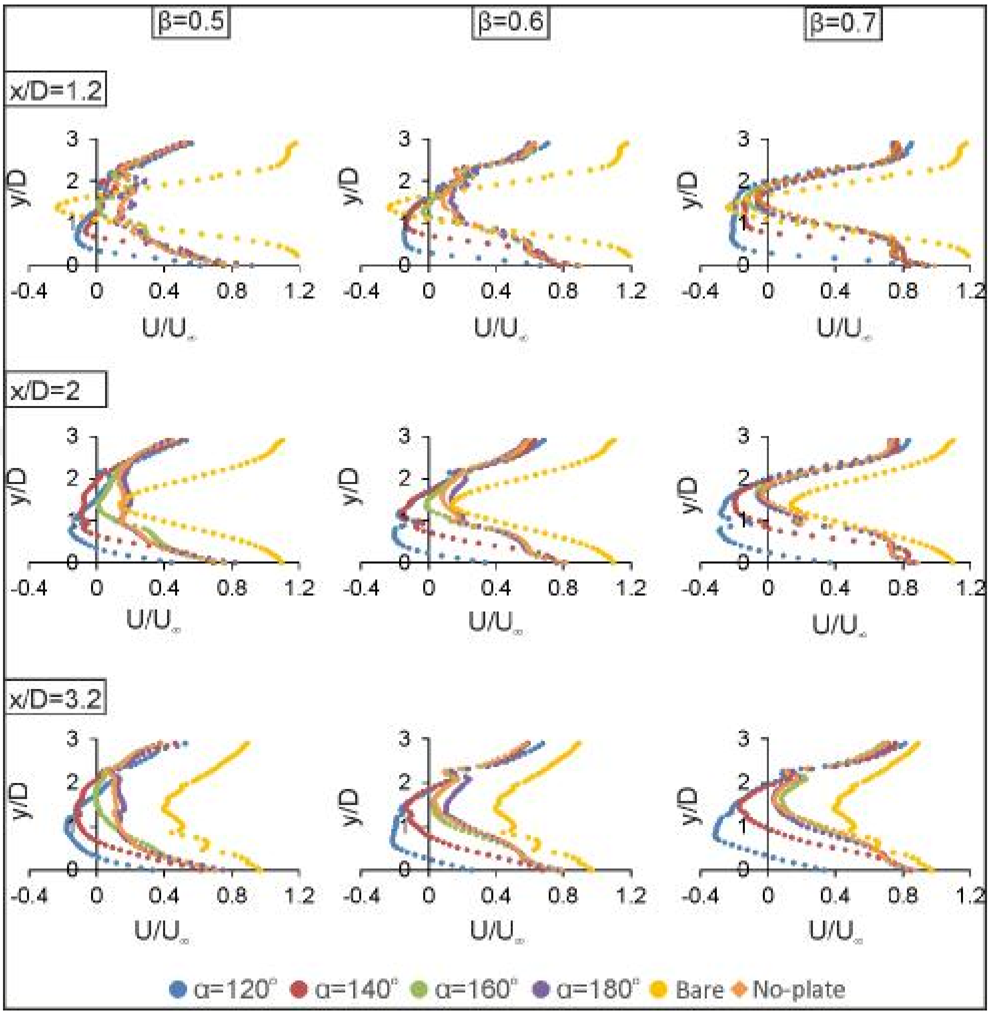

Figure 4.11. Profiles of mean stream-wise velocity of D/D_s=0.4 for cases of β=0.5, 0.6 and 0.7 and various plate angle, α at x/D=1.2, 2 and 3.2.

Figure 4.12a presents the time-averaged velocity vector map, <V> superposed with the stream-wise velocity contours, <u> for the plate length of L_p=1 case for the plate angles of 120^o ≤ α ≤140^o at the diameter ratio of D/D_s = 0.5. Effect of the splitter plate angle on the flow structure of the near-wake region has similar trend with the results obtained from the diameter ratio of D/D_s = 0.4. The reversed flow occurs in the near-wake region and the magnitude of velocity of the reverse flow decreases with the increasing plate angle, α. The width of reversed flow zone in the near-wake region is lower than the diameter ratio of D/D_s = 0.4 due to increasing cross sectional area of the splitter plate.

Figure 4.12b provides the time averaged velocity vector map, <V> superposed with the stream-wise velocity contours for the plate angles of 150^o ≤ ≤ 180^o. By increasing the splitter plate angle, α, it brings out slight changes in the flow structure compared to the no-plate case of the diameter ratio of D/D_s = 0.4. Especially for plate angle of α ≥170^o, the magnitude of velocity in the near-wake region is higher than the no-plate case for porosity values of β=0.5. Also, the size of reversed flow zone is lower than the no-plate case for the porosity value of β=0.6 and 0.7.

The time-averaged vorticity, <ω> contours of the diameter ratio of D/D_s = 0.5 is presented in Figures 4.13a and 4.13b for the plate angles 120^o≤ α ≤ 180^o, at different porosity, β. The vorticity in the leading edge is effective on the flow structure up to the plate angle α=140^o owing to fact that the plate causes to enhance the momentum transfer into the near-wake region. For the plate angles of α ≥ 150^o, the plate has insignificant effect on the flow structure of near-wake region in comparison with the no-plate case. The vorticity, <ω> in the leading edge disappears for the plate angles of α ≥ 150^o, since the plate does not distribute the shear layer in the lower side of the cylinder.

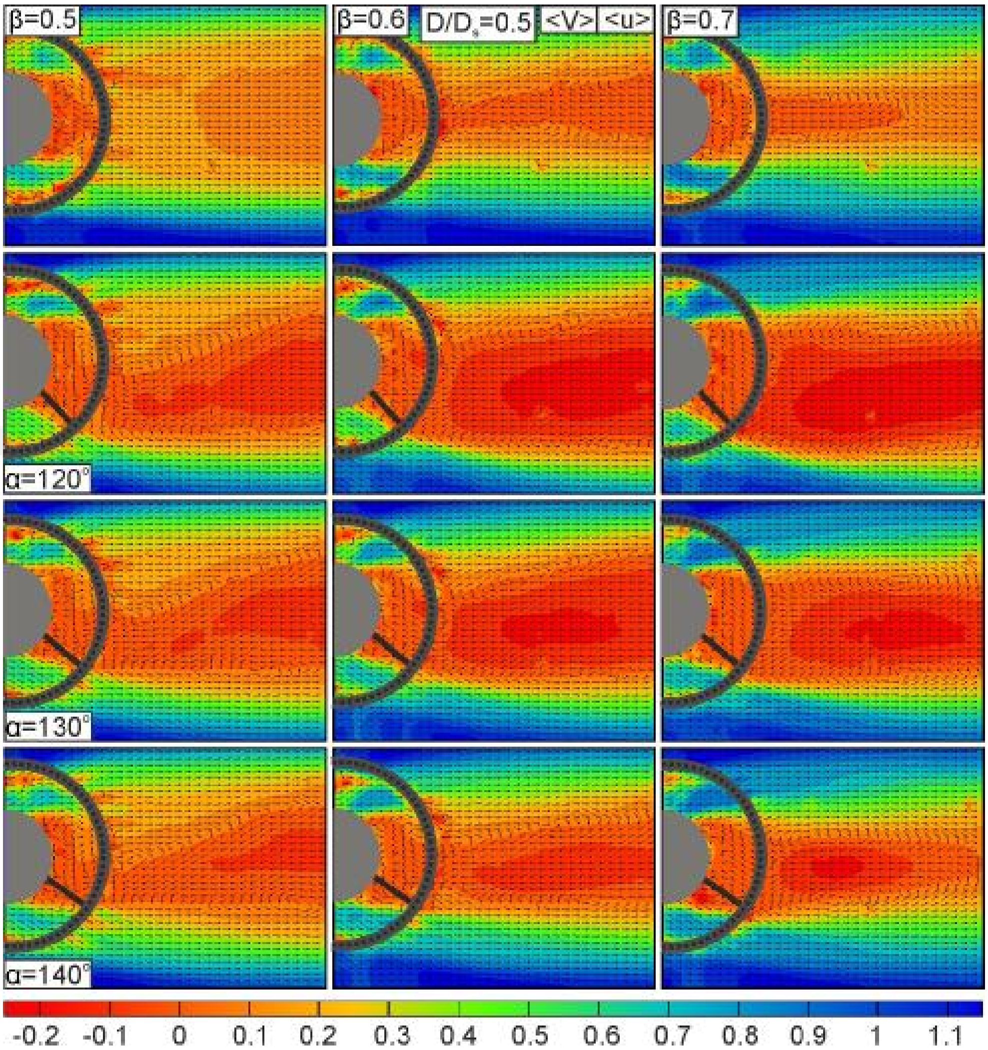

Figure 4.12a. Time averaged velocity vector field, <V> superposed with the stream-wise velocity contours, <u> for $120^o \leq \alpha \leq 140^o$ plate angles for various porosity of the perforated cylinders, β at the diameter ratio of D/D_s=0.5.

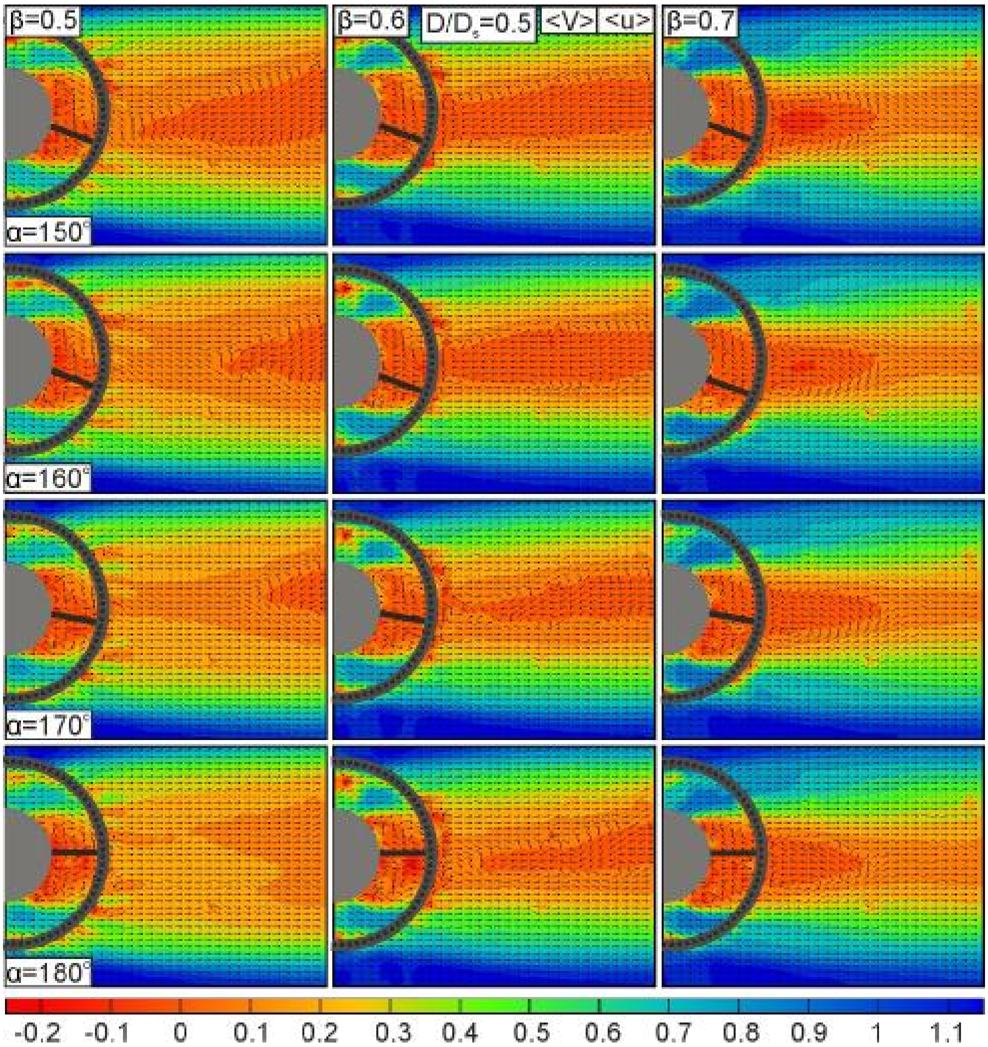

Figure 4.12b. Time averaged velocity vector field, <V> superposed with the stream-wise velocity contours, <u> for $150^o \leq \alpha \leq 180^o$ plate angles for various porosity of the perforated cylinders, β at the diameter ratio of D/D_s=0.5.

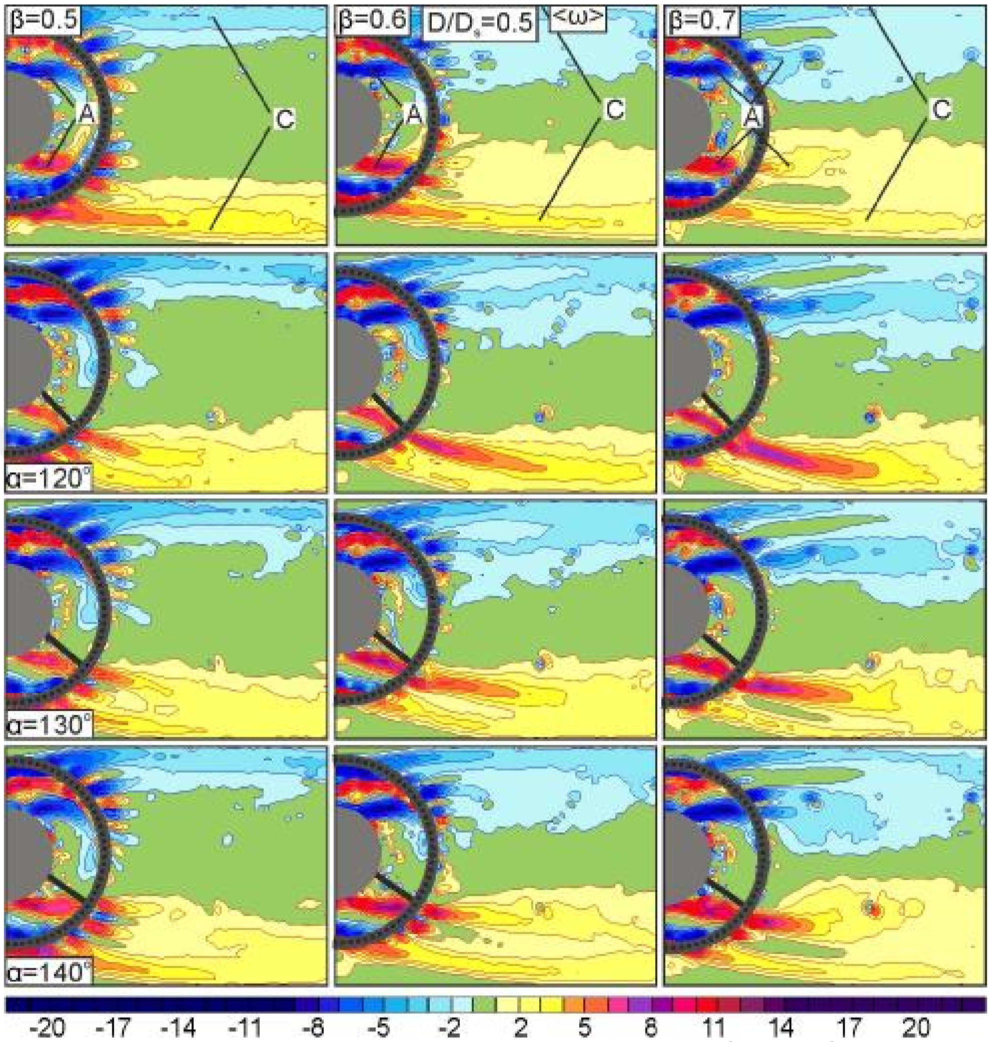

Figure 4.13a. Time averaged vorticity contour, <ω> for $120^o \leq \alpha \leq 140^o$ plate angles for various porosity of the perforated cylinders, β at the diameter ratio of $D/D_s=0.5$.

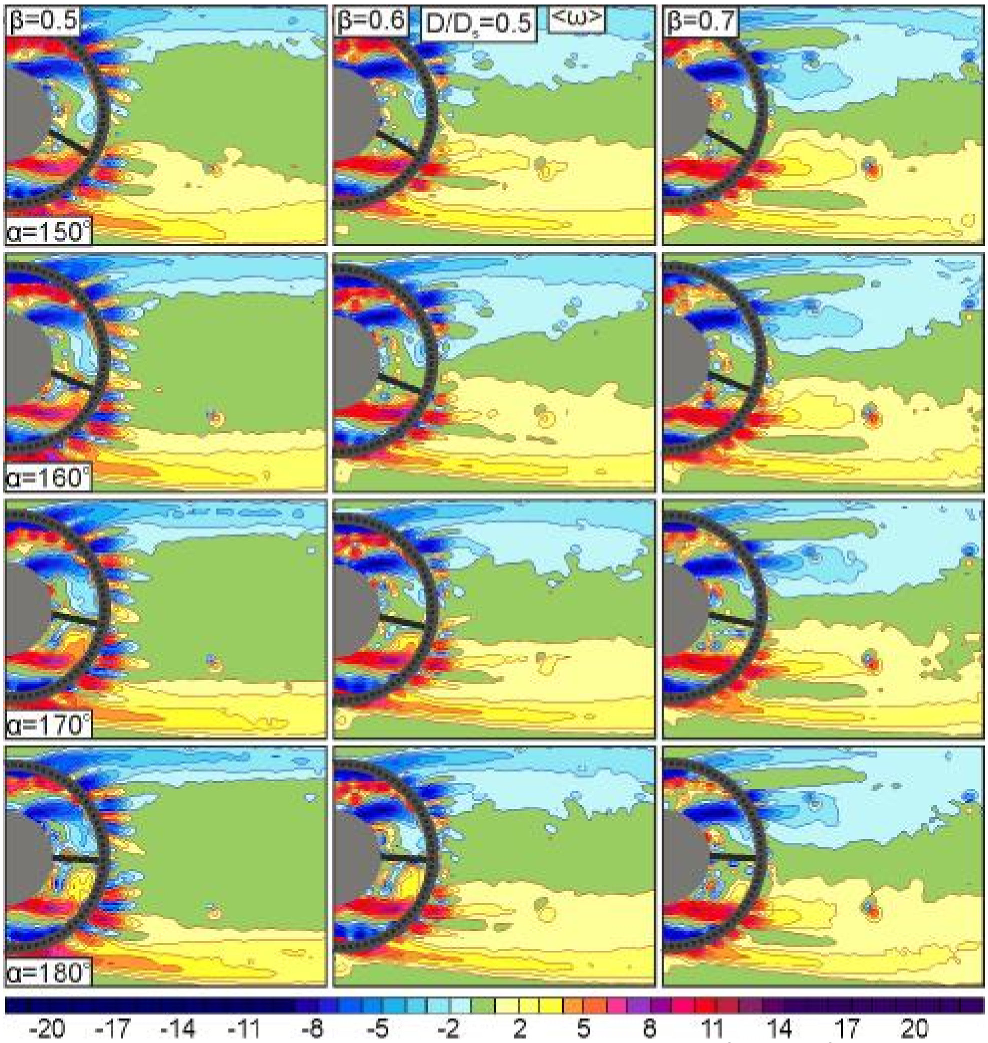

Figure 4.13b. Time averaged vorticity contour, <ω> for $150^o \leq \alpha \leq 180^o$ plate angles for various porosity of the perforated cylinders, β at the diameter ratio of D/D_s=0.5.

The profile of time-averaged mean stream-wise velocity of D/D_s=0.5 is presented in Figure 4.14 for the porosities of β=0.5, 0.6 and 0.7 at location of x/D=1.2, 2 and 3.2. The results obtained from the diameter ratio of D/D_s=0.5 depict that the plate angles of α=160° and 180° show similar trend with the diameter ratio of D/D_s=0.4 for all porosity, β. Also, it is observed that the velocity deficit for the plate angle of $\alpha=120^o$ is approximately same at the all locations contrary to the diameter ratio of $D/D_s=0.4$. It should be pointed out even for the porosity of $\beta=0.7$, the velocity deficit for the plate angle of $\alpha=140^o$ is decreased at the location of x/D=3.2.

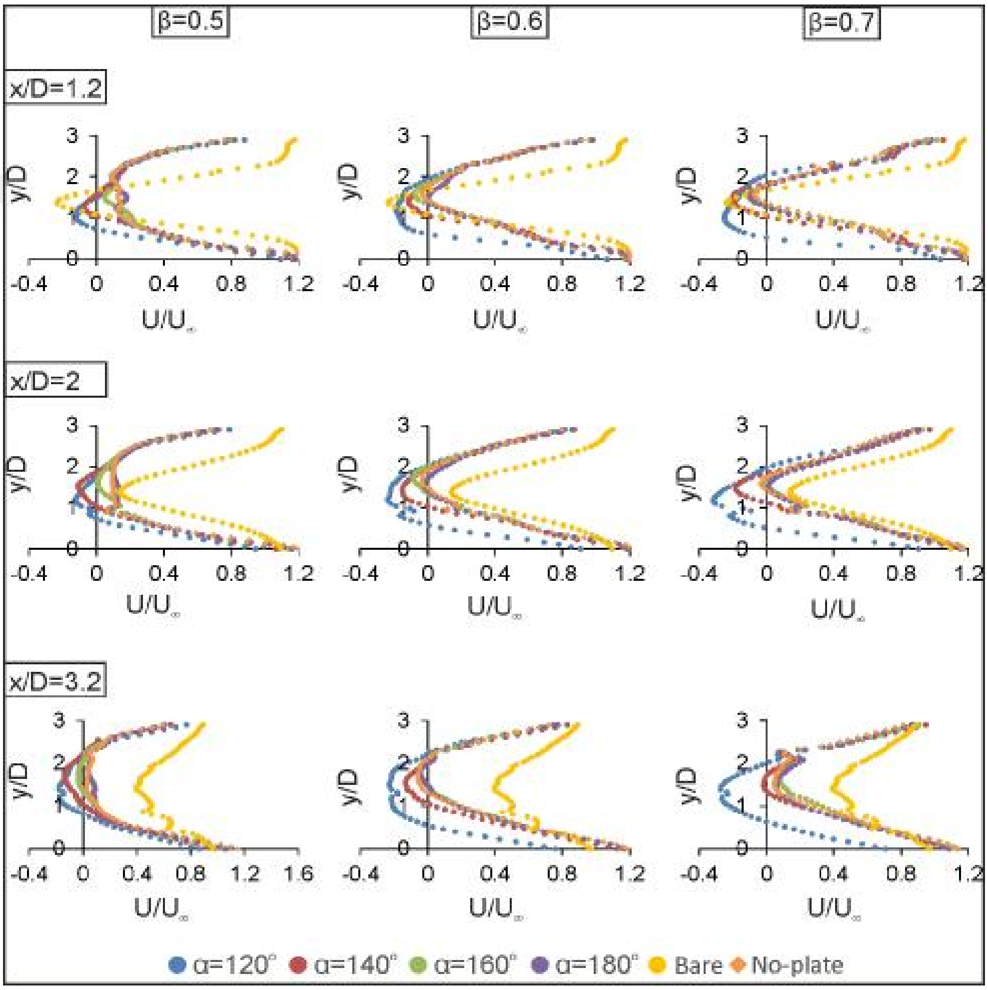

Figure 4.14. Profiles of mean stream-wise velocity of $D/D_s=0.5$ for cases of $\beta=0.5$, 0.6 and 0.7 and various plate angle, α at x/D=1.2, 2 and 3.2.

Figure 4.15 shows that variation of total drag coefficient with the plate angle for various porosities of the perforated cylinder for different diameter ratios at $Re=5\times10^3$. Figure 4.15a and 4.15b indicate that total drag coefficient, $<C_{DC}>$ which is calculated based on the frontal area of the cylinder slightly reduces with the increasing plate angle, α. Furthermore, the total drag coefficient of the diameter ratio $D/D_s=0.4$ is higher than diameter ratio of $D/D_s=0.5$, since it has larger cross sectional area. On the other hand, Figures 4.15c and 4.15d indicate that the plate angle, α and the diameter ratio, D/D_s have insignificant effect on the total drag coefficient, $<C_{DS}>$, which is calculated based on the frontal area of the perforated cylinder. The total drag coefficients of $D/D_s=0.4$ and 0.5 have nearly same with bare cylinder case for all porosity, β.

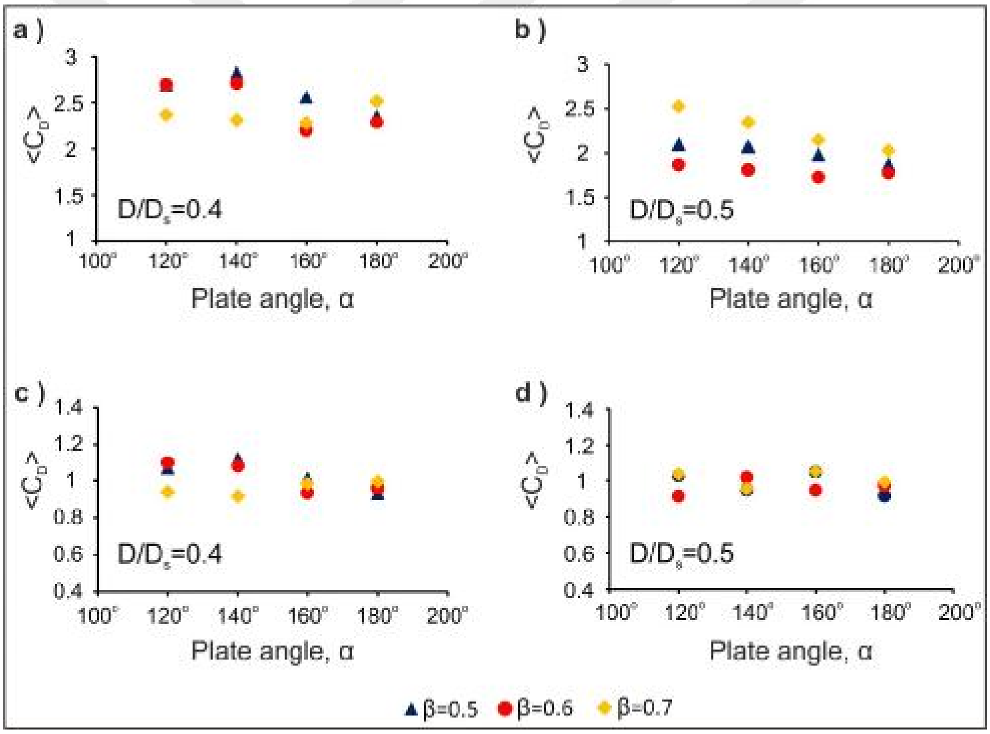

Figure 4.15. The effect of the plate angle, α on the total drag coefficient at $Re=5\times10^3$; a) total drag coefficient, $<C_{DC}>$ for $D/D_s=0.4$, b) total drag coefficient, $<C_{DC}>$ for $D/D_s=0.5$, c) total drag coefficient, $<C_{DS}>$ for $D/D_s=0.4$, d) total drag coefficient, $<C_{DS}>$ for $D/D_s=0.5$.

At Re=15×10[3], the variation of total drag coefficient, <C_{DC}>, which is calculated based on the frontal area of the cylinder, with the plate angle, α are presented in Figures 4.16a and 4.16b for the diameter ratios D/D_s = 0.4 and 0.5, respectively and the variation of total drag, <C_{DS}>, which is calculated based on the frontal area of the perforated cylinder, are presented in the Figures 4.16c and 4.16d for D/D_s = 0.4 and 0.5, respectively. At Re=15×10[3], it is observed that the variation of total drag coefficient with the plate angle, α has a similar trend by comparing with the Re=5×10[3] for diameter ratios of D/D_s = 0.4 and 0.5. The total drag coefficient slightly reduces with the increasing plate angle, α. It is clearly seen that the porosity of perforated cylinder, β has insignificant effect on the total drag coefficient.

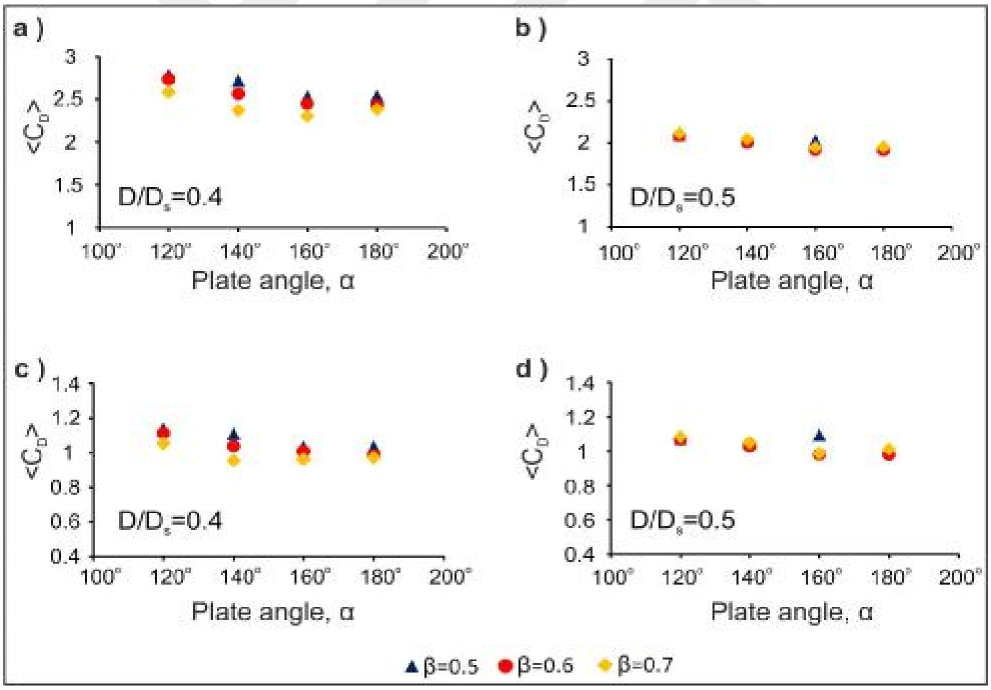

Figure 4.16. The effect of the plate angle, α on the total drag coefficient at Re=15×10[3]; a) total drag coefficient, <C_{DC}> for D/D_s=0.4, b) total drag coefficient, <C_{DC}> for D/D_s=0.5, c) total drag coefficient, <C_{DS}> for D/D_s=0.4, d) total drag coefficient, <C_{DS}> for D/D_s=0.5.

Time averaged total lift coefficient is calculated both based on the lateral area of the cylinder, A_C and the lateral area of the perforated cylinder, A_S for the diameter ratios of D/D_s=0.4 and 0.5 for all cases. The total lift coefficient is evaluated as zero for no-plate cases. Nevertheless, using of the splitter plate in the gap region between the cylinder and the perforated cylinder significantly affects total lift coefficient. Table 4.1 presents the variation of total lift coefficient with the plate angle, α at the $Re=15\times10^3$. For the diameter ratio of D/D_s=0.4, the total lift coefficients which are calculated based on lateral area of the cylinder, A_C and the lateral area of perforated cylinder, A_S are displayed in tables 4.1a and 4.1b, respectively. The maximum total lift coefficient is evaluated for the porosity of β=0.7 at the plate angle $\alpha=120^o$, since increasing porosity, β enhances momentum transfer into the gap region, and decreasing plate angle, α causes asymmetric flow in the gap region between the cylinder and the perforated cylinder. The total lift coefficient decreases gradually with the increasing splitter plate angle, α. The total lift coefficient values are approximately zero for all porosity at the plate angle of $\alpha=180^o$ due to symmetric flow downstream of the cylinder. For the diameter ratio of D/D_s=0.5, total lift coefficients which are calculated based on the lateral area of the cylinder, A_C and the lateral area of perforated cylinder, A_S are shown in the Tables 4.1c and 4.1d, respectively. Although the variation of total lift coefficients with the plate angle, α have a similar trend with the results obtained from the diameter ratio D/D_s=0.4, the total lift coefficients are lower than the diameter ratio of D/D_s=0.4 because the lateral area of this diameter ratio, D/D_s=0.4 is higher.

Table 4.1. The effect of the plate angle, α on the total lift coefficient at Re=15×10^3; a) total lift coefficient based on the A_C for D/D_s=0.4, b) total lift coefficient based on the A_S for D/D_s=0.4, c) total lift coefficient based on the A_C for D/D_s=0.5 d) total lift coefficient based on the A_S for D/D_s=0.5.

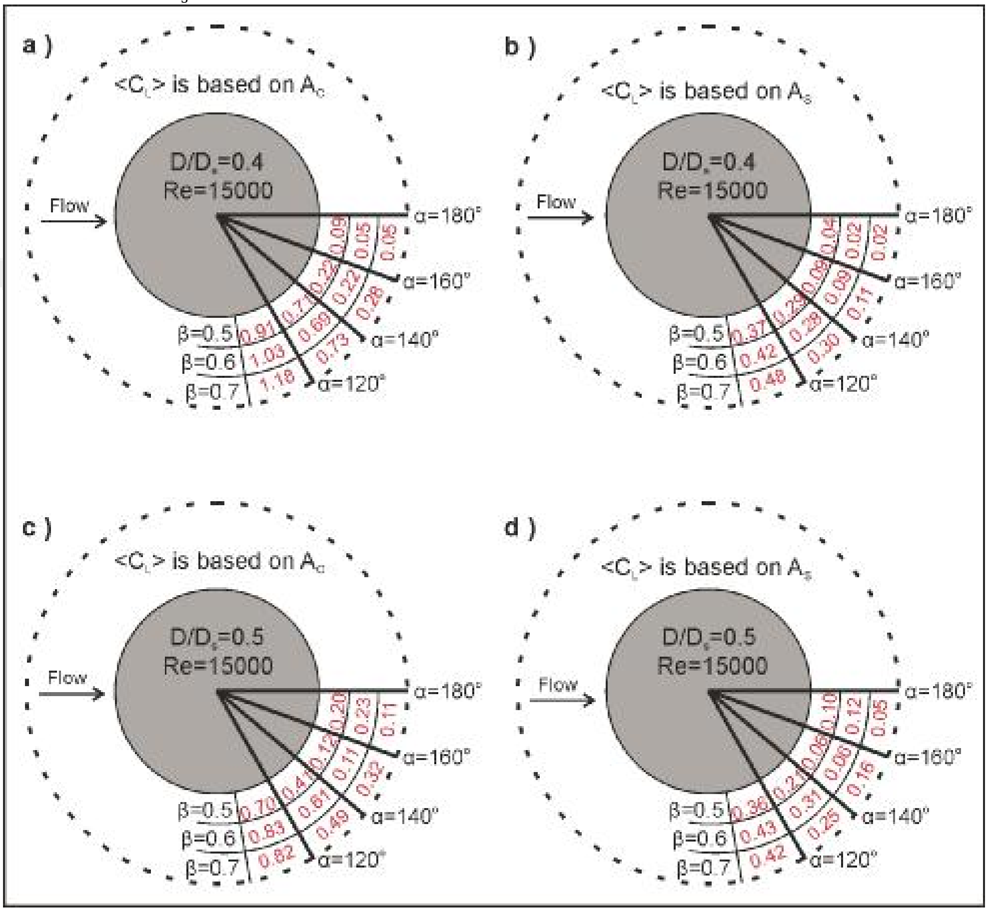

In order to investigate the effect of the plate length, Figure 4.17 presents the time averaged velocity vector map, <V> superposed with the stream-wise velocity contours, <u> for the plate length of L_p=3/4 case for the plate angles of 120^o ≤ α ≤ 180^o at the diameter ratio of D/D_s = 0.4. The plate is located in contact with the cylinder in the gap region between the cylinder and the perforated cylinder. Although using of L_p=3/4 in contact with the cylinder have similar effect on the flow structure of the gap region, the flow structure in the near-wake region is affected compared to the plate length of L_p=1. For the plate angle of α=140^o, the size of reversed flow in the near-wake region remarkably decreases in comparison with the plate length of L_p=1. Furthermore, the reversed flow disappears in the near-wake region for the plate angle of α=160^o at porosities values of β=0.5 and 0.6. The size of the recirculation zone in the lower side of the cylinder is lower than the plate length of L_p=1 for the plate angle of α=160^o at all porosity values.

The results obtained from the plate length of L_p=3/4 and in contact with the perforated cylinder are shown in figure 4.18 for the plate angles of $120^o \leq \alpha \leq 180^o$ at the various porosities of perforated cylinder. The flow structure in the gap region between the cylinder and the perforated cylinder changes significantly compared to the plate in contact with the cylinder for the plate angle of α=120^o. The flow emanating from the gap where between the splitter plate and the cylinder causes a jet alike flow towards upper side of the cylinder. Therefore, the occurrence of recirculation zone in the upper size of the cylinder is remarkably disturbed. The plate angles of $\alpha \geq 160^o$ have nearly same effect on the flow structure of both inside and outside of the perforated cylinder.

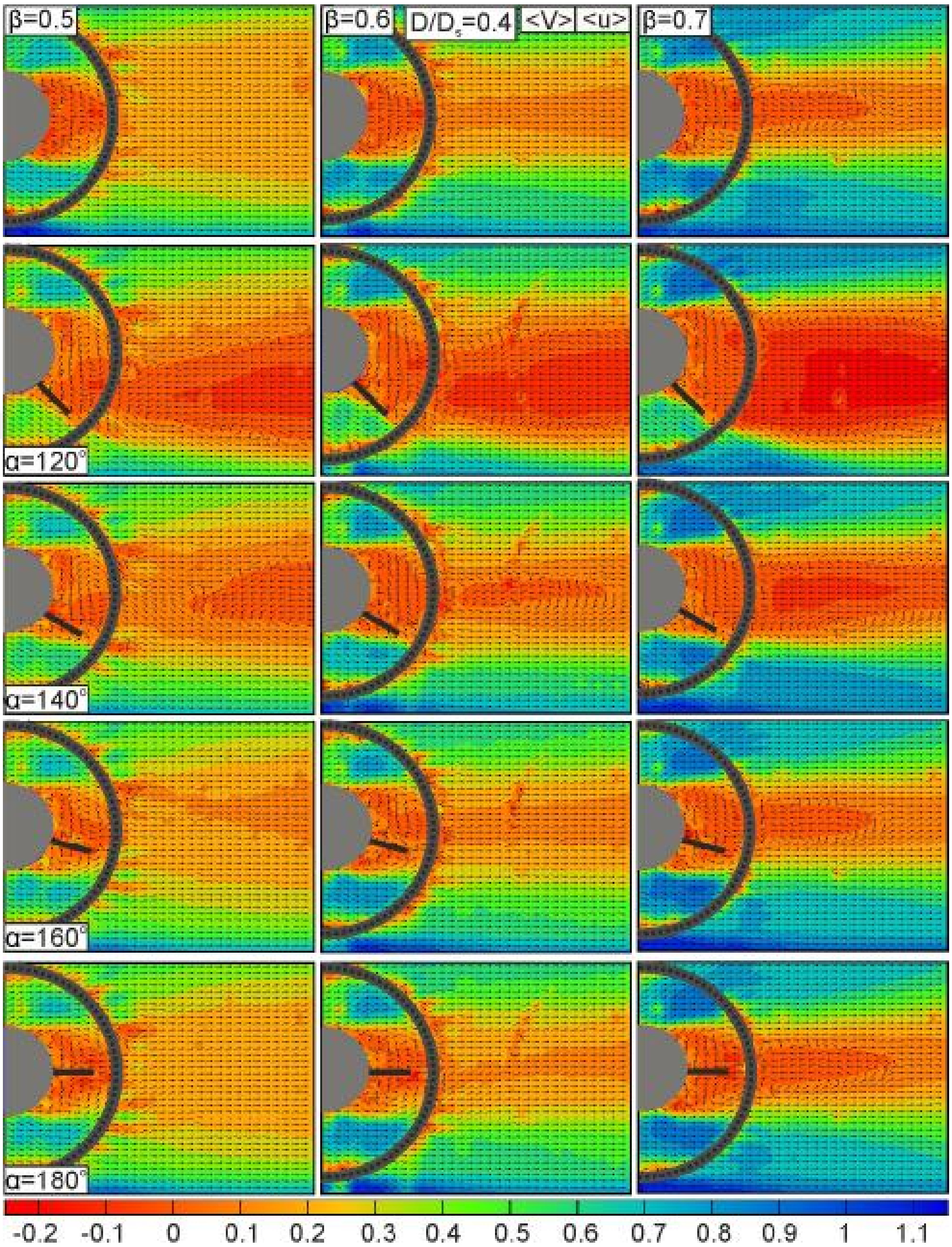

Figure 4.17. Time averaged velocity vector field, <V> superposed with the stream-wise velocity contours, <u> for the plate length of L_p=3/4 and in contact with the cylinder case for various plate angles and porosity of the perforated cylinders, β at the diameter ratio of D/D_s=0.4.

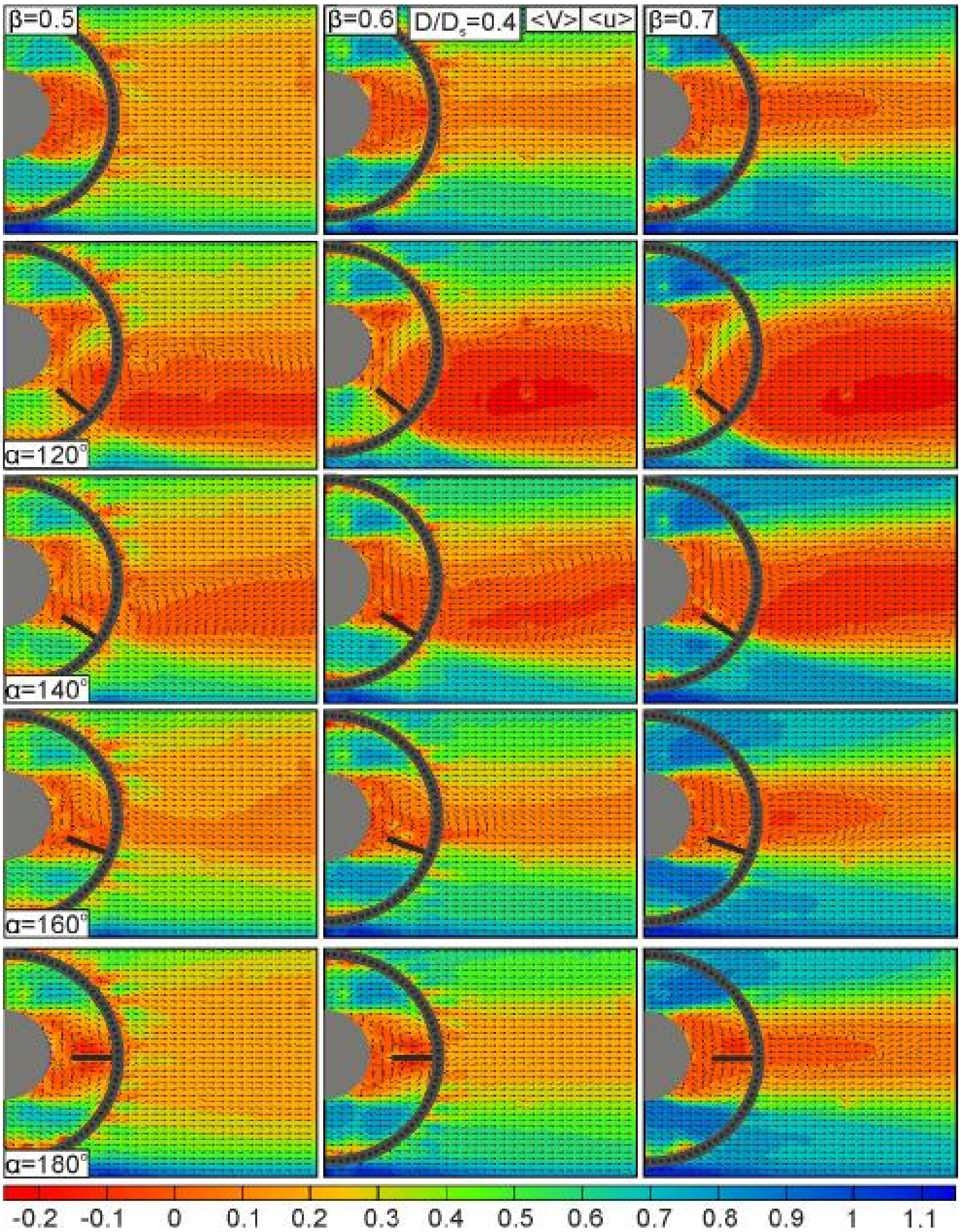

Figure 4.18. Time averaged velocity vector field, <V> superposed with the streamwise velocity contours, <u> for the plate length of L_p=3/4 and in contact with the perforated cylinder case for various plate angles and porosity of the perforated cylinders, β at the diameter ratio of D/D_s=0.4.

Figures 4.19 and 4.20 presents the time averaged vorticity contours, $<\omega>$ obtained for the splitter plate in contact with both the cylinder and the perforated cylinder, respectively. For the splitter plate in contact with the cylinder, the formation of vorticity in the gap region between the cylinder and the perforated cylinder and the near-wake region is nearly similar with the plate length of L_p=1 except for the case of the β=0.5 of α=160^o. For the porosity value of β=0.5 at the plate angle of α=160^o, it is not observed occurrence of the vorticity in the leading edge of the splitter plate compared to the plate length of L_p=1. Furthermore, the flow structure in the gap region between the cylinder and the perforated cylinder dramatically changes for the plate in contact with the perforated cylinder at the plate angle of α=120^o. A distinct vorticity pair which is designated by 'D' occurs in the upper side of cylinder due to jet-like flow where between the cylinder and the splitter plate. The splitter plate in contact with the perforated cylinders have similar effect on the formation of the vorticity in both the inside of perforated cylinder and the outside of the perforated cylinder for the plate angle of $\alpha \geq 140^o$.

For the diameter ratio of D/D_s=0.4, the profiles of mean stream-wise velocity of the L_p=3/4 in contact with the cylinder and the perforated cylinder are given in Figures 4.21, 4.22 and 4.23 at locations of x/D=1.2, 2 and 3.2, respectively. Within the porosities ranges of $0.5 \leq \beta \leq 0.7$, mean stream-wise velocity deficits for the plate angle of α=120^o in contact with the cylinder are approximately same by comparing with the same plate angle in contact with the perforated cylinder at all locations. Moreover, this trend is similar with the L_p=1 with slight changes. The negative velocity region is also taken place for all cases. The velocity deficits for L_p=3/4 of α=140^o are remarkably smaller than the case of L_p=1 of α=140^o. On the other hand, the velocity deficits for α=160^o and 180^o are approximately same with the no-plate case at all locations.

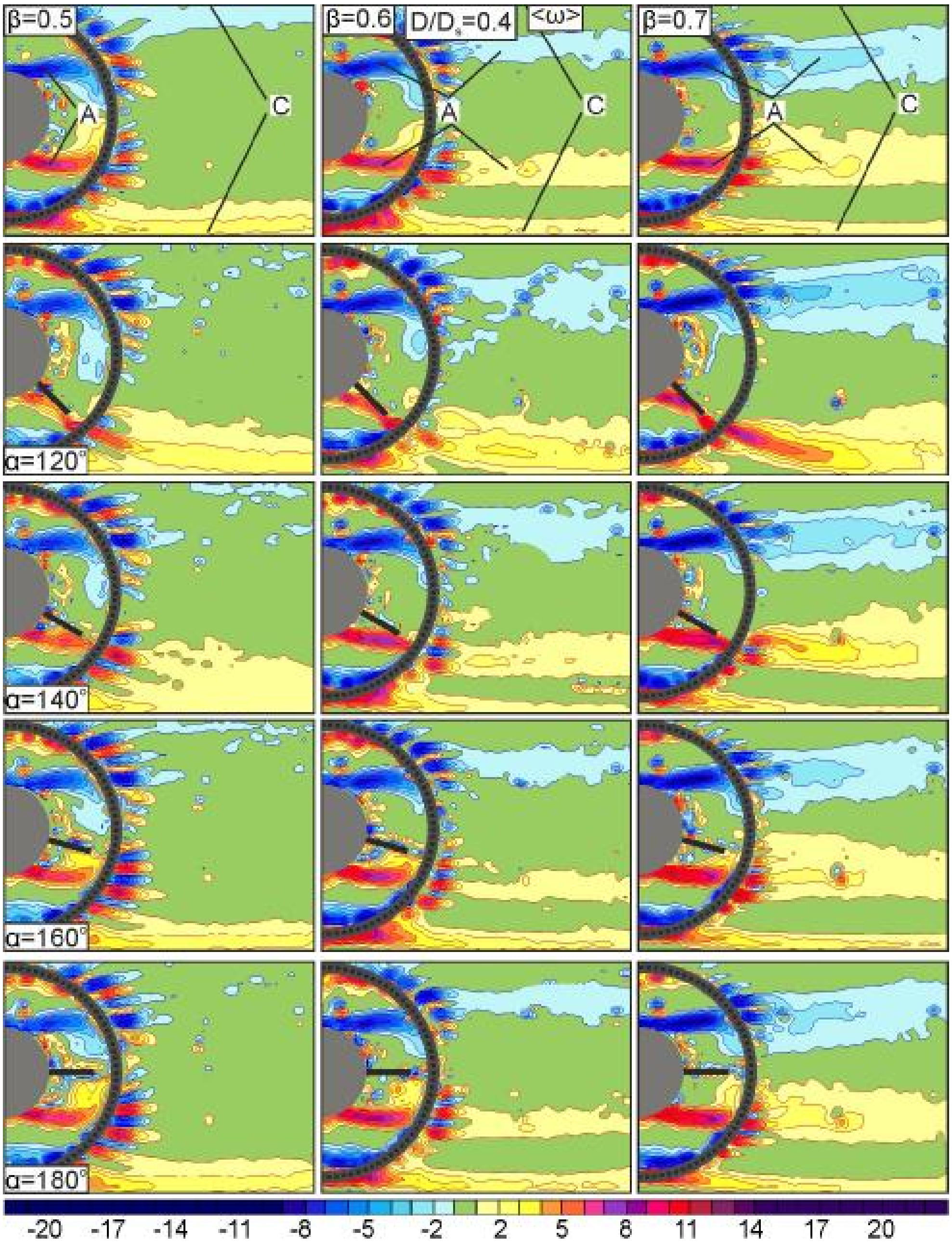

Figure 4.19. Time averaged vorticity contour, <ω> for the plate length of L_p=3/4 and in contact with the cylinder case for various plate angles and porosity of the perforated cylinders, β at the diameter ratio of D/D_s=0.4.

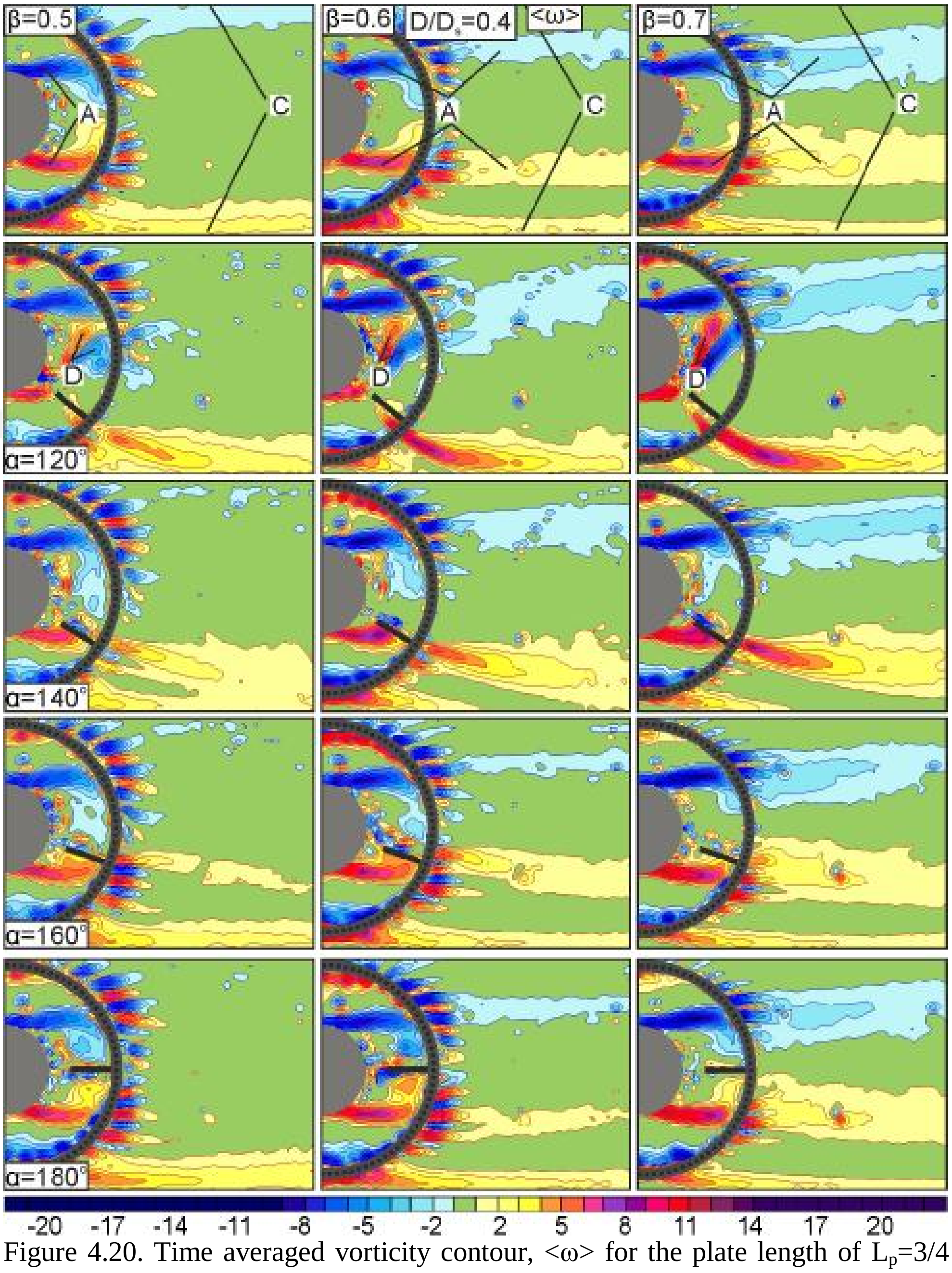

Figure 4.20. Time averaged vorticity contour, <ω> for the plate length of L_p=3/4 and in contact with the perforated cylinder case for various plate angles and porosity of the perforated cylinders, β at the diameter ratio of D/D_s=0.4.

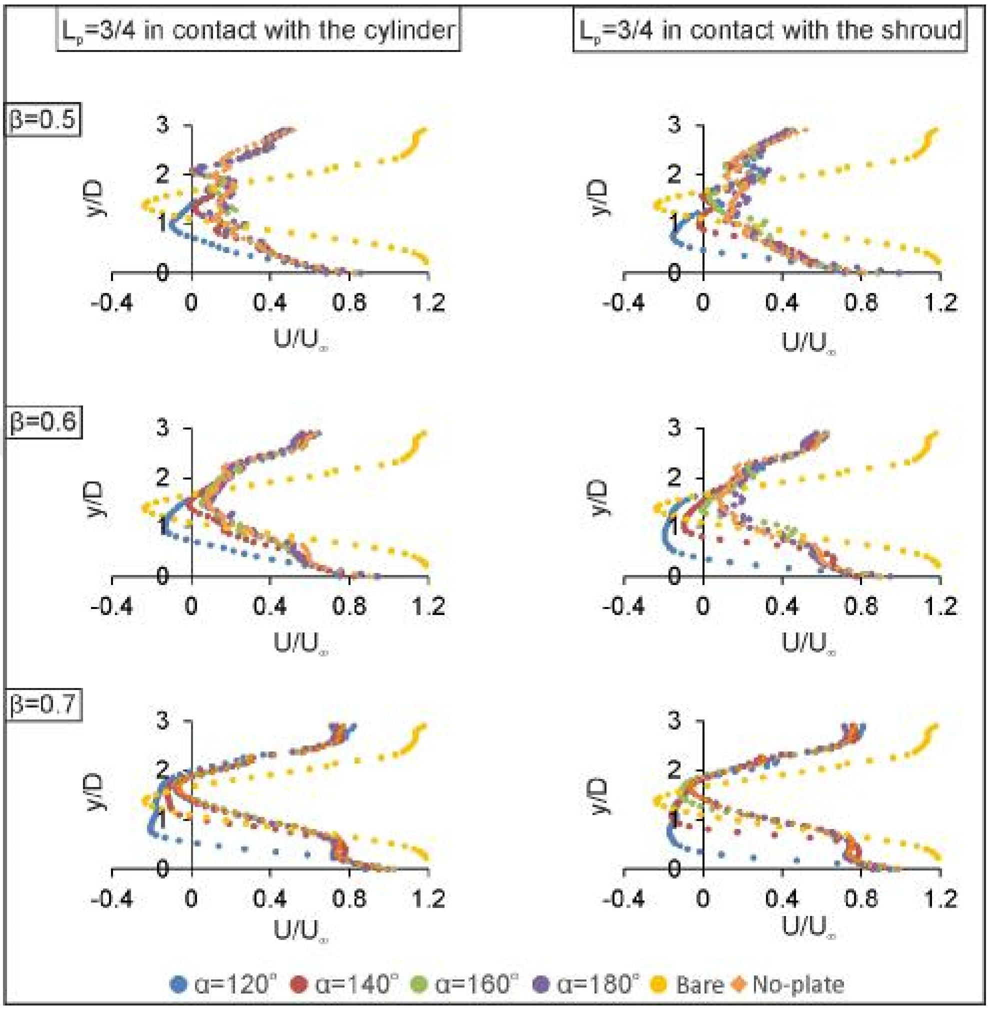

Figure 4.21. Profiles of mean stream-wise velocity of D/D_s=0.4 for L_p=3/4 in contact with the cylinder and the perforated cylinder cases at x/D=1.2.

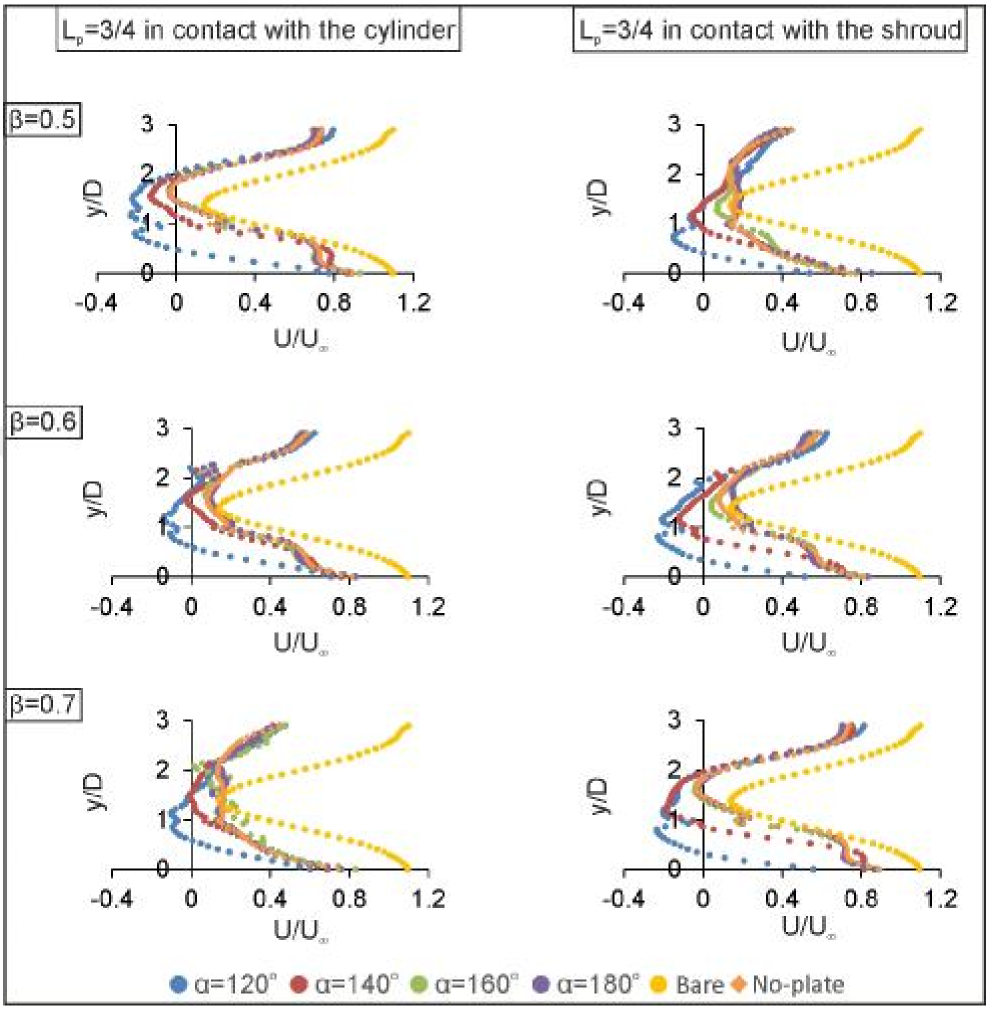

Figure 4.22. Profiles of mean stream-wise velocity of D/D_s=0.4 for L_p=3/4 in contact with the cylinder and the perforated cylinder cases at x/D=2.

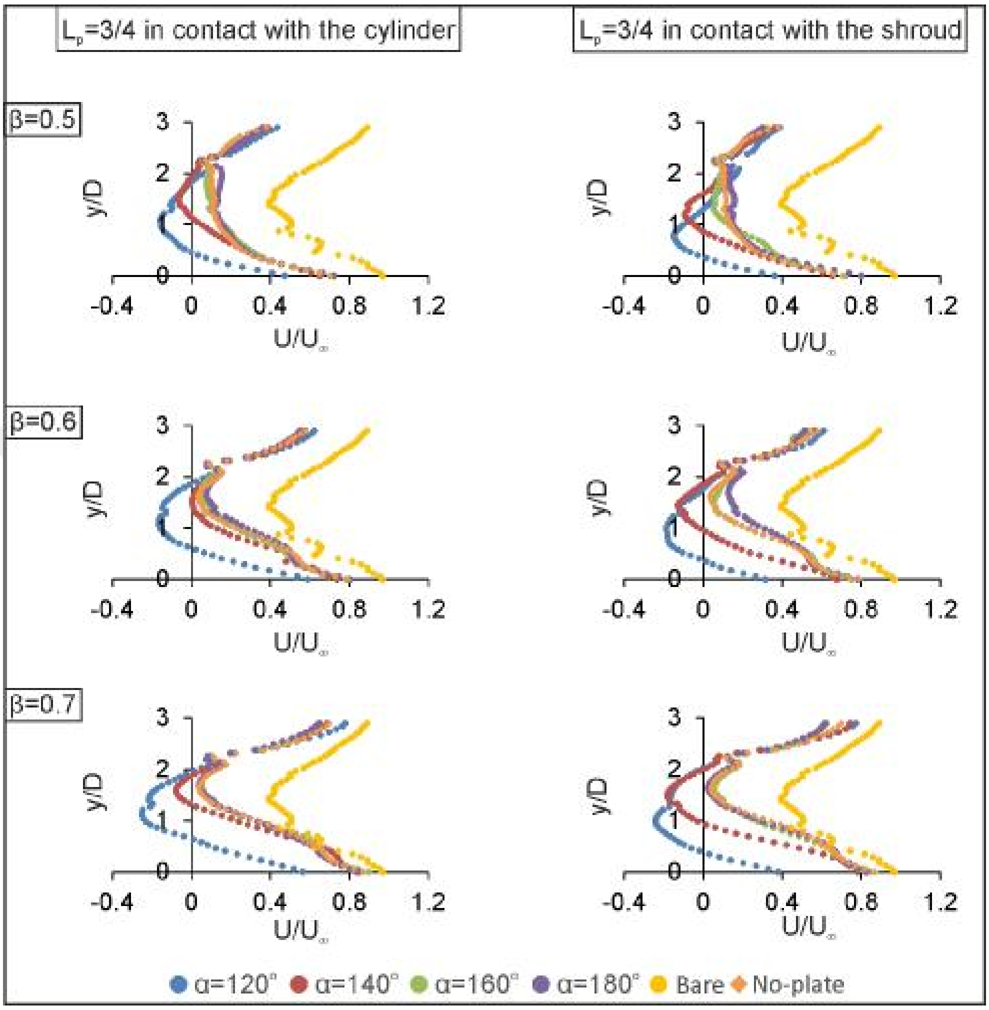

Figure 4.23. Profiles of mean stream-wise velocity of D/D_s=0.4 for L_p=3/4 in contact with the cylinder and the perforated cylinder cases at x/D=3.2.

For the diameter ratio of D/D_s =0.5, the effect of plate length of L_p=3/4 on the flow structure is shown in Figures 4.24, 4.25, 4.26 and 4.27. Time averaged velocity vector map, <V> superposed with the stream-wise velocity contours, <u> is presented for the splitter plate in contact with the cylinder and the splitter plate in contact with the perforated cylinder in Figures 4.24 and 4.25, respectively. The time averaged vorticity contours, <ω> of the splitter plate in contact with the cylinder and the splitter plate in contact with the perforated cylinder are shown in Figures 4.26 and 4.27, respectively. It is observed that the effect of the plate length of L_p=3/4 on the flow structure is almost same when compared with the results obtained from the diameter ratio of D/D_s =0.4 for the plate angle of $\alpha \geq 160^o$. However, the jet-like flow has insignificant effect on the disruption of the recirculation flow in the upper side of cylinder for the plate angle of $\alpha=120^o$ for the plate in contact with the perforated cylinder due to reducing momentum transfer towards the upper side of the cylinder.

The mean stream-wise velocity profiles obtained from the D/D_s=0.5 of L_p=3/4 are presented in Figures 4.28, 4.29 and 4.30 at the locations of x/D=1.2, 2 and 3.2, respectively. Especially for the splitter plate angles of $\alpha=120^o$ and 140^o, the results depict that the velocity deficits of L_p=3/4 in contact with the cylinder are smaller than L_p=3/4 in contact with the perforated cylinders at the all locations. For the porosity of β=0.7 with the plate angle of $\alpha=120^o$, the negative velocity region of L_p=3/4 in contact with the perforated cylinder is larger than the splitter plate in contact with the cylinder at all locations. It is clearly seen that the plate has insignificant effect on the mean stream-wise velocity for the plate angles of $\alpha=160^o$ and 180^o when compared to the no-plate case. The velocity deficits for $\alpha=160^o$ and 180^o are extremely similar with the no-plate case at all locations.

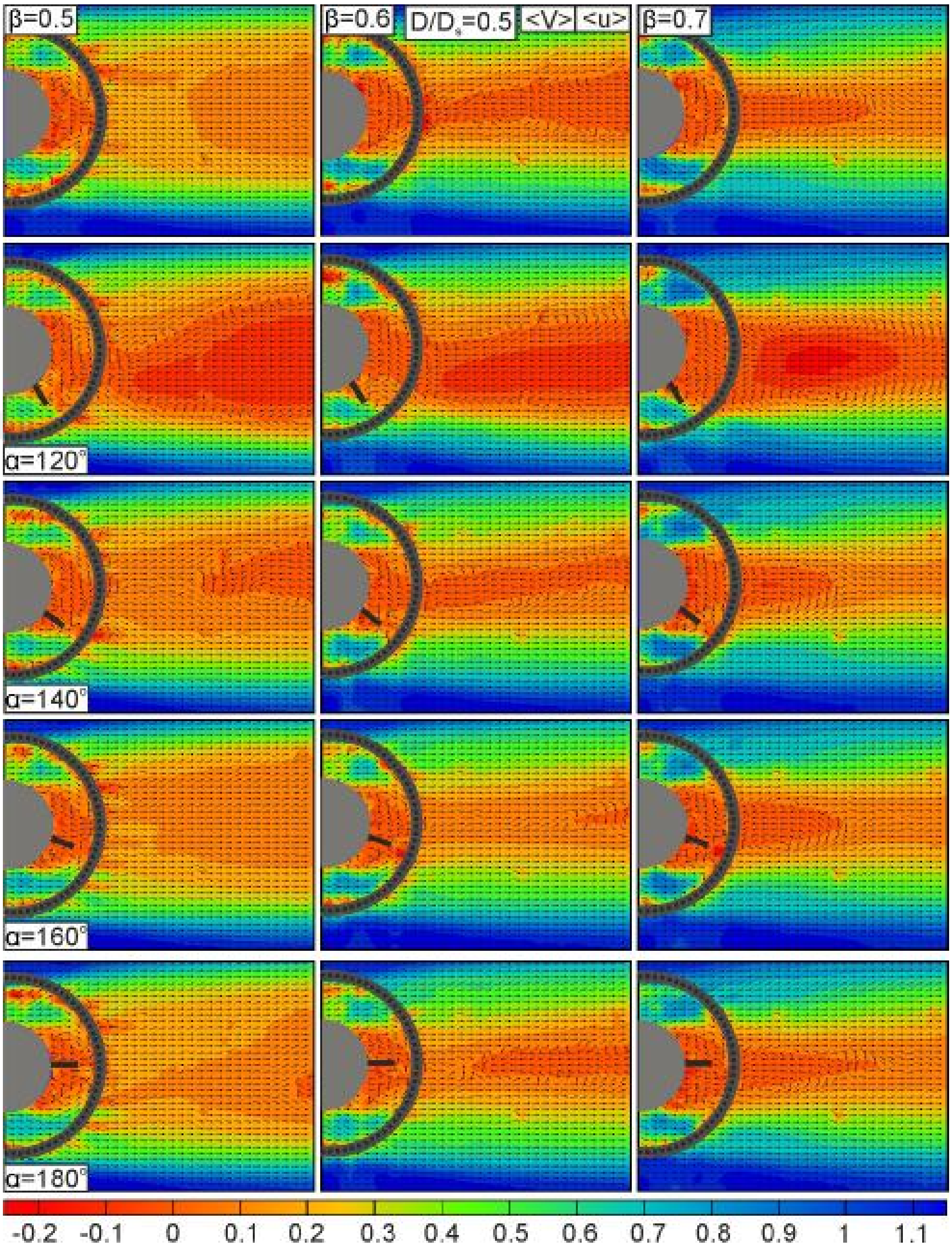

Figure 4.24. Time averaged velocity vector field, <V> superposed with the streamwise velocity contours, <u> for the plate length of L_p=3/4 and in contact with the cylinder case for various plate angles and porosity of the perforated cylinders, β at the diameter ratio of D/D_s=0.5.

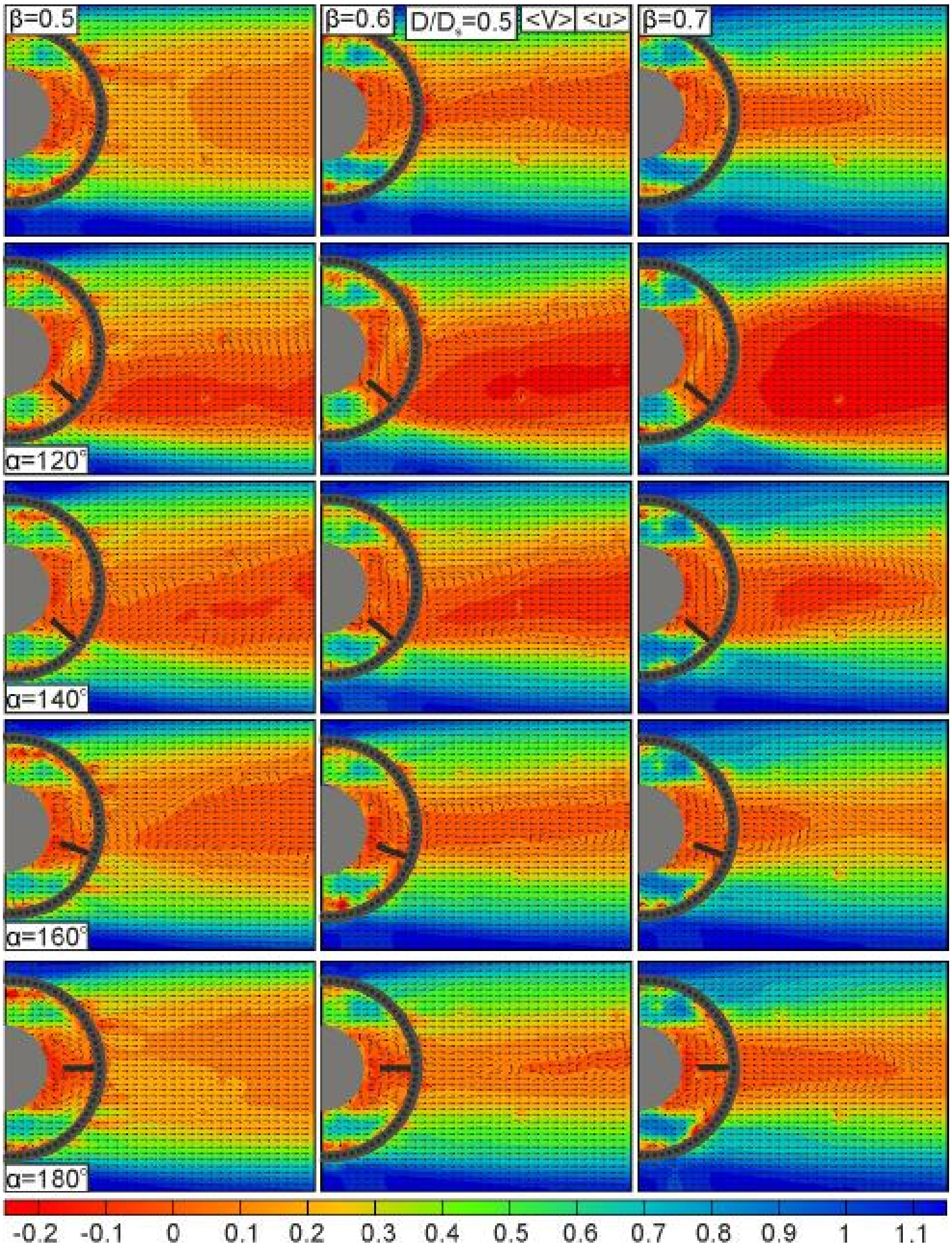

Figure 4.25. Time averaged velocity vector field, <V> superposed with the stream-wise velocity contours, <u> for the plate length of L_p=3/4 and in contact with the perforated cylinder case for various plate angles and porosity of the perforated cylinders, β at the diameter ratio of D/D_s=0.5.

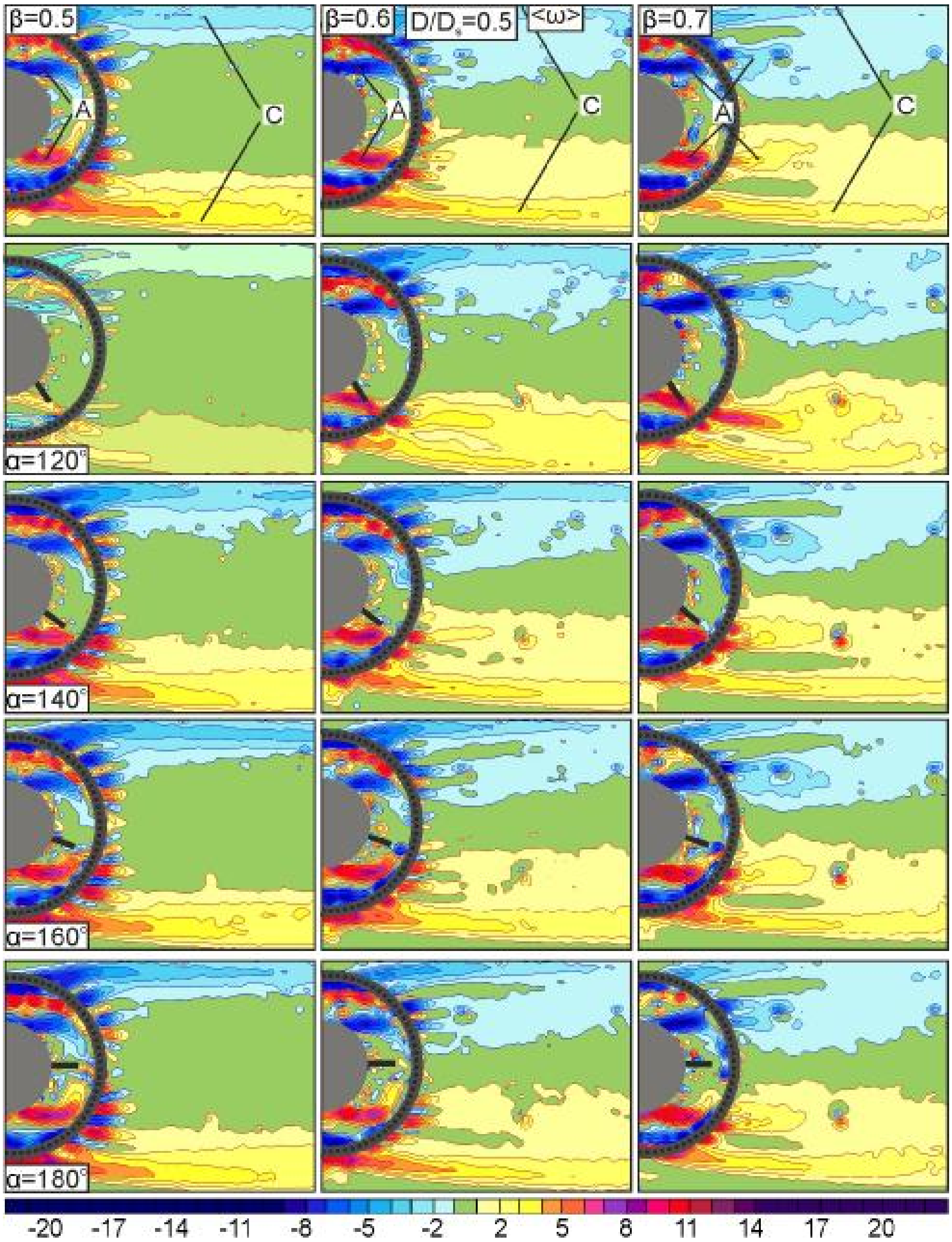

Figure 4.26. Time averaged vorticity contour, <ω> for the plate length of L_p=3/4 and in contact with the cylinder case for various plate angles and porosity of the perforated cyliders, β at the diameter ratio of D/D_s=0.5.

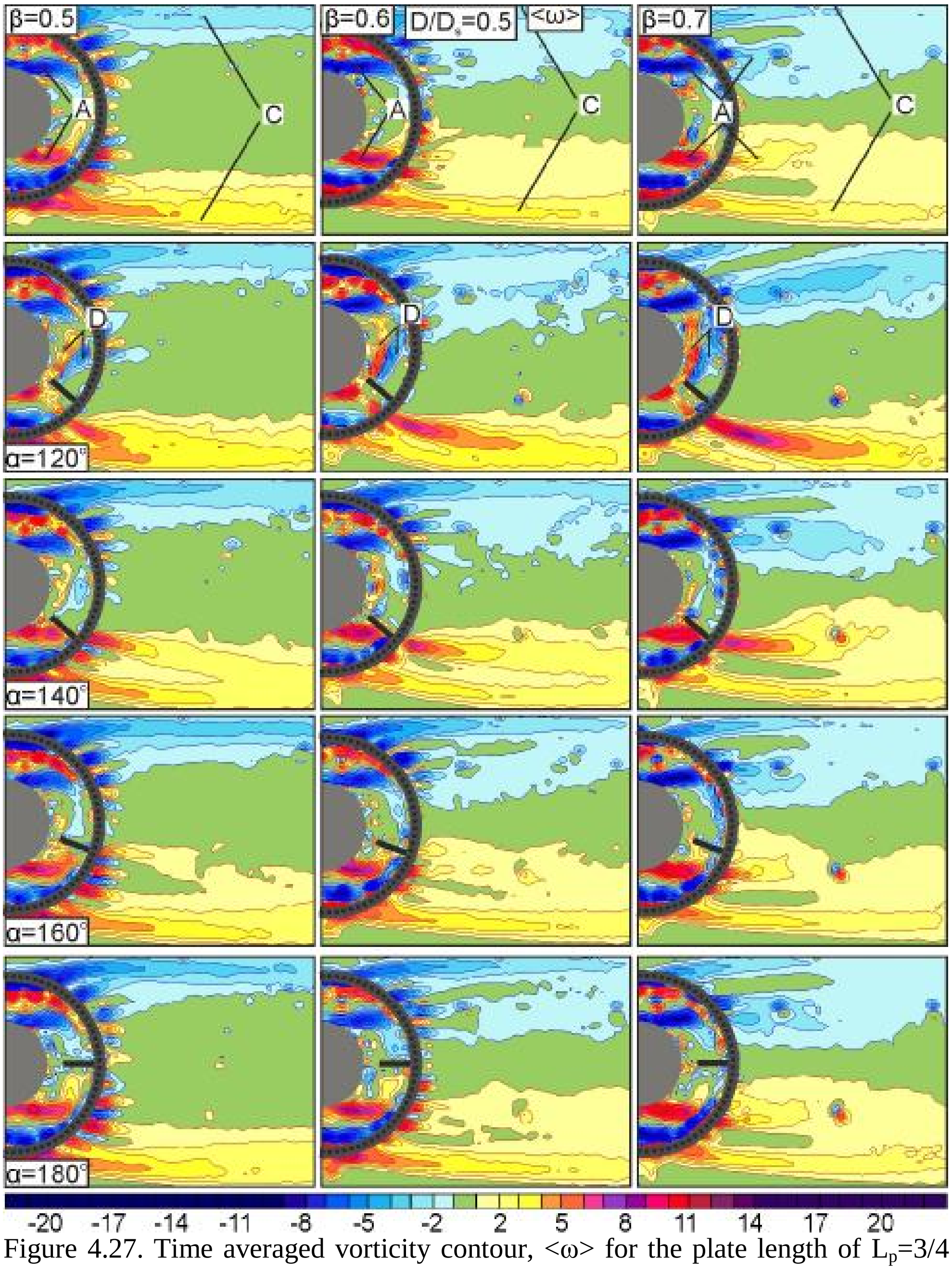

Figure 4.27. Time averaged vorticity contour, <ω> for the plate length of L_p=3/4 and in contact with the cylinder case for various plate angles and porosity of the perforated cylinders, β at the diameter ratio of D/D_s=0.5.

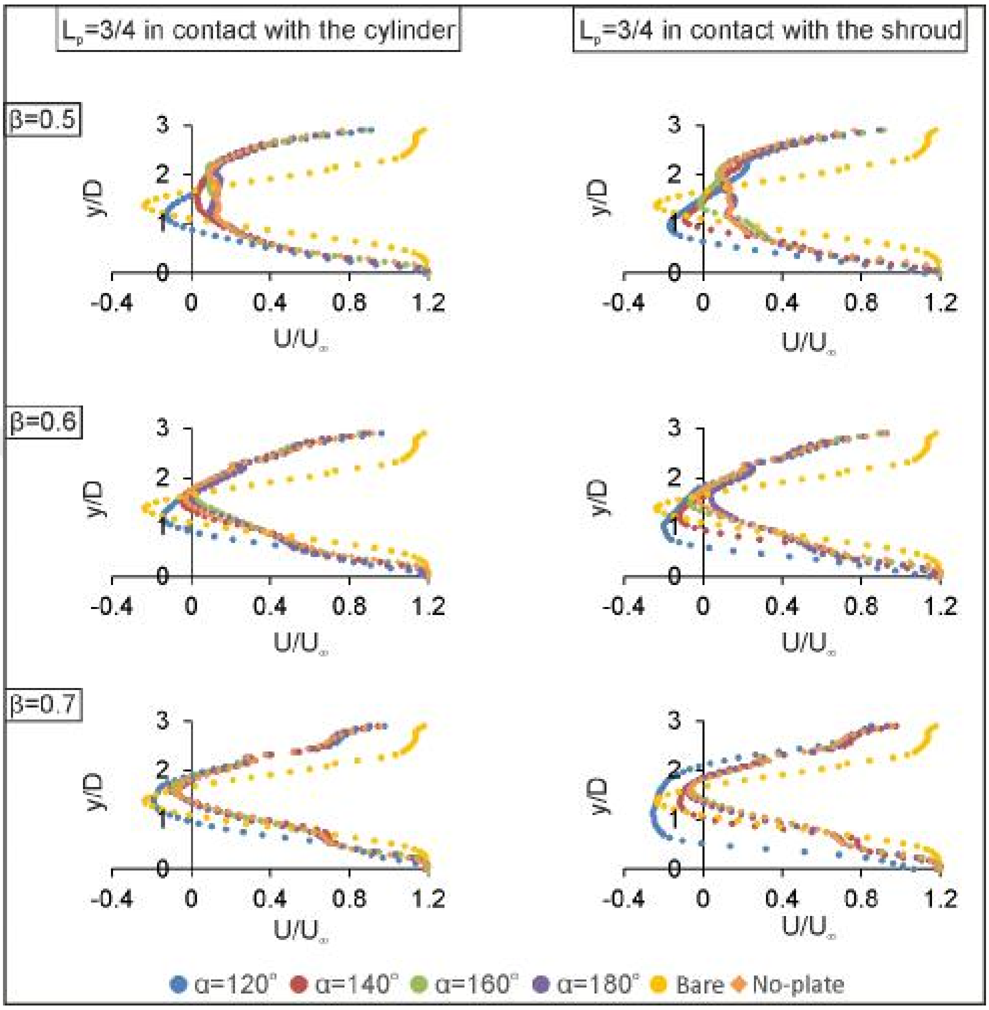

Figure 4.28. Profiles of mean stream-wise velocity of D/D_s=0.5 for L_p=3/4 in contact with the cylinder and the perforated cylinder cases at x/D=1.2.

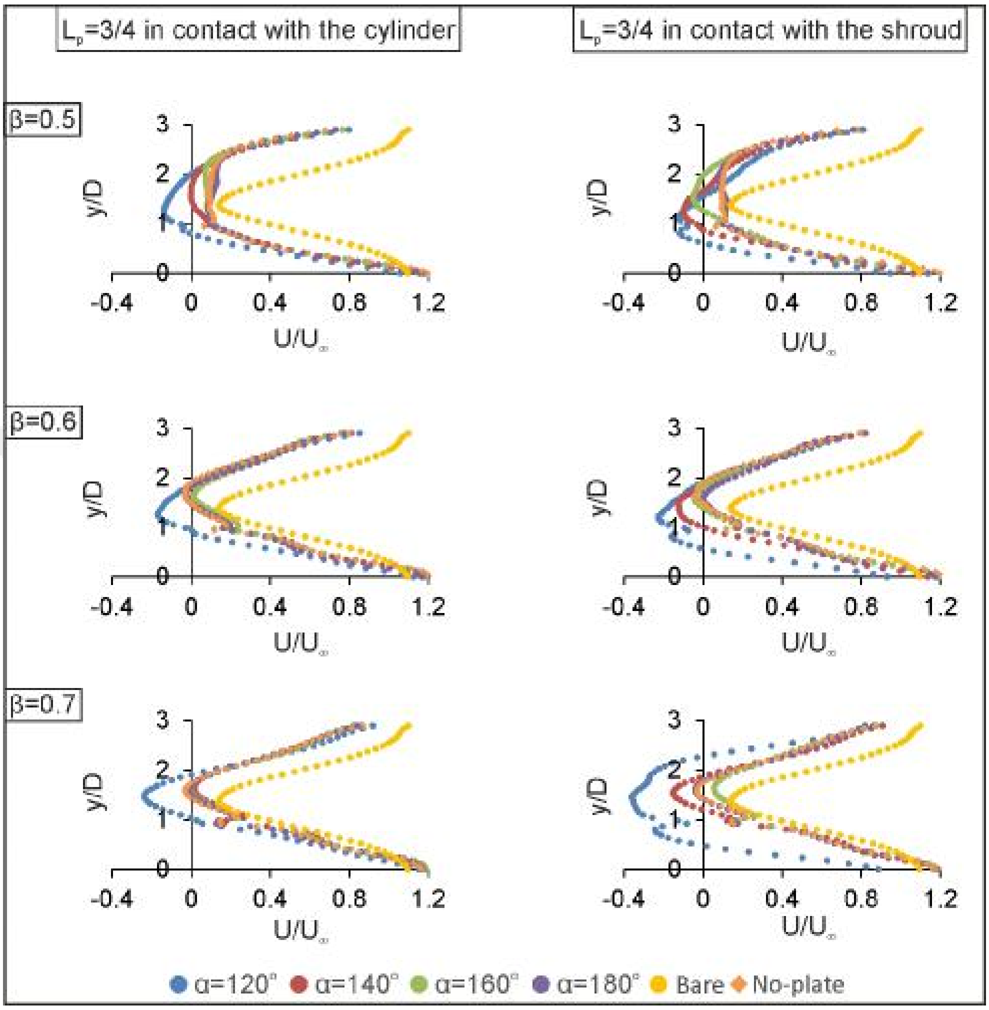

Figure 4.29. Profiles of mean stream-wise velocity of D/D_s=0.5 for L_p=3/4 in contact with the cylinder and the cylinder cases at x/D=2.

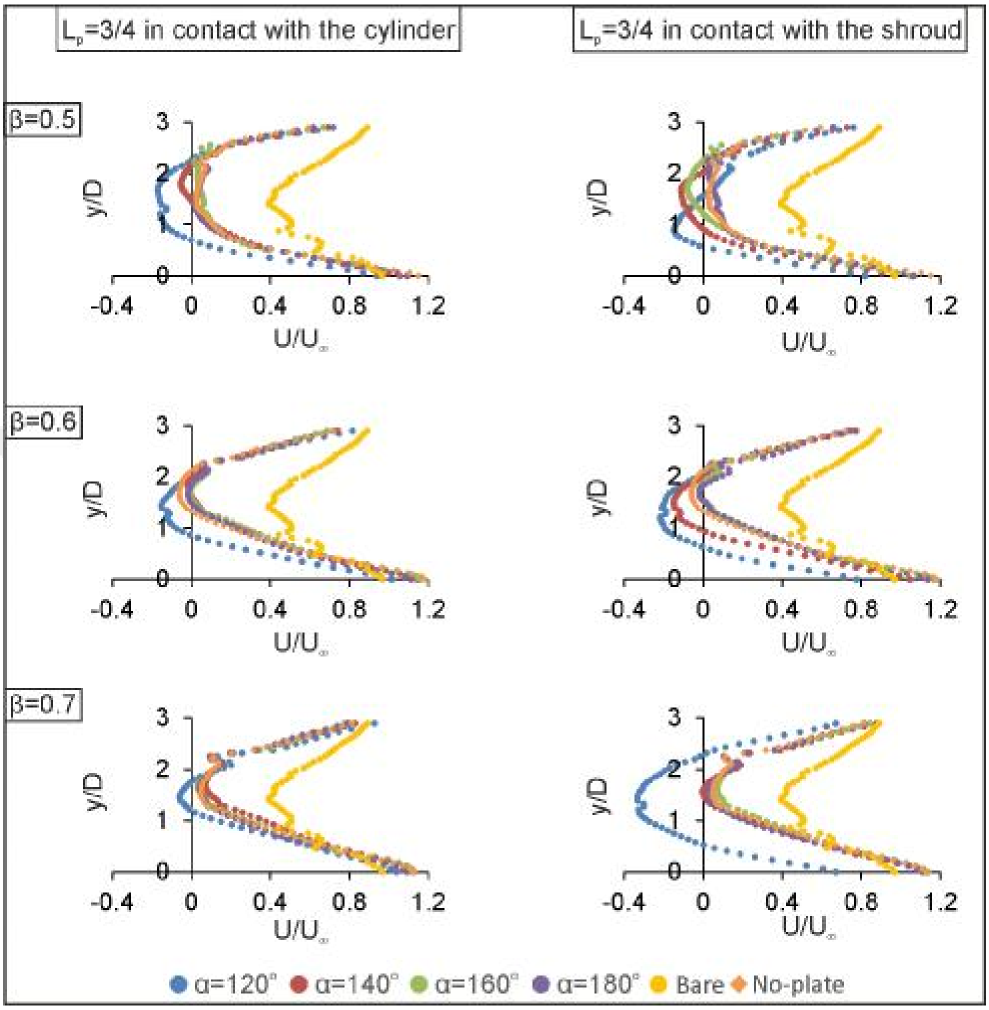

Figure 4.30. Profiles of mean stream-wise velocity of D/D_s=0.5 for L_p=3/4 in contact with the cylinder and the cylinder cases at x/D=3.2.

5. CONCLUSIONS AND RECOMMENDATIONS

The drag reduction and the flow control downstream of the circular cylinder are important research topics in order to reduce or eliminate the adverse effects of VIV. Although the shrouds have been studied in this regard, the controlled wake region of the shroud has not been fully understood. Perforated cylinders were used in this study as shroud. The diameter of the cylinder was kept constant as D=50 mm where the free stream velocity was also kept constant as U_∞=100 mm/s which corresponds to a Reynolds number of Re=5×10^3 according to the cylinder diameter, D. The perforated cylinders have five different porosities which are β=0.3, 0.4, 0.5, 0.6 and 0.7 and three different diameters which are D_s=83.33 mm, 100 mm and 125 mm. Firstly, it was focused on the flow structure in the gap region between the cylinder and the perforated cylinder as well as the near-wake region of the perforated cylinder, and also to investigate the effect of the perforated cylinder on the drag reduction. Secondly, it was investigated the effect of the splitter plate and the perforated cylinder combination on the flow control of the circular cylinder. During the experiments, two different plate lengths, L_p were used (L_p=3/4 and 1) and also the plate was located in seven different rotation angles, α which are α=120^o, 130^o, 140^o, 150^o, 160^o, 170^o and 180^o. It was also investigated that the effect of the splitter plate and the perforated cylinder combination on the total drag and lift coefficients.

It can be concluded in the light of obtained PIV results that the flow structure of the cylinder in the near-wake region is significantly affected by the perforated cylinder for all diameter ratios, D/D_s. The perforated cylinders are dominant on the flow structure for the porosity value of β=0.3. The negative velocity contours indicate that the reverse flow occurs in the near wake region owing to the detainment of the main flow by using perforated cylinder at porosity value of β=0.3. At diameter ratio of D/D_s=0.4, increasing the number of holes on the perforated cylinder enhances momentum transfer into the gap region between the cylinder and the perforated cylinder and the near-wake region. Thus, the velocity magnitudes of the gap region are higher compared to the porosity value of β=0.3 and reverse flow is disappeared in the near-wake region for the porosity values of $0.4 \leq \beta \leq 0.6$. The magnitude of velocity in near-wake region is affected not only by the porosity of perforated cylinder, but also by the diameter ratio of the perforated cylinder. At diameter ratio of D/D_s=0.6, the negative velocity contours for porosity values of β=0.4 and 0.5 indicate that the narrow gap is inadequate to transfer the momentum from inside of perforated cylinder into the near-wake region. The reverse flow, therefore, occurs in the near-wake region as a result of the momentum transfer from the shear layers of the perforated cylinder into the near – wake region. On the other hand, the flow control is achieved in the near – wake region for porosity values of β=0.5 and 0.6 at diameter ratios of D/D_s=0.4 and 0.5. Also, the drag coefficient of cylinder is reduced by 65% for porosity value of β=0.5 at diameter ratio of D/D_s=0.4. However, the vortex formation of the cylinder is observed in the gap region between the cylinder and the perforated cylinder for all cases.

The results obtained from dye experiments for the further downstream depict that perforated cylinders behave like bare cylinder and dominant on the flow structure for porosity values of $\beta \leq 0.4$. The shear layers on the both side of the perforated cylinder rolls up in to the near wake region and von Karman vortex Street emerged from the downstream of the cylinder and the perforated cylinder configuration. The results obtained for porosity value of β=0.5 indicated that the location of rolling up of shear layers, R_L is shifted to further region of downstream for diameter ratios $D/D_s \geq 0.5$. However, the results obtained for the porosity value of β=0.5 at the diameter ratio of D/D_s=0.4 is slightly different compared with the cases of diameter ratio $D/D_s \geq 0.5$. The wake region exhibits ‘S’ shaped unsteady oscillating flow behavior similar to von Karman vortex street. On the contrary, the width of wake regions, W_w are decreased up to porosity values of $\beta<0.6$ and they are approximately same at porosity values of $\beta \geq 0.6$ for all dimeter ratios, D/D_s.

Additionally, the formation of von Karman vortex street is suppressed in the flow region further downstream of the cylinder at diameter ratios of D/D_s=0.4 and 0.5.

Using the splitter plate and the perforated cylinder combination remarkably affects flow structure in the near-wake. For plate angles of $120^o \leq \alpha \leq 140^o$, the incoming flow through the perforated cylinder is blocked by the splitter plate. Therefore, the reverse flow occurs in the near-wake region and re-enters into the gap region between the cylinder and the perforated cylinder. A lower magnitude vorticity in the lower side of the cylinder elongates in the downstream direction and the magnitude of the vorticity dramatically increases in the leading edge of the splitter plate due to the fact that transfer of the momentum into the near-wake region increases at this point. On the other hand, the reverse flow disappears in the near – wake region for the porosity values of β=0.5 and 0.6 at the plate angles of $\alpha=170^o$ and 180^o. The plate angle of $\alpha=180^o$ presents the well-known splitter plate method within the literature and could be the best way of preventing the interaction of vortices formed by the cylinder in the near-wake region. Total drag coefficient which is calculated based on the frontal area of cylinder slightly reduces with the increasing plate angle, α. It is worth to note that the plate angle has a significant effect on the total lift coefficient. The maximum total lift coefficient is evaluated at plate angle $\alpha=120^o$ for porosity of β=0.7 because increasing porosity, β enhances momentum transfer into the gap region between the cylinder, and the perforated cylinder and decreasing plate angle, α causes asymmetric flow in the gap region between the cylinder and the perforated cylinder. The total lift coefficient decreases gradually with increasing plate angle, α. The total lift coefficient values are approximately zero for all porosities at plate angle of $\alpha=180^o$ due to symmetric flow downstream of the cylinder.

Since this study has revealed benign results on the drag reduction by using perforated cylinders, it can be expected that the results would benevolently guide the engineers for further investigations. The future work about this topic will be studied numerically and this study would be excellent example as a reference for the researchers as well.

REFERENCES

Ahmed, A., and Bays-Muchmore, B., 1992. Transverse Flow over a Wavy Cylinder. Phys. Fluids A, 4: 1959-1967.

Akilli, H., Sahin, B., and Tumen, N.F., 2005. Suppression of Vortex Shedding of Circular Cylinder in Shallow Water by a Splitter Plate. Flow Measurement and Instrumentation, 16:211–219.

Akilli, H., Karakus, C., Akar, A., Sahin, B., and Tumen, N.F., 2008. Control of Vortex Shedding of Circular Cylinder in Shallow Water Flow Using an Attached Splitter Plate. Journal of Fluids Engineering-T ASME, 130:041401.

Amitay, M., Honohan, A., Trautman, M., and Glezer, A., 1997. Modification of the Aerodynamic Characteristics of Bluff Bodies Using Fluidic Actuators. AIAA 97-2004.

Assi, G.R.S., Bearman, P.W., and Kitney, N., 2009. Low Drag Solutions for Suppressing Vortex-Induced Vibration of Circular Cylinders. Journal of Fluids and Structures, 25: 666–675.

Assi, G.R.S., Bearman, P.W., Kitney, N., and Tognarelli, M.A., 2010. Suppression of Wake-Induced Vibration of Tandem Cylinders with Free-to-Rotate Control Plates. Journal of Fluids and Structures, 26:1045–1057.

Baek, H., and Karniakidis, G.E., 2009. Suppressing Vortex-Induced Vibrations via Passive Means. Journal of Fluids and Structures, 25:848–866.

Badr, H., Coutanceau, M., Dennis, S., and Menard, C., 1990. Unsteady Flow Past a Rotating Circular Cylinder at Reynolds Numbers 1000 and 10000. Journal of Fluid Mechanics, 220:459– 484.

Bandyopadhyay, PR., 1986. Review—Mean Flow in Turbulent Boundary Layers Disturbed to Alter Skin Friction, Trans. ASME Journal of Fluids Engineering 108, 127-140.

Bao, Y. and Tao, J., 2013. The Passive Control of Wake Flow behind a Circular Cylinder by Parallel Dual Plates. Journal of Fluids and Structures, 37:201-209.

Bearman, P.W., 1965. Investigation of Flow behind a Two-dimensional Model with Blunt Trailing Edge and Fitted with Splitter Plates, Journal of Fluid Mechanics, 21, 241–255.

Bearman, P.W., 1967, The Effect of Base Bleed on the Flow behind a Two dimensional Model with a Blunt Trailing Edge, The Aeronautical Quaterly,18; 207-224.

Bearman, P.W., 1984. Vortex Shedding From Oscillating Bluff Bodies. Annual Review of Fluid Mechanics, 16: 195-222.

Bearman, P.W., 1997. Near Wake Flows behind Two and Three dimensionel Bluff Bodies. Journal of Wind Eng. And Inds. Aero., 71: 33-54.

Bearman, P.W., 2011. Circular Cylinder Wakes and Vortex-Induced Vibrations, Journal of Fluids and Structures, 27: 648–658.

Bearman, P., and Brankovic, M., 2003. Experimental Studies of Passive Control of Vortex-Induced Vibration. European Journal of Mechanics B/Fluids, 23: 9-15.

Boorsma, K., Zang, X., and Molin, N., 2010. Landing Gear Noise Control Using Perforated Fairings. Acta Mechanica Sinica, 26:159-174.

Bovand, M., Rashidi, S., Dehghan, M., Esfahani, J.A., and Valipour, M.S., 2015. Control of Wake and Vortex Shedding Behind a Porous Circular Obstacle by Exerting an External Magnetic Field, J. Magn. Magn. Mater, 385:198-206.

Chen, Z.H., and Aubry, N., 2005. Active Control of Cylinder Wake. Communications in Nonlinear Science and Numerical Simulation, 10:205-216.

Choı, H., Jeon, W-P., and Kim, J., 2008. Control of Flow over a Bluff Body. Annual Review of Fluid Mechanics, 40:113-139.

Cimbala, M., and Garg, S., 1991. Flow in the Wake of a Freely Rotatable Cylinder with Splitter Plate. AIAA Journal, 29:1001-1003.

Delaunay, Y. and Kaiktsis, L., 1999. Active Control of Cylinder Wakes: Use of Base Suction and Blowing. ESAIM: Proceedings, 7:104-119.

Durhasan, T., Aksoy M.M., Pinar, E., Ozkan, G.M., Akilli, H., and Sahin, B., 2016. Vortex Street Suppression of a Circular Cylinder Using Perforated Semi-Circular Fairing in Shallow Water, Experimental Thermal and Fluid Science, 79:101-110.

Every, M.J., King, R., and Weaver, D.S., 1982. Vortex- Excited Vibrations of Cylinders and Cables and their Suppression. Ocean Engineering, 9: 135-157.

Feng, L.H., and Wang, J.J., 2010. Circular Cylinder Vortex-Synchronization Control with a Synthetic Jet Positioned at the Rear Stagnation Point. Journal of Fluid Mechanics, 662:232-259.

Firat, E., 2015. The Effects of Different Opening (ventilation) Configurations on Drag Reduction and/or Vortex-Induced Vibration (VIV) Suppression of a Circular Cylinder. PhD Thesis, 4.

Fujisawa, N., Takeda, G., and Ike, N., 2003. Flow Control around a Circular Cylinder by Internal Acoustic Excitation. Journal Fluid Structures, 17:903–913.

Gabbai, R.D., and Benaroya, H., 2004. An Overview of Modeling and Experiments of Vortex Induced Vibration of Circular Cylinder. Journal of sound and Vibration, 282:575-616

Gad-El-Hak, M., 2000. Flow Control- Passive, Active and Reactive Flow Management, Cambridge University Press, New York.

Galvao, R., Lee, E., Farrell, D., Hover, F., Triantafyllou, M., Kitney, N., and Beynet, P., 2008. Flow Control in Flow–Structure Interaction. Journal of Fluids and Structures, 24: 1216-1226.

Gao, Y., Fu, S., Wang, J., Song, L., and Chen, Y., 2015. Experimental Study of the Effects of Surface Roughness on the Vortex-Induced Vibration Response of a Flexible Cylinder. Ocean Engineering, 103: 40-54.

Gerrard, J.H., 1966. The Mechanics of the Formation Region of Vortices behind Bluff Bodies. Journal of Fluid Mechanics, 25: 401-413.

Glezer, A., and Amitay, M., 2002. Synthetic Jets. Annual Review of Fluid Mechanics, 34: 503-529.

Gozmen, B., Akilli, H., and Sahin, B., 2013. Passive Control of Circular Cylinder Wake in Shallow Flow. Measurement, 46:1125-1136.

Gozmen, B., and Akilli, H., 2014. Flow Control Downstream of a Circular Cylinder by a Permeable Cylinder in Deep Water. Wind structure Int. j., 19:389-404.

He, J.W., Chevalier, M., Glowinski, R., Metcalfe, R., Nordlander, A. and Periaux, J., 2000. Drag Reduction by Active Control for Flow Past Cylinders. In Computational mathematics driven by industrial problems, Berlin, 287–363.

Hsiao, F.B., and Shyu, J.Y., 1991. Influence of Internal Acoustic Excitation upon Flow Passing a Circular Cylinder. Journal of Fluids and Structures, 5: 427-442.

Igarashi, T., 1978. Flow Characteristics around a Circular Cylinder with a Slit. Bulletin of the Japan Society of Mechanical Engineers, 21;656–664.

Ingham, D.B., 1983. Steady Slow Past a Rotating Cylinder, Computers & Fluids, 11(4); 351-366

Ingham, D.B., and Tang, T., 1990. A Numerical Investigation into the Steady Flow Past a Rotating Circular Cylinder at Low and Intermediate Reynolds Numbers, Journal of Computational Physics, 87(1);91-107.

Jukes, T. N., and Choi, K.S., 2009. Flow Control around a Circular Cylinder Using Pulsed Dielectric Barrier Discharge Surface Plasma. Physics of Fluids, 21:127-139.

Kieft, R., Rindt, C.C.M., and Van Steenhoven, A.A., 2007. Near-Wake Effects of a Heat Input on the Vortex-Shedding Mechanism, International Journal of Heat and Fluid Flow, 28(5);938-947.

Kim, S., Lee, and C. M., 2001. Control of Flows around a Circular Cylinder: Suppression of Oscillatory Lift Force. Fluid Dynamics Research, 29, 47-63.

Kiu, K.Y., Stappenbelt, B.., and Thiagarajan, K.P., 2011. Effects of Uniform Surface Roughness on Vortex-Induced Vibration of Towed Vertical Cylinders. J. Sound Vib, 330, 4753-7463.

Kumar, R.A., Sohn, C-H., and Bangalore, H.L., 2008. Passive Control of Vortex-Induced Vibrations: An Overview. Recent Patents on Mechanical Engineering, 1:1-11.

Kuo, C.-H., Chiou, L.-C., and Chen, C.-C., 2007. Wake Flow Pattern Modified by Small Control Cylinders at Low Reynolds Number. Journal of Fluids and Structures, 23:938–956.

Kuo, C.-H., and Chen, C.-C., 2009. Passive Control of Wake Flow by Two Small Control Cylinders at Reynolds Number 80. Journal of Fluids and Structures, 25:1021–1028.

Kwon, K., and Choi, H., 1996. Control of Laminar Vortex Shedding behind a Circular Cylinder Using Splitter Plates. Physics of Fluids, 10:479– 485.

Lachman, G, 1961. Boundary Layer and Flow Control, Oxford: Pergamon Press vols.1,2.

Lam, K., Wang, F.H., Lib, J.Y., and Soa, R.M.C., 2004. Experimental Investigation of the Mean and Fluctuating Forces of Wavy (varicose) Cylinders in a Cross-Flow. Journal of Fluids and Structures, 19: 321–334.

Lee, S-J., and Kim, H-B., 1997. The Effect of Surface Protrusions on the Near Wake of a Circular Cylinder, Journal of Wind Engineering and Industrial Aerodynamics, 69–71:351-361.

Lee, S-Y., and Lee, J-Y., 2006. Flow Structure of Wake behind a Rotationally Oscillating Circular Cylinder, Journal of Fluids and Structures, 22(8);1097-1112.

Li, Z., Navon, I.M., Hussaini, M.Y., and Le Dimet, F.X., 2003. Optimal Control of Cylinder Wakes via Suction and Blowing. Computers and Fluids, 32(2):149–171.

Lienhard, J.H., 1966. Synopsis of Lift, Drag and Vortex Frequency Data for Rigid Circular Cylinders. Washington State University College of Engineering Research Division Bulletin, 300:3.

Lim, H.C., and Lee, S.J., 2004. PIV Measurements of Near Wake behind a U-Grooved Cylinder. Journal of Fluids and Structures, 18:119–130.

Lin, J.C., and Rockwell, D., 1995. Evolution of a Quasi-Steady Breaking Wave. Journal of Fluid Mechanics, 302, 29-44.

Lin, S-Y., and Wu, T-M., 1993. Flow Control Simulation around a Circular Cylinder by a Finite Volume Schema. Numerical Heat Transfer, Part A: Application: An International Journal of computation and Methodology, 2(3):301-319.

Mansingh, V., and Oosthuizen, P.H., 1990. Effects of Splitter Plates on the Wake Flow behind a Bluff Body, AIAA J. 28:778-783.

Marris, A.W., 1964. A Review on Vortex Streets, Periodic Wakes, and Induced Vibration Phenomena. Journal of Basic Engineering, 86(2), 185-193.

Miau, J.J., Yang, J.H., and Lee, K.R., 1993. Suppression of Low Frequency Variations in Vortex Shedding by a Splitter Plate behind a Bluff Body, Journal of Fluids and Structure, 7:897-912.

Mimeau, C., Mortazavai, I., and Cottet, G-H., 2014. Passive Flow around a Semi-Circular Cylinder Using Porous Coatings. International Journal of Flow Control, 6(1);43-60.

Mittal, S., and Raghuvanshi, A., 2001. Control of Vortex Shedding behind Circular Cylinder for Flows at Low Reynolds Numbers. International Journal of Numerical Methods for Heat & Fluid Flow, 35:421–447.

Molin, B., 1993. A Potential Flow Model for the Drag of Shrouded Cylinders. Journal of Fluids and Structures, 7: 29-38.

Muddada, S., and Patnaik, B.S.V., 2010. An Active Flow Control Strategy for the Suppression of Vortex Structures behind a Circular Cylinder. Europian Journal of Mechanics B/Fluids, 29:93–104.

Nakamura, Y., 1996. Vortex Shedding from Bluff Bodies with Splitter Plates, Journal of Fluids and Structures, 10(2):147-158.

Nakamura, H., Igarashi, T., 2008. Omnidirectional Reductions in Drag and Fluctuating Forces for a Circular Cylinder by Attaching Rings. Journal of Wind Engineering, 96:887–899.

Nebres, J., Batill, S., 1993. Flow about a Circular Cylinder with a Single Large-Scale Surface Perturbation. Experiments in Fluids, 15(6):369-379.

Nosenchuck, D.M., Brown, G.L., Culver, H.C., Eng. T.I., and Huang, I.S., 1995. Spatial and Temporal Characteristics of Boundary Layers Controlled with the Lorentz Force. Twelfth Australasian Fluid Mechanics Conference, Australia.

Oruc, V., 2012. Passive Control of Flow Structures around a Circular Cylinder by Using Screen. Journal of Fluids and Structures, 33:229-242.

Oruc, V., 2017. Strategies for the Applications of Flow Control Downstream of a Bluff Body. Flow Measurement and Instrumentation, 53:204-214.

Oruc, V., Akilli, A., and Sahin, B., 2016. PIV Measurements on the Passive Control of Flow past a Circular Cylinder. Experimental Thermal Fluid Science, 70:283-291.

Owen, J.C., Bearman, P.W., and Szewczyk, A.A., 2001. Passive Control of VIV with Drag Reduction. Journal of Fluids and Structures, 15:597-605.

Ozkan, G.M., Firat, E., and Akili, H., 2017. Passive Flow Control in the Near Wake of a Circular Cylinder Using Attached Permeable and Inclined Short Plates. Ocean Engineering, 134:35-49.

Ozkan, G.M., Oruc, V., Akili, H. and Sahin, B., 2012. Flow Around a Cylinder Surrounded by a Permeable Outer Cylinder in Shallow Water. Experiments in Fluids 53:1751-1793.

Ozono, S., 1999. Flow Control of Vortex Shedding by a Short Splitter Plate Asymmetrically Arranged Downstream of a Cylinder. Physics of Fluids, 11 (10):2928 –2934.

Parkinson, G.V., 1974. Mathematical Models of Flow-Induced Vibrations of Bluff Bodies. Flow Induced Structural Vibrations, 81-127.

Price, P., 1956. Suppression of the Fluid-Induced Vibration of Circular Cylinders. J. Eng. Mech. Div., Am. Soc. Civ. Eng., 82: 1030.

Rashidi, S., Hayatdavoodi, M., and Esfahani, J. A., 2016. Vortex Shedding Suppression and Wake: a review. Ocean Engineering, 126: 57-80.

Ruck, B., Klausmann, K., and Wacker, T., 2012. The Flow Around Circular Cylinders Partially Coated with Porous Media. AIP Conference Proceedings 1453;49-54.

Roshko, A. 1954. On the Development of Turbulent Wakes from Vortex Streets. NACA Rep. 1191.

Roshko, A. 1955. On the Drag and Shedding Frequency of Two-dimensional Bluff Bodies, NACA Tech. Note no.3169.

Roshko, A. 1993. Perspectives on Bluff Body Aerodynamics. Journal of Wind Induced Aerodynamics, 49:79.

Sarpkaya, T., 1979. Vortex-Induced Oscillations. Journal of Applied Mechanics, 46: 241–258.

Sarpkaya, T., 2004. A Critical Review of the Intrinsic Nature of Vortex-Induced Vibrations. Journal of Fluids and Structures, 19:389–447.

Schubauer, G. B., and Skramstad, H. K., 1947. Laminar Boundary Layer Oscillations and Transitions on a Flat Plate. J Aero Sci., 14:69–79

Shukla, S., Govardhan R.N., and Arakeri J.H., 2009. Flow over a Cylinder with a Hinged-Splitter Plate. Journal of Fluids and Structures, 25: 713-720.

Son, D., Jeon, S., and Choi, H., 2011. A Proportional-Integral-Differential Control of Flow over a Circular Cylinder. Philos. Trans. R. Soc. A, 369: 1540-1555.

Son, J.S., Hanratty, T. J., 1969. Velocity Gradients at the Wall for around a Cylinder at Reynolds Number from 5000 to 100000. Journal of Fluids Mechanics, 35(2): 353-368.

Unal, M.F., and Rockwell, D., 1987. On Vortex Formation from a Cylinder, Part 1: The Initial Instability. Journal of Fluid Mechanics, 190: 491-512.

Unal, M.F., and Rockwell, D., 1988. On Vortex Formation from a Cylinder, Part 2: Control by Splitter-Plate Interference. Journal of Fluid Mechanics, 190: 513-529.

Wang, C., Tang, H., Duan, F., and Yu, S.C.M., 2015. Control of Wakes and Vortex-Induced Vibrations of a Single Circular Cylinder Using Synthetic Jets, Journal of Fluids and Structures, 60;160-179.

Wang, J., Zheng, H., and Tian, Z., 2015. Numerical Simulation with a TVD-FVM Method for Circular Cylinder Wake Control by a Fairing, Journal of Fluids and Structures, 57;15-31.

Weier, T., Gerbeth, G., Mutschke, G., Platacis, E., and Liealausis, O., 1998. Experiments on Cylinder Wake Stabilization in an Electrolyte Solution by Means of Electromagnetic Forces Localized on the Cylinder Surface, Experimental Thermal and Fluid Science, 16:84-91.

Williamson, C.H.K., and Govardhan, R., 2004. .Vortex-Induced Vibrations. Annual Review of Fluid Mechanics, 36:413-455.

Wong, H. Y., 1985. Wake Stabilization by the Action of Base Bleed. Trans. ASME: J. Fluids Engineering, 107, 378–384.

Wood, C. J., 1964. The Effect of Base Bleed on a Periodic Wake. J. R. Aero. Soc. 68, 477–482.

Wood, C. J., 1967. Visualization of Incompressible Wake with Base Bleed, Journal of Fluid Mechanics, 29, (2) 259–272.

Xu, J.C., Sen, M., and Gad-El-Hak, M., 1993. Dynamics of Rotable Cylinder with Splitter Plate in Uniform Flow. Journal of Fluids and Structures, 7(4):401-416.

Yu, M-H., and Monkewitz, P. A. 1990. The Effect of Nonuniform Density on the Absolute Instability of Two-Dimensional Inertial Jets and Wakes Physics of Fluids A 2(7):1175-1181.

Zdravkovich, M. M., 1981. Review and Classification of Various Aerodynamic and Hydrodynamic Means for Fuppressing Vortex-Shedding. Journal of Wind Engineers and Industrial Aerodynamics, 7:145–189.

Zdravkovich, M. M, and Soutworth, P.J., 1973. Effect of Shroud Eccentricity on Suppression of Flow Induced Vibrations. Journal of Sound and Vibration, 27(1); 77-84.

Zhang, H., Fan, B.-C.., and Chen, Z.-H., 2010. Computations of Optimal Cylinder Flow Control in Weakly Conductive Fluids. Computers and Fluids, 39:1261–1266.

Zhao, M., and Cheng, L., 2010. Finite Element Analysis of Flow Control Using Porous Media. Ocean Engineering, 37:1357-1366.

Zhou, B., Wang, X., Guo, W., Gho, W.M., and Tan, S.K., 2015. Experimental Study on Flow Past a Circular Cylinder with Rough Surface. Ocean Engineering, 109:7-13

Zou, L., and Lin, Y., 2009. Force Reduction of Flow around a Sinusoidal Wavy Cylinder. Journal of Hydrodynamics, 21(3):308-315.

CURRICULUM VITAE

Tahir DURHASAN was born in Adana in 1987. He finished his high school education in Adana and after the graduation he entered in Mechanical Enginnering Department of Erzurum Atatürk University. He graduated as a Mechanical Engineer from the university in June 2009. He finished his master education in Mechanical Enginnering Department of Cukurova University in February, 2013 and began his Doctor of Philosophy at the same department in 2013. He is married and has a son.